農研機構報告　農村工学部門 2
1 ～ 56, 2018

ESTIMATION OF DAMAGED ZONE IN SOIL USING RESISTIVITY MONITORING

INOUE Keisuke

Disaster Prevention Unit, Division of Facilities and Geotechnical Engineering

Abstract

In this research, we investigated the applicability of methods that estimate the 3D resistivity structure using 2D resistivity survey data to numerical and field experiments. When the resistivity structure is in 3D and does not match the assumption of 2D inversion, the resistivity distribution derived from 2D inversion can result in artifacts. However, 2D inversion using 2D resistivity survey data can estimate the depth of the target body with orthogonal survey lines after estimating the length of the target body with parallel survey lines. Moreover, 2D difference inversions from multiple 2D resistivity survey data could estimate the vertical and horizontal water flow and help in 3D modeling of nonuniform sequential recharging. When 3D inversion of 2D resistivity survey data is conducted, parallel lines are useful to highlight areas of particular interest where further detailed work with an intersecting line should be carried out. The 3D inversion of 2D resistivity survey data is more suitable than 2D inversion to describe the 3D phenomena associated with groundwater recharge. This method can be applied to monitor relatively fast infiltration in the vadose zone. Moreover, 3D simulations of the groundwater flow and 2D resistivity survey can estimate high hydraulic conductivity locations. Although these methods use 2D resistivity survey data, 3D information of the subsurface can be estimated considering proper line arrangement, estimation order, or a combination of simulations.

Key words *:2D Resistivity survey, 3D resistivity structure, Survey line arrangement, Farm pond, Crack, Leakage, water from simulation*

CONTENTS

1. Introduction

1.1 Motivation for this thesis

Whenever a large earthquake occurs, soil structure is damaged. The damage results in the formation of a high hydraulic conductivity zone in the soil. The high hydraulic conductivity zone of soil often leads to problems such as leakage of water from a reservoir or a paddy field, and slope failures after heavy rain. Although it is important to properly evaluate the infiltration, identifying of such high hydraulic conductivity locations is difficult. Tensiometers and time-domain reflectometry (TDR) moisture meters are often used to assess infiltration (Faybishenko, 2000; Huisman et al., 2002). Although these techniques are effective for measuring the amount of soil water, the measurements refer to discrete points and the soil structure is disturbed. By contrast, geophysical methods such as electrical resistivity survey can provide spatial geological information non-invasively. The

resistivity survey is an effective tool with which to ascertain water flow in the vadose zone, because electrical resistivity is strongly affected by the level of water saturation in the soil. Several methods have been applied to determine the water flow in soil by monitoring the resistivity change that is associated with variation in water saturation or water salinity (Daily et al., 1992; Binley et al., 1996; Park, 1998; Binley et al., 2002; Oldenborger et al., 2007; Amidu and Dunbar, 2007; Koestel et al., 2008; Nimmo et al., 2009; Batlle-Aguilar, 2009; Suzuki et al., 2010; Coscia et al., 2011; Takakura et al., 2013; Suzuki et al., 2015).

The soil water flow at a field scale is three-dimensional (3D) because of the heterogeneous hydraulic conductivity of the soil. For a detailed understanding of the soil water flow, a 3D distribution of resistivity is required. To monitor soil water infiltration, 3D resistivity survey is conducted (Oldenborger et al., 2007; Koestel et al., 2008; Coscia et al., 2011). For rapid water flow, the measurement time and the number of data should be small. To reduce the measurement time and produce a 3D distribution of resistivity, a 3D inversion method using two-dimensional (2D) resistivity survey data is applied (Jackson et al., 2001; Sugimoto et al., 2004; Gharibi and Bentley, 2005; Inoue et al., 2016). Since the 2D resistivity survey is more frequently used than the 3D resistivity survey, an estimation of 3D resistivity structure using 2D resistivity survey data can reduce the cost and improve the results on the field.

1.2 Research aim and objectives

This research investigates methods that estimate the 3D resistivity structure using 2D resistivity survey data. First, we propose a method to estimate resistivity structure using 2D inversion of 2D resistivity survey data. The 2D inversion require less time than the 3D inversion and 2D inversion is efficient to promptly estimate damage zones. When the resistivity structure is in 3D and does not match the assumption of the 2D inversion, the resistivity distribution derived from 2D inversion often provides artifacts. However, by considering the characteristics of resistivity distribution of 2D inversion with different line arrangements, 2D inversion of 2D resistivity survey data may interpret the results that include artifacts. Moreover, when the location of infiltration is unknown in the leaked paddy field, a 3D resistivity structure is useful to estimate the location. When the survey line is properly arranged, the semi 3D structure of resistivity can be estimated, because the 2D resistivity survey data include 3D information of the resistivity structure. Next, we propose a method to use 3D inversion of 2D resistivity data. A 3D inversion provides more precise information than 2D inversion, although 3D inversion requires more time than 2D inversion. When a 3D inversion of the 2D resistivity survey data is conducted, the arrangement of the survey line for 2D resistivity survey is also important. This effective arrangement has to be investigated. Moreover, when the water content varies with time, the distribution derived from 3D inversion of the 2D resistivity survey data includes data at different measurement times. The interpretation of the results based on the characteristics of inversion results is needed. Finally, we propose a method that uses 3D simulation data of soil water flow and 2D resistivity survey data to estimate locations of infiltration. Since the water flow in soil is governed by infiltration phenomena, considering the water flow simulation may improve the results, because the constraint from water flow is added to the resistivity structure. Therefore, the main objectives of this research are as follows:

1. To propose a method using 2D inversion of 2D resistivity survey data for efficiently detecting of crack ranges.
2. To examine a semi 3D resistivity monitoring method using the 2D resistivity survey data of four traverse survey lines in a groundwater recharge experiment.
3. To propose effective electrode configurations and line layouts commonly used in 2D resistivity surveys to 3D inversion.
4. To examine a 3D resistivity monitoring for an artificial groundwater recharge experiment using 3D inversion of 2D resistivity data.
5. To propose a method that uses the 3D simulation data of soil water flow and 2D resistivity survey data during a groundwater recharge experiment to estimate high hydraulic conductivity locations.

1.3 Structure of the thesis

This thesis is comprised of seven chapters.

In Chapter 2, we propose a method which uses two survey lines of orthogonal and parallel to the crack to efficiently detect the range of cracks. In the numerical experiment, the pattern of resistivity changes with different crack length or depth using orthogonal and parallel survey lines to the crack is investigated. By using numerical experiment results, the crack range is estimated for a field experiment (Inoue et al., 2014).

Chapter 3 examines a semi 3D resistivity monitoring method using 2D resistivity survey data of four traverse survey lines at a groundwater recharge experiment site. The resistivity change ratio distributions are derived using 2D difference inversion to make 3D soil water flows easily visible (Inoue et al., 2008).

In Chapter 4, we propose effective electrode configurations and line arrangement of 2D resistivity surveys for 3D inversion. We also conduct field experiments in a loam area including a backfilled pit. Finally, we apply these electrode configurations and line arrangements to the investigation of geological structure near the Nojima Fault in Awaji Island (Inoue et al., 2017b).

Chapter 5 examines the applicability of 2D resistivity survey data for 3D inversion to monitoring water flow in the vadose zone. Distributions of the resistivity change ratio are verified by the volumetric water content observed in boreholes in the test site. Furthermore, other 3D resistivity change ratio distributions are recovered from a 1-hr. time-shifted dataset to investigate the time dependency of measurements (Inoue et al., 2017a).

In Chapter 6, we propose a method that uses 3D simulation data of soil water flow and 2D resistivity survey data during a groundwater recharge experiment to estimate high hydraulic conductivity locations. First, we show the difficulty in estimating the infiltration path from the inversion of the 2D resistivity survey data. Next, proposed method is described in detail. Finally, to evaluate this method, numerical and field experiments are conducted (Inoue et al., 2017c).

Finally, summary and conclusions of this study and comments on future works are given in Chapter 7.

2. Simplified methods for detecting ground damage using 2D resistivity surveys

This research investigates methods that estimate damaged zones using 2D resistivity survey data. In this and the next chapters, we propose methods to estimate the resistivity structure using 2D inversion of 2D resistivity survey data. Because less time is required for 2D inversion of the survey data than that for 3D inversion, 2D inversion is efficient to promptly estimate the damaged zones.

When the resistivity structure is in 3D and does not match the assumption of 2D inversion, the resistivity distribution derived from 2D inversion can provide artifacts. However, when we consider the characteristics of the resistivity change derived from 2D inversion with different line arrangements, 2D inversion of 2D resistivity survey data can interpret the results that includes the artifacts.

This chapter describes a method using 2D inversion of 2D resistivity survey data to efficiently detect the range of cracks that could result from a large earthquake. In this method, we use two survey lines, one orthogonal and one parallel to the crack, before and after injecting of lime water into the crack. In the numerical experiment, characteristics of resistivity distributions with different crack length or depth are investigated using survey lines orthogonal and parallel to the crack. By using these results, the crack range is estimated during field experiments.

2.1 Introduction

A large earthquake can damage an agricultural reservoir by causing cracks in the embankments (Morii and Teradate, 2006; Hori et al., 2012; Masukawa et al., 2012). Cracks often can extend to the bottom of the embankment (Mohri et al., 2008). This type of damage can cause many secondary risks in rural areas such as flooding after the earthquake event. To reduce these risks, a prompt estimate of the damage to a reservoir is needed after the earthquake. In general, when a soil structure is damaged by a crack, lime water or methylene blue solution is injected into the crack and the damaged zone is observed by excavating the embankment (Hori et al., 2012; Masukawa et al., 2012). Although this method reliably estimates the crack range, the estimate is only carried out after the excavation. The reconstruction planning, therefore, cannot occur before the excavation. It is also difficult to excavate the embankment when the reservoir is filled with water. In this case, a geophysical method that non-invasively images the geological conditions from the surface may be used to estimate the crack range. An electrical resistivity survey, which is one of the geophysical methods, can repeatedly measure resistivity and calculate resistivity change. Injecting of a lime water into the crack increases the water content in infiltrated zones and decreases the porosity, because the crack is filled with the lime water, and decreases a resistivity in the pore waters. Because these factors decrease the resistivity of the water in and around the crack, the infiltrated range of lime water can be estimated.

A crack induced by an earthquake usually exhibits a planar shape that extends in a direction parallel to a dam's axis (Hori et al., 2012). A 2D resistivity survey line orthogonal to the planar-shaped crack almost matches with the assumption of 2D resistivity survey. However, the length of the crack is limited and the crack is a 3D structure. Therefore, a 3D resistivity survey would appear to be the best way to assess damages. On the other hand, a 3D resistivity survey increases the amount of measuring equipment and the time required to take the measurement, and it is difficult to promptly conduct. Although a 2D resistivity survey is easier to conduct than the 3D resistivity survey, artifacts can appear at incorrect places in the inverted cross section when the target is a 3D structure (Sasaki, 1993; Batlle-Aguilar et al., 2009). This means that a 2D resistivity survey can include the information around the survey line and can represent the 3D geological structure

(Inoue et al., 2008), because the electrical current flows three-dimensionally and the derived resistivity is affected by the anomaly, which is at a distance from the survey line. The 2D resistivity surveys have been conducted to estimate the extent of soil cracks (Samouelian et al., 2003) and to estimate the extent of slope weakness (Suryo et al., 2011). Nakazato et al. (2012) estimated damaged zones using a 2D resistivity survey by injecting sanitary water into the cracks on earth dams produced by a large earthquake. However, there are few investigations that study the influence of artifacts from 2D resistivity surveys on estimating the extent of cracks. If the influence of artifacts can be estimated, then the 2D resistivity survey also can produce information to estimate the 3D geological structure.

The purpose of this chapter is to propose a method to estimate the range of the crack with the injecting of lime water and conducting 2D resistivity surveys. We use two survey lines, one orthogonal and one parallel to a crack. We investigate the pattern of resistivity change indicated by different crack lengths or depths using survey lines that are both orthogonal and parallel to the crack. By using the numerical experiment results, the crack range is estimated in a field experiment.

2.2 Methods

2.2.1 Flow of the proposed method

Figure 1 illustrates the conceptual model and shows the crack and the survey lines. In this thesis, the horizontal distance of the crack is called "length," the vertical distance of the crack is called "depth," and the width of the crack is called "width." Although a survey line is usually placed in a direction that is orthogonal to the crack, a 2D resistivity survey often cannot precisely estimate the depth (Batlle-Aguilar et al., 2009). The estimation error depends on the crack length. Also, the estimation error along the direction of the crack length using the survey line parallel to a crack may be small. Therefore, it is more efficient to estimate a crack depth after its length is estimated. **Figure 2** illustrates a flow of the proposed method. First, two survey lines are placed parallel and orthogonal to the crack, as drawn in **Fig.1**, and initial electrical responses are measured. After the injection of lime water into the crack, the electrical response is measured using the two survey lines. The change in resistivity is calculated from the measurement data of each survey line. The length of the crack is estimated from the

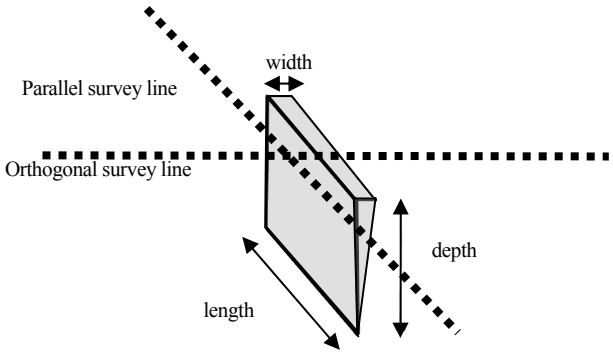

Fig.1 Conceptual model of the crack and the survey lines.

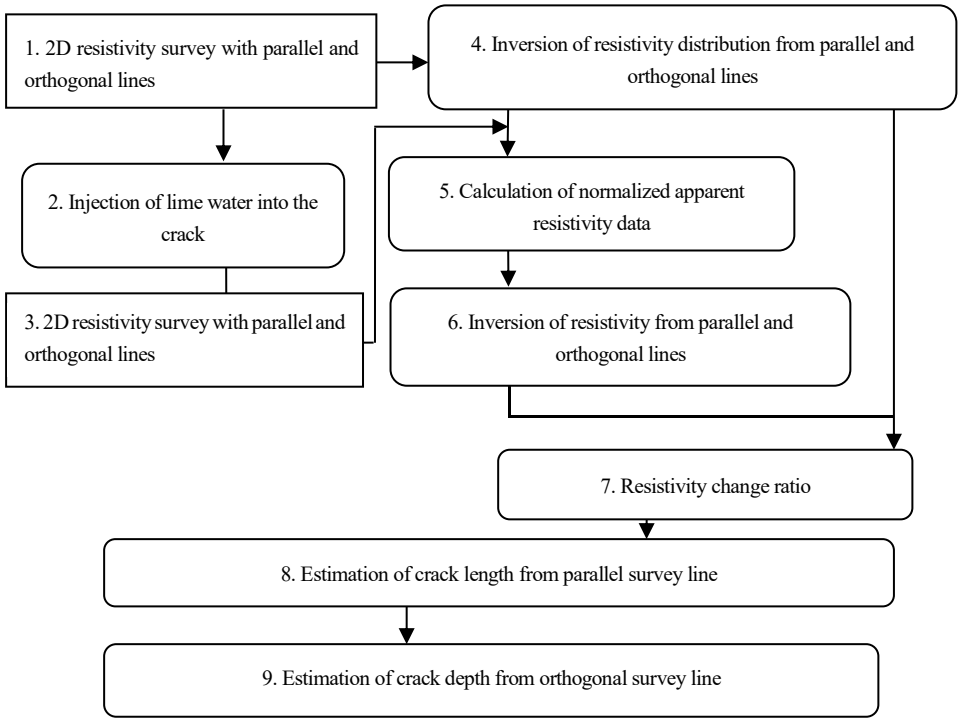

Fig.2 Flow of the proposed method illustrating the steps.

change in resistivity along the parallel survey line and the depth of the crack is estimated from the change in resistivity along the orthogonal survey line. The reason we use a change in resistivity is described in subsection 2.2.2 and the effects of measuring a change in resistivity are described in Section 2.4.

2.2.2 Theoretical background of resistivity survey

Measurements of soil resistivity can indicate the condition of the soil. Archie (1942) developed an empirical formula for the effective resistivity of a formation that takes into account porosity, ϕ, pore water saturation, S_r, and water resistivity, ρ_w:

$$\rho_s = a\phi^{-m} S_r^{-n} \rho_w \tag{1}$$

where ρ_s is the bulk resistivity of the formation, and a, m and n are constants. In the injection of lime water, the water saturation, porosity and water resistivity are expected to change. These factors decrease the resistivity.

Electrical potentials can be calculated from a resistivity model using a finite element method (FEM). We assume a 3D resistivity model $\rho(x, y, z)$ in a Cartesian system of coordinates (x, y, z) with the origin at the air-earth interface and z is positive downwards. The current source I is located at (x_0, y_0, z_0). The governing equation for the electrical potential $V(x, y, z)$ is

$$\nabla \cdot \left[\frac{1}{\rho(x, y, z)} \nabla V(x, y, z)\right] = -I\,\delta(x - x_0)\,\delta(y - y_0)\,\delta(z - z_0) \tag{2}$$

where δ is the Dirac's delta function. When model responses (apparent resistivity) are calculated from Equation (2), model parameters (resistivity) are updated to match the modelled responses to observed data (apparent resistivity). Let F be the forward mapping operator defined by Equation (3), the observed data vector $\boldsymbol{d}$ is then given by

$$\boldsymbol{d} = F(\boldsymbol{p}) \tag{3}$$

where $\boldsymbol{p}$ is the model parameter vector. The direct current resistivity inverse problem can be written in matrix form as

$$\Delta\boldsymbol{d} = \boldsymbol{A}\Delta\boldsymbol{p} \tag{4}$$

where $\Delta\boldsymbol{d}$ is the vector of differences between the observed data and modelled responses, $\boldsymbol{A}$ is the Jacobian matrix and $\Delta\boldsymbol{p}$ is the correction vector to be added to the initial model parameters of $\boldsymbol{p}_0$. Because the inverse problem is generally ill-posed, some constraints may be imposed on $\Delta\boldsymbol{p}$. Then the objective function to be minimized is expressed as

$$U = \|\Delta\boldsymbol{d} - \boldsymbol{A}\Delta\boldsymbol{p}\|^2 + \alpha^2\|\boldsymbol{C}\Delta\boldsymbol{p}\|^2 \tag{5}$$

where α is the degree of constrain and $\boldsymbol{C}$ is the matrix providing the constraint. Minimizing U in Equation (5) produces a system of linear equations in the normal equation form:

$$[\boldsymbol{A}^T\boldsymbol{A} + \alpha^2\boldsymbol{C}^T\boldsymbol{C}]\Delta\boldsymbol{p} = \boldsymbol{A}^T\Delta\boldsymbol{d} \tag{6}$$

The vector $\Delta\boldsymbol{p}$ is added to the initial vector $\boldsymbol{p}_0$ to obtain the updated parameters. In this chapter, $\boldsymbol{C}$ is the Laplacian filter (Lytle and Dines, 1980) and α is chosen such that

$$\mathrm{AIC} = -2\ln U + 2l \tag{7}$$

is minimized (Sugimoto, 1987), where AIC is the Akaike's Information Criterion (Akaike, 1974), and l is the number of independently adjusted parameters.

To estimate a resistivity change, we generally obtain two resistivity distributions from apparent resistivity data observed before and after the change, and then calculate the resistivity change ratio (RCR) between the two distributions. However, this approach may not give an accurate resistivity change due to the different noise levels at each measurement and the different convergence levels at each inversion. To reduce these influences, LaBrecque and Yang (2001) presented the difference inversion and Daily et al. (2004) described ratio inversion. Sasaki et al. (1985) proposed a method to obtain a resistivity change by directly inverting a change ratio of apparent resistivity data using a linearized model, which describes the relationship between changes in earth resistivity and apparent resistivity. Sugimoto (1995) improved this method by considering the non-linearity of the resistivity change. Sugimoto (1995) used normalized apparent resistivity data $\boldsymbol{d}_a^{\mathrm{nor}}$ to evaluate RCR:

$$d_{a,i}^{\mathrm{nor}} = \frac{d_{a,i}^{\mathrm{obs}}}{d_{b,i}^{\mathrm{obs}}} d_{b,i}^{\mathrm{cal}} \quad (i = 1, \cdots, N) \tag{8}$$

where $d_{b,i}^{\mathrm{obs}}$ and $d_{a,i}^{\mathrm{obs}}$ are the apparent resistivity values observed before and after the change, respectively, $d_{b,i}^{\mathrm{cal}}$ is the apparent resistivity calculated for the initial model $\boldsymbol{p}_b$ and N is the number of observation data. Let G be the inversion operator represented by Equation (5), the initial model parameter $\boldsymbol{p}_b$ is then derived from the apparent resistivity data observed before the change $\boldsymbol{d}_b^{\mathrm{obs}}$ by

$$\mathbf{p}_b = \mathrm{G}\left(\mathbf{d}_b^{\mathrm{obs}}\right) \tag{9}$$

Then the RCR after the change is expressed as

$$r_{a,j} = \frac{p_{a,j}^{\mathrm{nor}} - p_{b,j}}{p_{b,j}} \times 100\ (\%)\ (j = 1, \cdots, M) \tag{10}$$

with

$$\boldsymbol{p}_a^{\mathrm{nor}} = G(\boldsymbol{d}_a^{\mathrm{nor}}) \tag{11}$$

where $r_{a,j}$ is the RCR, M is the number of unknown parameters, $p_{b,j}$ is the parameter before the change, and $p_{a,j}^{\mathrm{nor}}$ is the parameter derived from normalised apparent resistivity data $\boldsymbol{d}_a^{nor}$. The resistivity inversion may be highly stabilised by

restricting the updating direction of the model parameters. In this process, we hypothesize that the resistivity after the injection of lime water will be lower than the initial resistivity, because the resistivity is expected to decrease as lime water infiltrates the crack. As the crack becomes saturated, the porosity decreases as the lime water fills the crack, and pore-water resistivity increases with low-resistivity lime water infiltration.

2.2.3 Two-dimensional resistivity survey

A resistivity survey induces electrical current between two electrodes and measures electrical potential between two other electrodes. Because the electrical potential is influenced by the resistivity structure of the ground, the resistivity of the geological structure is derived by changing the pair of the current and potential electrodes. **Figure 3 (a)** illustrates the 3D resistivity survey (Sasaki, 1994), where electrodes are arranged on the surface and the current and potential electrodes are positioned along not only one line, but also different lines. Although the 3D resistivity survey can obtain a large amount of 3D data, it is costly to place the survey lines, and obtaining data is time consuming. On the other hand, the 2D resistivity survey, as shown in **Fig.3 (b)**, can reduce the time or cost, because the electrodes are placed only along the line and a 2D inversion is conducted on the assumption that the resistivity is constant in a direction orthogonal to the analyzed cross section. However, when the resistivity structure of the target is not in 2D, artifacts (resistivity anomalies) often appear in the cross section (Sasaki, 1993). In these cases, a 3D inversion of 2D resistivity survey data is conducted (Nakazato et al., 2009). However, it is time consuming to create a 3D inversion model and to calculate the electrical potential. The estimate from the 2D inversion can produce a result faster than the 3D inversion.

When the electrical potential is calculated from FEM, a 2D inversion (Coggon, 1971) reduces the calculation time. However, a 2D inversion often produces artifacts of resistivity, even if the structure of the crack is almost two dimensional and the survey line is orthogonal to the crack. The reason for this is because the crack length is limited and it does not meet the assumption of 2D inversion. On the other hand, the estimated crack depth depends on the degree of 2D of the crack and the degree corresponds to the crack length. Therefore, it is efficient to estimate the crack depth after estimating the crack length. The proposed method aims to simply estimate the range of the crack using 2D resistivity inversion. In this method, two survey lines, one parallel and one orthogonal to the crack as shown in **Fig.1**, are used and the range of the crack is estimated from each 2D resistivity survey.

2.3 Numerical experiment

2.3.1 Method

We conducted a numerical experiment to investigate the applicability of this method to models with different depths and lengths. **Figure 4** illustrates a FEM mesh and resistivity model. Tetrahedron elements are FEM meshes, and hexahedron grids are inversion resistivity. The smallest size of a tetrahedron element is a quarter of the size of the smallest interval of electrodes. The FEM mesh is divided more roughly according to the distance from an electrode using the Delaunay triangulation (Sugimoto and Hishiya, 1993). The number of elements and nodes are 730,947 and 119,283, respectively. The grid size of the hexahedron is the smallest interval of electrodes within the survey lines and the number of the grid is 21 × 28 × 15 = 8,820. The ground model before the injection of limewater is a half-space resistivity distribution of 100 Ωm, and the ground models after the injection are 16 resistivity models that have a 10 Ωm conductive body in the homogeneous resistivity. The conductive bodies in each model have a plate with a width of

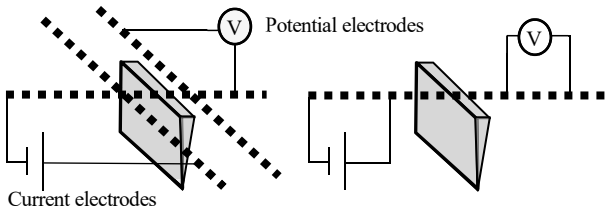

(a) 3D resistivity survey.　(b) 2D resistivity survey.

Fig.3 Comparison between 3D and 2D resistivity surveys.

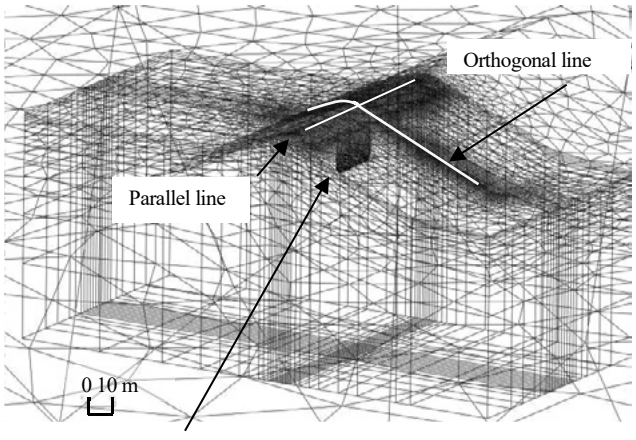

Injected lime water model (10 Ωm)　Homogeneous half-space model (100 Ωm)

Fig.4 FEM mesh incorporating the resistivity model in the numerical experiment (after injection of lime water).

Table 1 Configuration of each resistivity profiles in the numerical experiment.

Number of electrodes	43
Interval of electrodes	2 m
Length of survey line	84 m
Number of measurements	495
Array	modified pole-pole array

1 meter (m). They have four depths of 3, 6, 12 and 24 m, and four lengths of 4, 8, 12 and 24 m. The conductive body extending down under the parallel survey line in **Fig.4** is the model of injecting lime water. Since the width which a resistivity survey can detect depends on the smallest interval of the electrodes, a thin anomaly is difficult to detect because the interval of the electrodes is limited. However, because the lime water infiltrates around the crack, the width of the conductive body is set to be half of the smallest interval of the electrodes.

Synthetic observation data for the numerical experiment was obtained using a 3D FEM with survey lines that were both parallel and orthogonal to the crack. A Dirichlet boundary condition was applied to the current electrodes,

$$V = \bar{V} \tag{12}$$

a Neumann boundary condition was applied to the surface, where the flux of electrical current is zero,

$$\frac{\partial V}{\partial n} = 0 \tag{13}$$

and a mixed boundary condition was applied to the other boundary (Dey and Morrison, 1979), where the electrical current is a portion of V,

$$\frac{\partial V}{\partial n} + \frac{\cos\gamma}{r} V = 0 \tag{14}$$

where r is distance from the electrical current's point source to the boundary point, and γ is the angle between the distance r and the outward normal vector n.

Table 1 shows the synthetic observation data in the numerical experiment. The parallel survey line was placed at a distance of 2 m from the crack, which was the smallest interval of electrodes. The synthetic observation data was calculated using a 3D FEM and inversion program entitled "E-Tomo 3D" (Sugimoto and Inoue, 1998). The electrode arrangement was a modified pole-pole array in which remote electrodes were placed at the end of each survey line.

The change in resistivity were obtained from a resistivity distribution derived from a 2D inversion of the synthetic data. The number of measurements and the number of unknown parameters are 495 and 1,456, respectively. A 2D inversion program entitled "E-Tomo ver. 4.1" (Sugimoto et al., 1995) was used for the 2D inversion.

2.3.2 Results

Figure 5 illustrates resistivity changes from the survey line that is parallel to the crack. The decreased resistivity zone spreads in the direction of the crack length. The horizontal range of a resistivity change of more than −5% corresponds to the crack length. **Figure 6** plots the estimated

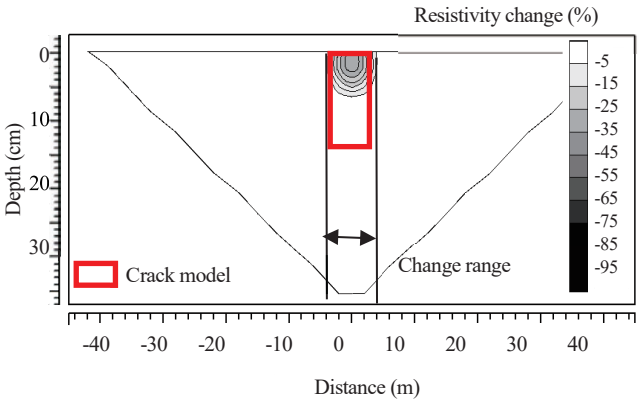

(a) Crack depth of 12 m and crack length of 8 m.

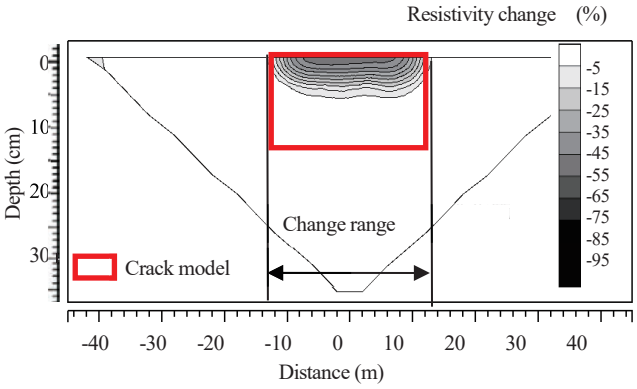

(b) Crack depth of 12 m and crack length of 24 m.

Fig.5 Cross sections of resistivity change (parallel to the crack).

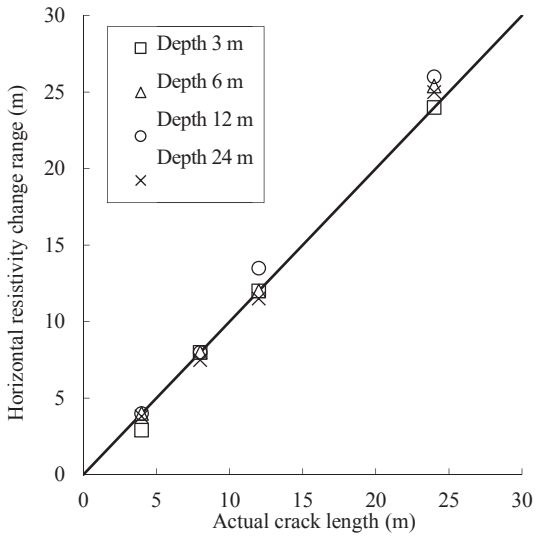

Fig.6 Estimated and actual length of crack along survey line that is parallel to the crack.

and actual length of the crack by the survey line that is parallel to the crack. The estimated length corresponds to the actual length, although some estimated length is longer than the actual one. These results indicate that the parallel survey line can detect the infiltrated range along the direction of the crack length. However, the resistivity change does not reach the bottom of the crack in **Fig.5.** It is difficult to estimate the depth of the crack from the survey line that is parallel to the crack.

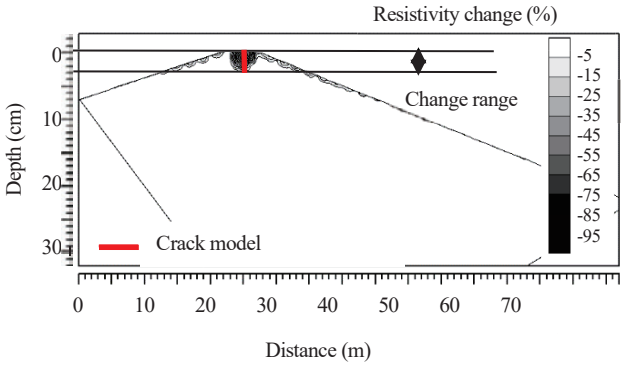

(a) Crack depth of 3 m and crack length of 12 m.

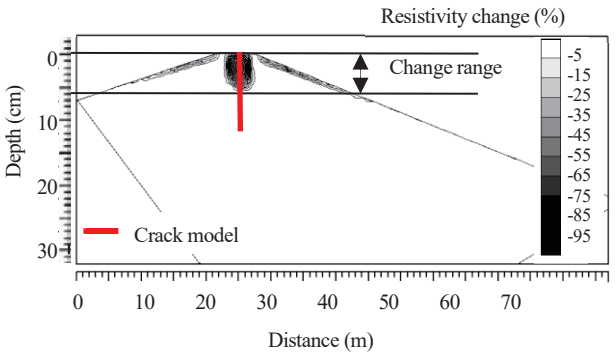

(b) Crack depth of 12 m and crack length of 12 m.

Fig.7 Cross sections of resistivity change (orthogonal to the crack).

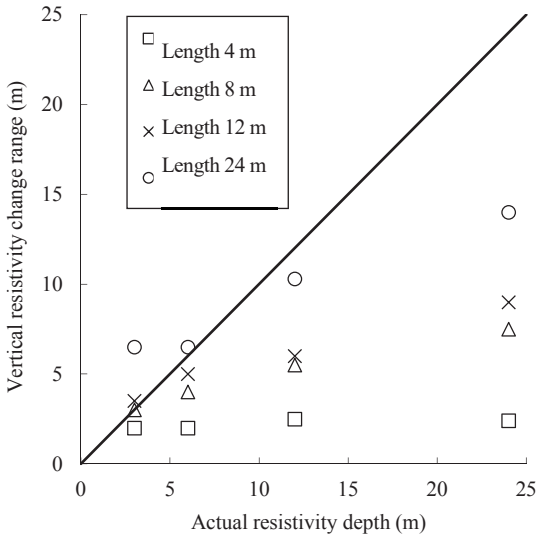

Fig.8 Estimated and actual depth of crack along the survey line that is orthogonal to the crack.

Figure 7 illustrates resistivity changes from the survey line that is orthogonal to the crack. The resistivity decreases around the crack and the decreased zone is deeper as the crack deepens. **Figure 8** plots the estimated and actual depth of the crack by the survey line that is orthogonal to the crack. The estimated depth is less than the actual depth as the crack depth becomes longer with the crack length. However, when the crack depth is less than half of the crack length, the estimated depths correspond to the actual depths. This relation indicates that an orthogonal survey line can estimate the infiltrated range on the vertical direction when the crack length is sufficiently longer than the crack depth. This relation also indicates that when the resistivity structure becomes more two dimensional, it matches with the assumption of 2D inversion.

In **Fig.8**, the estimated depth of the model with 24 m length and 3 m depth is the same as the model with 24 m length and 6 m depth. This means that the accuracy is low for the model with 24 m length and 3 m depth. **Figure 9**

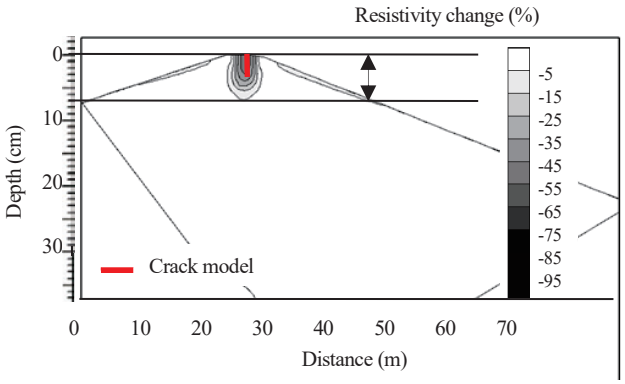

(a) Crack depth of 3 m and crack length of 24 m.

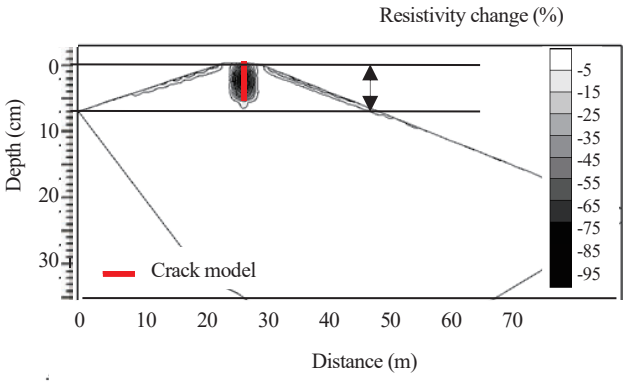

(b) Crack depth of 6 m and crack length of 24 m.

Fig.9 Cross sections of resistivity change (orthogonal to the crack).

Table 2 Properties of cracks produced for field experiment.

	Vertical	vertical	inclining
Length (cm)	60	30	60, 120
Depth (cm)	25, 50	25, 50	40
Width (cm)	1.5	1.5	1.5
Way to produce	iron plate	continuous wall	continuous wall
Survey line	orthogonal	orthogonal	parallel

compares the results of these models. The resistivity changes of the model with 3 m depth in **Fig.9 (a)** is smaller than that of the model with 6 m depth in **Fig.9 (b)**, and the zone where the resistivity decreased drastically is around 3 m depth. In this study, the threshold for estimation of the crack depth is −5%, and these factors caused the result shown in **Fig.8**. In future studies, the threshold for estimation of crack depth should be investigated.

2.4 Field experiment

2.4.1 Method

To investigate the applicability of this method to a crack in soil, a field experiment was conducted. The site was in an experimental field at the Institute for rural engineering, part of the National Agriculture and Food Research Organization. The geology of subsurface was homogeneous. An iron plate of 1.5 cm width and 60 cm length was buried at different depth and then pulled up to produce cracks of 25 and 50 cm depth. Electrodes of 1.5 cm diameter was also buried straight into soil and then pulled up to produce vertical cracks of 30 cm length, and 25 and 50 cm depth, and the electrodes was buried diagonally into soil and then pulled up to produce diagonal cracks of 60 and 120 cm length (vertical:horizontal = 40 cm:30 cm). **Table 2** identifies the properties of these cracks produced for the field experiment, and the injected lime water was 1 Ωm (water:lime = 2 :1) (Inoue et al., 2010).

Before and after the injection of the lime water, 2D resistivity surveys were conducted on the survey line that was orthogonal to the vertical cracks and on the survey line that was parallel to the diagonal crack, which were inclined apart from the survey line. The reason we used the parallel survey line only for the diagonal crack was to investigate the applicability of this method to severe conditions, because the farther the survey line is from the crack, the more difficult it is to obtain the information. The parallel survey line was placed at the distance of 10 cm from the crack, which was the smallest interval between electrodes. The electrodes were stainless steel nails of 2 mm diameter and 5 cm length. The electrode arrangement was a modified pole-pole array. A resistivity survey equipment entitled “Profiler-4”, manufactured by OYO Corporation, was used for the measurement.

The 2D resistivity distribution was derived from the 2D inversion of resistivity survey data. **Figure 10 (a)** illustrates the FEM mesh used to calculate electrical potentials. The Dirichlet boundary condition shown in Equation (12) was used at the current electrodes, the Neumann boundary condition show in Equation (13) was used at surface, and the mixed boundary condition shown in Equation (14) was used for the other boundary. **Figure 10(b)** illustrates the resistivity grid derived in the inversion. The numbers of measurements and unknown parameters were 312 and 1,567, respectively. E-Tomo ver. 4.1 was used for the inversion of resistivity. In each case, number of the iterations was 10, and the residuals were less than 4%.

2.4.2 Results

Figure 11 illustrates the change in resistivity derived from the survey line that was parallel to the crack. The vertically decreased resistivity zone reached less than 30 cm depth in **Fig.11 (b)** although the depth of the crack was 40 cm. The horizontally decreased resistivity zone reached the same range with the actual crack length, although some resistivity changes were beyond the actual crack length. **Figure 11**

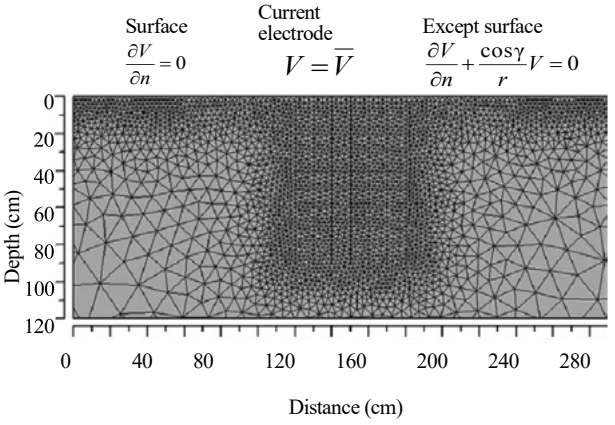

(a) FEM mesh.

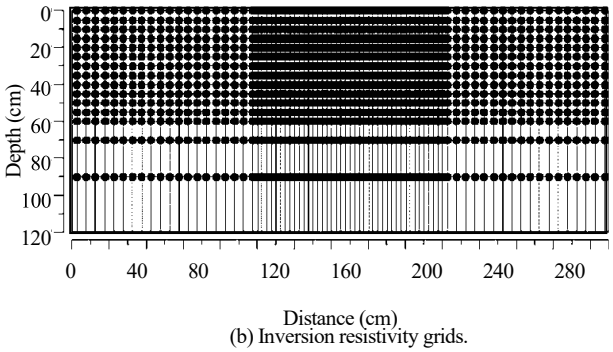

(b) Inversion resistivity grids.

Fig.10 FEM mesh and inversion resistivity grid.

shows the results of the inclined crack, which was located away from the survey line. Although the inclined crack is more difficult to detect than the vertical crack, the results of the survey line that was parallel to the crack can estimate the crack length. At a real disaster site, although it may be difficult to observe the spreading of a crack from the surface, lime water injected to the limited crack could infiltrate along the direction of the crack length. To estimate the direction of crack length from the surface, a survey line that is parallel to the crack would be effective.

Figures 12 and **13** show the resistivity distribution and the resistivity change using the survey line that is orthogonal to the crack. **Figure 12** presents the resistivity derived from the orthogonal survey line to the crack with a length of 60 cm. **Figures 12 (a)** and **(b)** illustrate the resistivity of the cracks at 25 and 50 cm depth before the injection of lime water. The resistivity near the surface is more than 1,000 Ωm around the crack. Because the porosity of the crack is high, the resistivity of the crack is also high. The high resistivity zone does not reach the bottom of the actual crack depth, although the result depends on the crack depth.

Figures 12 (c) and **(d)** illustrate the resistivity after the injection of the lime water. The high resistivity zone of 1,000 Ωm near the surface seen in **Figs.12 (a)** and **(b)** disappears. This may indicate that a low-resistivity zone spread down to 80 cm depth. However, it is difficult to estimate the crack depth from these results. Although a low-

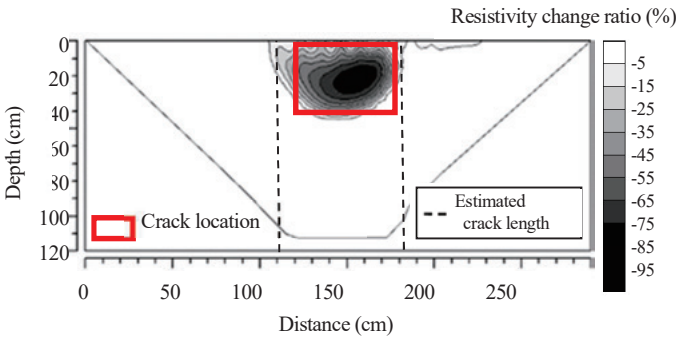

(a) Crack length of 60 cm.

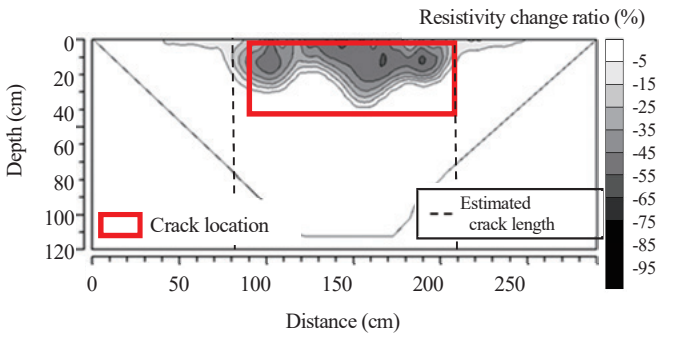

(b) Crack length of 120 cm.

Fig.11 Cross sections of resistivity change for the survey line that was parallel to the crack (inclined crack, vertical:horizontal = 40 cm:30 cm).

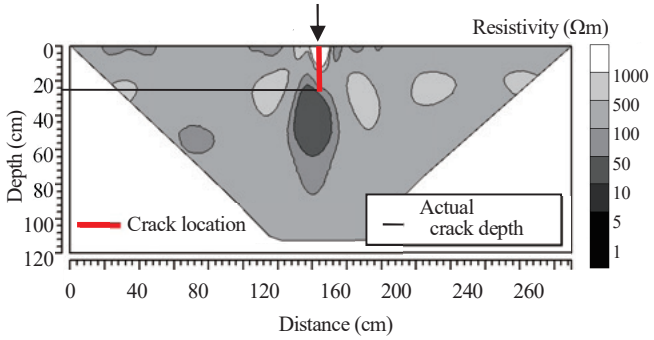

(a) Before injection (crack depth of 25 cm).

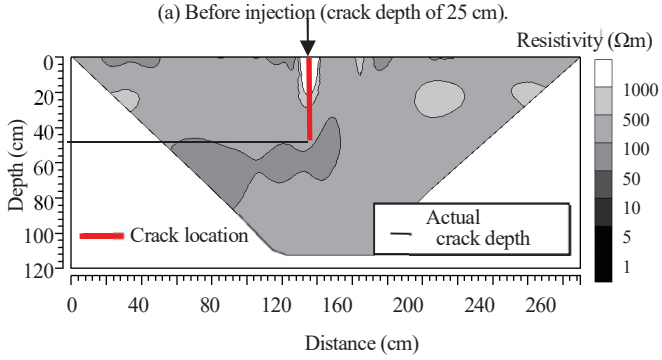

(b) Before injection (crack depth of 50 cm).

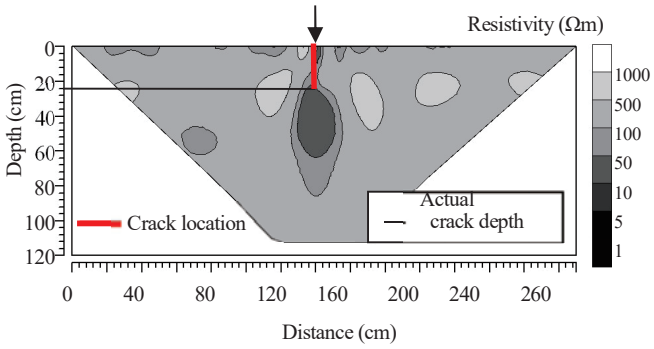

(c) After injection (crack depth of 25 cm).

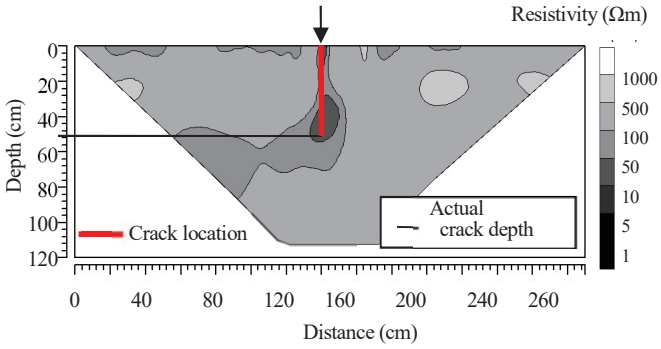

(d) After injection (crack depth of 50 cm).

Fig.12 Cross sections of resistivity along the survey line that was orthogonal to the crack (crack length of 60 cm).

resistivity zone was calculated under the crack in **Figs.12 (a)** and **(c)**, no low-resistivity zone was calculated in **Fig.12 (b),** which may indicate a difference in the degree of compaction when the crack was backfilled. Because resistivity varies from many factors, it is difficult to judge the ground conditions only on the basis of the resistivity cross sections.

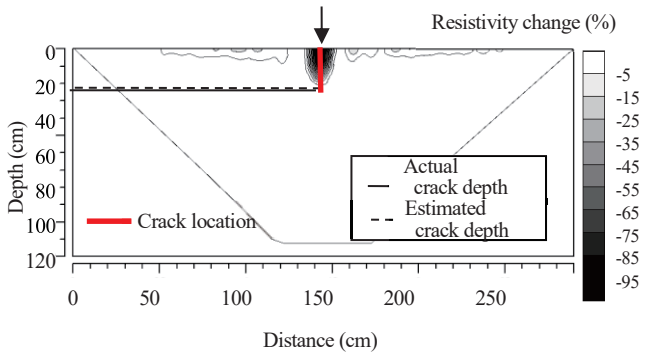

(a) Crack length of 60 cm and crack depth of 25 cm.

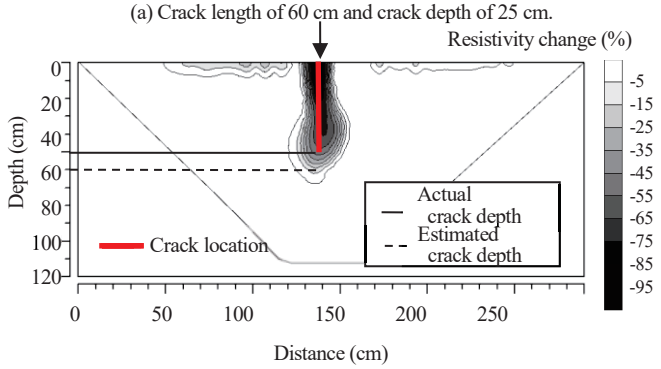

(b) Crack length of 60 cm and crack depth of 50 cm.

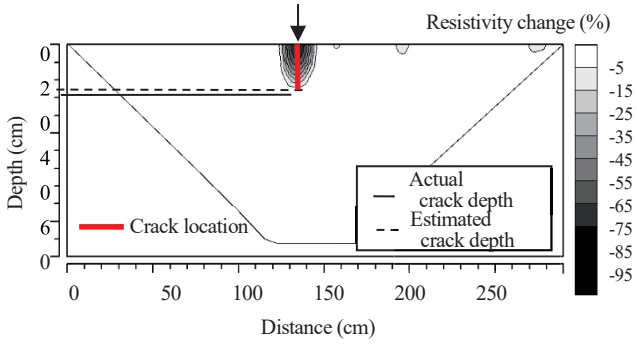

(c) Crack length of 30 cm and crack depth of 25 cm.

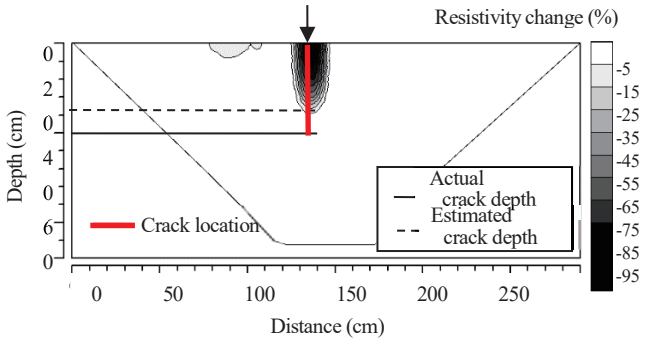

(d) Crack length of 30 cm and crack depth of 50 cm.

Fig.13 Cross sections of resistivity change along the survey line that was orthogonal to the crack.

Figure 13 shows the changes in resistivity derived from the survey line that is orthogonal to the crack after the injection of lime water. **Figures 13 (a)** and **(b)** illustrate the resistivity changes from **Figs.12 (c)** and **(d)** against the resistivity from **Figs.12 (a)** and **(b)** with the crack depth of 60 cm. The resistivity around the crack decreased and the vertical change in resistivity corresponded to the crack depth. These results indicate that resistivity change distribution is more effective than the resistivity distributions to estimate the crack depth. **Figures 13 (c)** and **(d)** show the result at half the crack length of 30 cm. Although the resistivity around the crack decreased, the resistivity in **Fig.13 (d)** decreased down to shallower range than the actual depth. As shown in **Figs.13 (a), (b)** and **(c)**, when the crack length is longer than the crack depth, the resistivity change reaches the crack depth. However, as shown in **Fig.13 (d)**, when the crack length is shorter than the crack depth, the range of the resistivity change is a shallower than the actual crack depth. Attention must be paid to the fact that the crack depth can be underestimated when the crack depth is longer than the crack length.

Figure 14 shows a cross section excavated orthogonally to the crack after the field experiment. Although the buried depths of the iron plate were 30 and 60 cm, lime water was filled to depths of 25 and 50 cm and the maximum width was 1.5 cm. There is a possibility that the decreased resistivity zones spread beyond the crack filled with the lime, because the lime water can infiltrate through the porosity of the soil. Apparent resistivities were measured along the cross section in a direction that was orthogonal to the crack shown in **Fig.15**. A Wenner array with a 1-cm interval of electrodes was used to measure the apparent resistivity, because a Wenner array produces the average resistivity around the electrodes and the apparent resistivity is almost the resistivity of the excavated wall when the interval of electrodes is small. **Table 3** shows the apparent resistivity. Although the zones filled with the lime indicate low resistivity, the zones located 10 cm from the crack indicate high resistivity. However, the location filled with lime of No.3 indicated high resistivity, which may be because the crack is narrow. Therefore, in this experiment, the only zone filled with lime indicated low resistivity.

2.5 Conclusions

This chapter described a method to simply estimate the range of crack induced by an earthquake. This method involves injection of lime water into the crack, and deriving

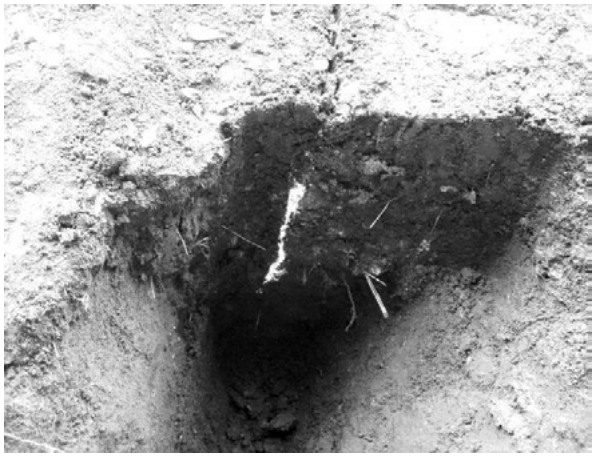

(a) Crack depth of 25 cm.

(b) Crack depth of 50 cm.

Fig.14 Cracks and injected lime water along the cross section.

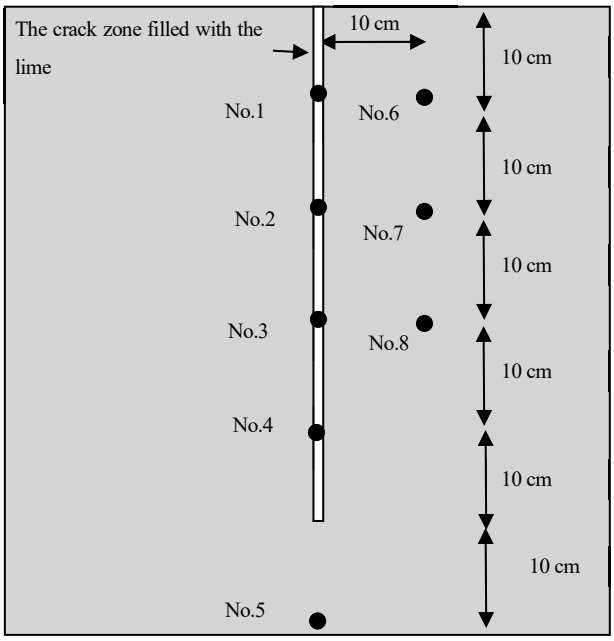

Fig.15 Measurement points for apparent resistivity along the cross section.

Table 3 Apparent resistivity measured along the cross section.

No.	Apparent resistivity (Ωm)
1	6.02
2	6.39
3	34.02
4	3.25
5	99.70
6	95.10
7	114.30
8	107.65

resistivity change from 2D resistivity surveys conducted before and after the injection. The crack depth is then estimated according to the crack length. The applicability of the method to numerical and field experiments was investigated and the following findings were demonstrated.

1. The numerical experiment indicated that the survey line that was parallel to the crack produces a resistivity change whose horizontal range corresponds to the crack length. The survey line parallel to the crack can estimate the range of the lime water injected in the direction of the crack length. In actual disaster sites, although it is difficult to detect the crack from the surface, injection of limewater even from a limited location can estimate the range on the direction of the crack length.
2. In the survey line orthogonal to the crack, the correlation between the estimated and actual depths decrease when the crack depth is larger than the crack length. When the crack depth is smaller than the crack length, a correlation exists between the estimated crack depth and the range of lime water injected in the direction of the crack depth.
3. The field experiment showed that by using the survey line parallel to the crack, the horizontal range of resistivity change corresponds to the crack length filled with lime. By using the survey line orthogonal to the crack, the vertical range of resistivity change corresponds to the crack depth filled with lime in case when the crack depth is less than half of the crack length.
4. The lime water may possibly infiltrate around the crack. However, in this experiment, all zones except the crack zone filled with lime indicate high resistivity.

Thus, we can estimate the range infiltrated with lime water using 2D inversion of 2D resistivity survey data by c onsidering the characteristics of resistivity distribution of 2D inversion with different line arrangements. However, it is difficult to detect the crack under the water table where the

injected lime water does not infiltrate. Additional considerations are needed when the survey line crosses the crack diagonally or the crack width is less than 0.1 times the electrode interval. This chapter showed results for crack widths of 0.1 – 0.5 times the electrode interval. In this experiment, artificial cracks of simple structure were used to investigate basic property of the proposed method. In actual disaster sites, however, the crack shape and the ground condition around the crack vary. Moreover, the injected liquid can infiltr ate around the crack and the resistivity may change temporally. Therefore, various possibilities of cracks must be investigated in the disaster site and a method needs to be developed to monitor the time-lapse resistivity change in future.

3. Semi 3D resistivity monitoring of groundwater recharge using 2D difference inversions

In the preceding chapter, we described a method to estimate the extent of the crack in soil, where the crack can be observed from the surface. However, in paddy fields that exhibit water leakage, locations of infiltration cannot be observed from the surface and the location has to be estimated. Although 2D inversion can provide artifacts, the 2D resistivity survey data include 3D information of the resistivity structure. When the survey line is properly arranged, the semi 3D structure of resistivity can be estimated.

This chapter describes a method to monitor semi 3D water flow using 2D inversions of 2D resistivity survey data with four traverse survey lines at a groundwater recharge experimental site. The resistivity change ratio distributions are derived from 2D difference inversion to make 3D soil water flows easily visible.

3.1 Introduction

Many methods have been applied to estimate changes in soil water or groundwater. These methods include time-lapse resistivity surveys, i.e., an extension of 1D resistivity surveys (Takakura, 1991; Ushijima, 1997), comparisons of 2D apparent resistivity (Inoue, 1988; Takeuchi and Nagae, 1990; Wada at el.,1995; Suga, 2004), and comparisons of 2D inverted resistivity (Sasaki et al., 1985; Sugimoto, 1995, Suzuki, 1997; Suzuki et al., 2002; Nakazato et al., 2003; Inoue et al., 2006). For time-lapse inversion, Sugimoto (1995, 2002) demonstrated that artifacts arise from data noise and the different convergences at each iteration. He proposed a difference inversion method to reduce their impact. Nakazato et al. (2003) applied the difference inversion to 2D resistivity survey data using multi-channel resistivity survey equipment. They were able to image hourly soil water flow in an unsaturated gravel layer. However, they demonstrated the limitations of 2D inversion when estimating a 3D groundwater flow from a point source. Resistivity monitoring using a 3D resistivity survey is a best approach to the estimation of 3D phenomena. However, 3D resistivity surveys require the large amount of measuring equipment, extend the time needed for one cycle of measurement, and reduce the time resolution. Although Nakazato et al. (2003) used two orthogonal survey lines, four traverse survey lines are expected to be effective in the estimation of 3D ground water flow. If the characteristics of resistivity derived from the multi survey lines can be estimated, we can reduce the limitations of 2D inversion for the estimation of the 3D phenomenon.

The goal of this chapter is to develop a method to estimate a semi 3D water flow using 2D inversion of 2D resistivity survey data with multi survey lines to reduce the measurement and calculation costs. We conduct 2D resistivity surveys of four traverse survey lines at a groundwater recharge experiment site on a pyroclastic Plateau. Changes in resistivity before and during the recharge were derived from the 2D difference inversion. A semi 3D representation of groundwater recharge including vertical and horizontal water flows is created.

3.2 Methods

3.2.1 Site description

A recharge experiment and 2D resistivity surveys were conducted on a pyroclastic plateau. The survey area is test site of the Kagoshima Prefectural Institute for Agricultural Development, Osumi Branch. **Figure 16** illustrates the location of the survey area and geological map. The site is located on Kasanohara Plateau, between Kimotsuki and Kushira rivers at the center of Osumi Peninsula in Kagoshima prefecture (**Fig.16**). The Kasanohara Plateau is composed of the Ito pyroclastic flow deposits erupted by the Aira caldera some 26,000 - 29,000 years ago (Machida and Arai, 2003). **Figure 17** illustrates the survey area. Four intersecting survey lines, A, B, C and D, two recharge areas, RA1 and RA2, and four boreholes, B1, B2, B3 and B4, were set up at the experiment site. The surface of the site had an elevation of 100 m, a slight northwest-to-southeast incline, and gradient of 1/63. Four boreholes were drilled to a depth of 10 m, with a diameter of 66 mm. **Figure 18** shows the logs of the four boreholes. In each borehole, the loam layer, the secondary Shirasu layer (lacustrine or marine sediments of pyroclastic origin), and the Shirasu layer (pyroclastic) were observed in order of depth. The boundaries of the subsoil

layers were expected to have the same incline as that at the surface.

Nakazato et al. (2003) estimated the horizontal water flow using 2D resistivity survey with two orthogonal survey lines. However, their results demonstrated the limitation of using 2D inversion to estimate a 3D groundwater flow from a point source that is 2 m in diameter and 3 m in depth. In the current experiment, the recharge areas RA1 and RA2 were set as the infiltrated zone under the recharge area was almost 2D structure for survey line B. For estimation of 3D soil water

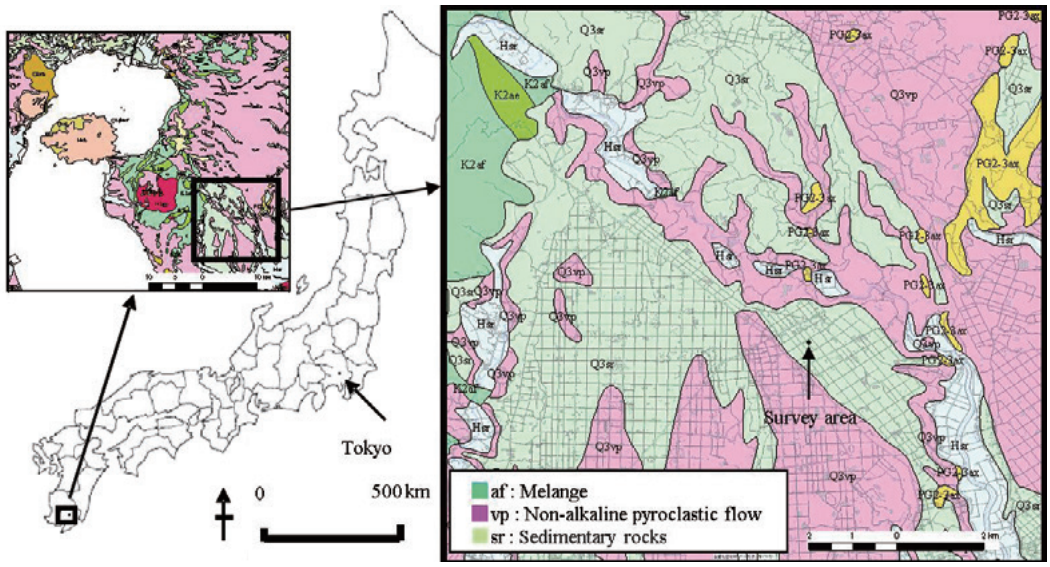

Fig.16 Location of the survey area and geological map (Geological Survey of Japan, AIST (ed.), 2014).

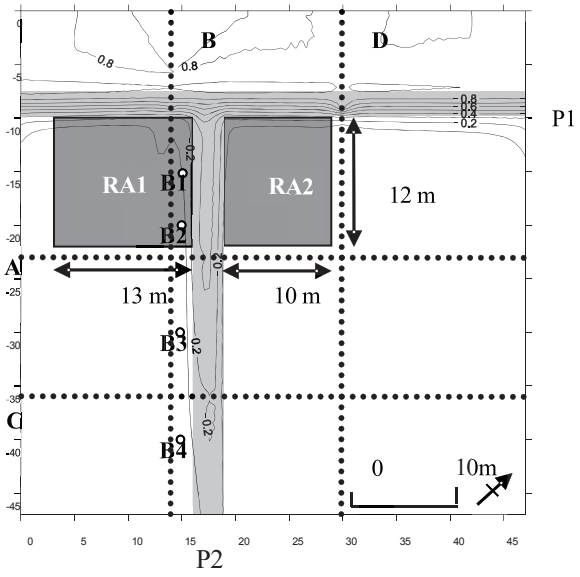

Fig.17 Survey area where the groundwater recharge experiment was conducted. Four lines A, B, C and D (black dots), four boreholes B1, B2, B3 and B4 (white dot), and two recharge areas RA1 (12 m × 13 m) and RA2 (12 m × 10 m) were set up in the area. Symbols P1 and P2 indicate the roads in the survey area.

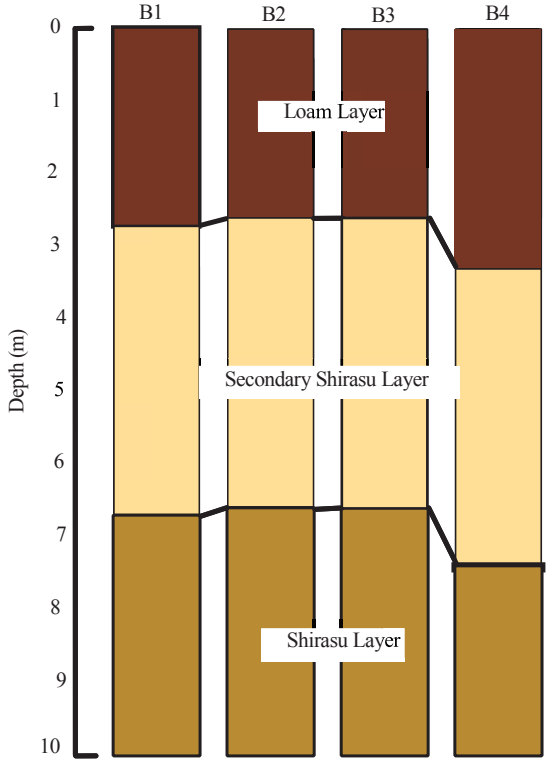

Fig.18 Logs of boreholes B1, B2, B3 and B4 shown in **Fig.17**. The loam layer, the secondary Shirasu layer (lacustrine or marine sediments of pyroclastic origin), and the Shirasu layer (pyroclastic) were observed in order of depth.

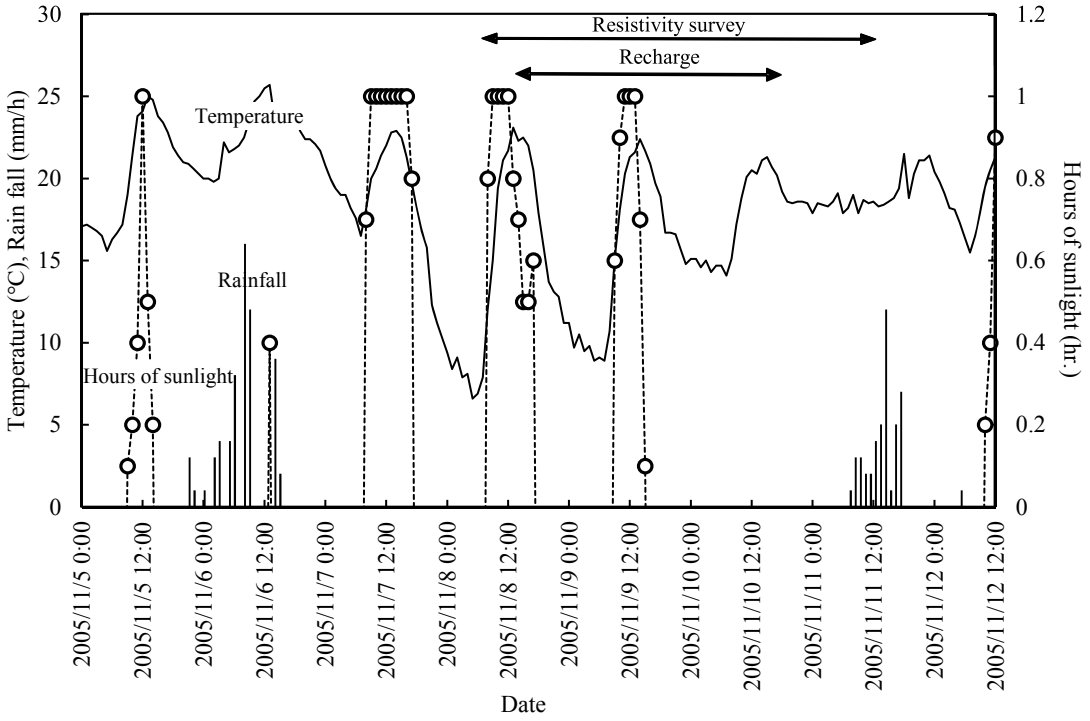

Fig.19 Temperature (°C), rainfall (mm/h) and hours of sunlight (h) observed near the survey area from November 5 to November 12, 2005 (Kanoya Magnetic Observatory).

flow, the traverse survey lines A, C and D were set to take account of the terrain and geology at the site.

Near the survey area, Inoue et al. (2004) estimated saturated hydraulic conductivity at $5.5 \times 10^{-7} - 3.1 \times 10^{-5}$ m/s in the loam layer, $1.3 - 1.7 \times 10^{-5}$ m/s in the secondary Shirasu layer and 1.3×10^{-5} m/s in the Shirasu layer. The loam layer usually has much lower hydraulic conductivity than that of the other layers. The groundwater level was estimated to be deeper than 10 m, because groundwater was not observed in any borehole in the test site before the recharge experiment. Thus, the depth of the unsaturated zone was considered to be more than 10 m. In the loam layer, it was confirmed that some clastic dikes of sands penetrate from the lower secondary Shirasu (Naruo and Kobayashi, 2002). Kubota et al. (2005) considered the dikes of sand to function as bypass that discharges soil water from the loam layer to the secondary Shirasu layer only when heavy rain occurs.

Figure 19 shows the temperature, rainfall and hours of sunlight observed at the Kanoya Magnetic Observatory near the survey area during the experiment, from November 5 to November 12, 2005. Total rainfall of 55 mm and 45 mm on November 6 and 11, 2005, but no rain during the recharge experiment was recorded. The highest temperature was 23°C and the lowest 7°C.

3.2.2 Ground water recharge experiment

The recharge water was supplied from the centres of the recharge area RA1 (12 m × 13 m) and RA2 (12 m × 10 m) shown in **Fig.17**. The recharge areas were surrounded by plastic plates buried 0.3 m in depth. Water was supplied to each recharge area at the rate of 16.0 m^3/h, and its electrical conductivity was 8.9 mS/m (119 Ωm). The duration of the recharge was 56 hr., from 13:00 on November 8 to 21:00 on November 10, 2005.

3.2.3 Tow-dimensional resistivity survey

To decide of the specifications of the 2D resistivity survey, the spatial and time resolutions were considered. Since the loam layer and the secondary Shirasu layer had a depth of 2–4 m, the interval of the electrodes for estimation of the resistivity change in the layers was set to 1 m. A dipole-dipole array was used to achieve high resolution (Takakura, 1999) and to allow a multi-channel resistivity survey to be efficiently conducted. The measuring time for each survey line was set at 1 hr. as shown in **Table 4**. The electrodes were stainless and had a length of 0.5 m and diameter of 0.01m.

Dipole-dipole resistivity surveys continued from 7:00 on November 8 to 12:00 on November 11, 2005, along the four lines shown in **Fig.17**. Each line had 48 electrodes which were arranged at an interval of 1 m. To reduce the total time of measurements, only 2D resistivity surveys were

conducted. Dipole spacings (*a*-spacings) were 1, 2, 3 and 4 m, and the maximum separations (*n*) were 8, 4, 4 and 8, respectively. A total of 698 data were collected along each line. The measurement time for one line was about 1 hr. and 4 hr. were required to complete a measurement cycle from line A to line D.

A Profiler-4 system, manufactured by OYO Corporation, was used for the resistivity measurements. It has four channels for measuring voltages. There are many resistivity measurement systems (Blome et al., 2011; Zhe et al., 2007; Imamura, 2007) that can acquire data much faster than the Profiler-4. However, as the saturated hydraulic conductivity in the study site is less than 3.1×10^{-5} m/s, it takes 4 hr. to move soil water by only 0.45 m. Therefore, 4 hr. for one cycle was considered to be fast enough, because the distance of 0.45 m is less than the electrode spacing of 1 m.

Table 4 The conditions of an 2D resistivity survey.

	one line content
Number of electrodes	48
Length of the survey	47 m
Electrode spacing	1, 2, 3, 4 m
Electrode separation index	1 – 8, 1 – 4, 1 – 4, 1– 8
Number of data	698
Electrode arrays	dipole-dipole array
Measurement times	1 hr.
Interval time of measurement	4 hr.

3.2.4 Difference inversion

Resistivity distributions were derived from the 2D inversions of the 2D resistivity survey data. E-Tomo 2D ver.4.1 (Sugimoto et al., 1995) was used for the inversions. **Figure 20** presents a schematic view of the mesh for FEM modelling, and the inversion grid. The model space was divided more roughly according to the distance from an electrode using the Delaunay triangulation (Sugimoto and Hishiya, 1993). The cell of the inversion grid in the horizontal direction is 2 m inside the survey site. The cell size also increased gradually in the vertical direction and outside the survey site. The Dirichlet boundary condition shown in Equation (12) was used at the current electrodes, the Neumann boundary condition show in Equation (13) was used at surface, and the mixed boundary condition shown in Equation (14) was used for the other boundary. Time-lapse RCR distributions during the recharge experiment was estimated using the method described in chapter 2, in which the distribution before the change was used as the initial state and the normalized apparent resistivity was inverted rather than the measured apparent resistivity itself. The resistivity after the recharge experiment started was maintained lower than the initial resistivity, based on the hypothesis that the resistivity was expected to decrease as the saturation level increased with water infiltrating. The constraint matrix shown in Equation (5) was the unit matrix, and the average apparent resistivity was used as the initial model for inversions along each survey line.

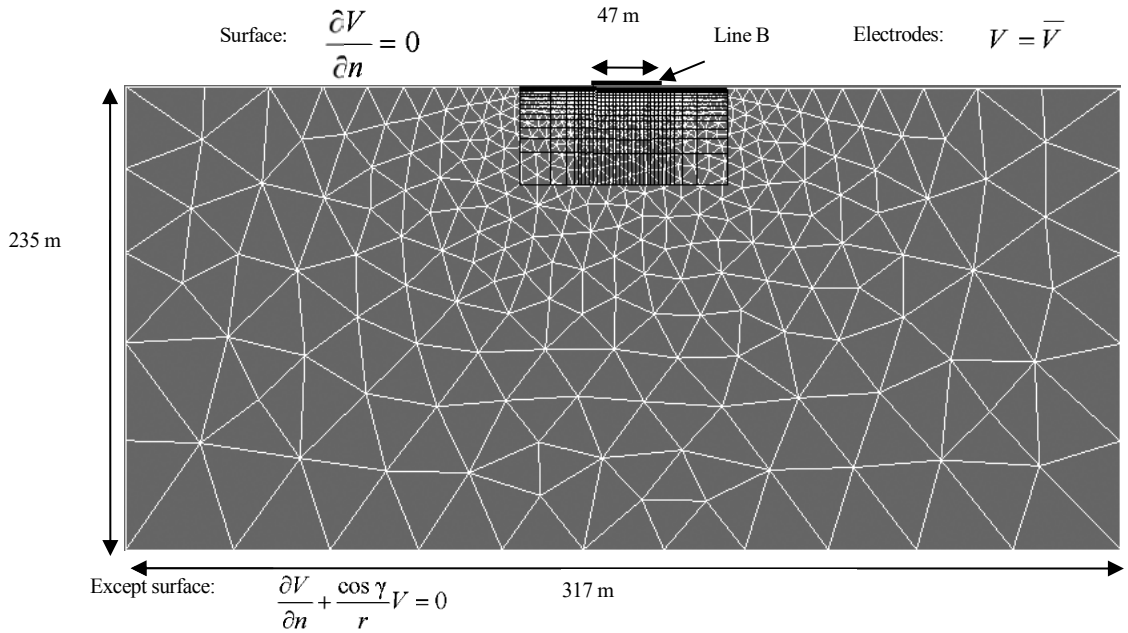

Fig.20 FEM mesh and inversion grid along line B.

3.2.5 Volumetric water content measurement

Changes in θ in the vadose zone during recharge were detected using a neutron moisture meter comprising a probe and a display. In the experiment, θ was measured periodically at borehole B1 in recharge area RA1 as shown in **Fig.21**. The probe measured the number of thermal neutrons discharge at different depths in the borehole. As the number of thermal neutrons reflects the volumetric water content, the volumetric water content can be derived from the neutron count. The measurement range was 0.3 m from the probe, and the measurement volume was averaged. The measurement at each depth was taken for approximately ten seconds. The calibration curve of Ishida et al. (2005) was used.

From the surface to 3 m depth, θ was almost constant at around 50% and little change occurred during the entire period. By contrast, at 4 – 7 m depths, θ was 20 – 25% before the experiment, 40 – 45% during the experiment, and 25 – 30% at the end of the experiment. Furthermore, θ at than 7 m was 30 – 40% before the experiment, increased by depths greater 5% during the experiment, and remained almost constant after the experiment. In particular, the period during which θ increased at 4 – 7 m depths correspond to the period of recharging.

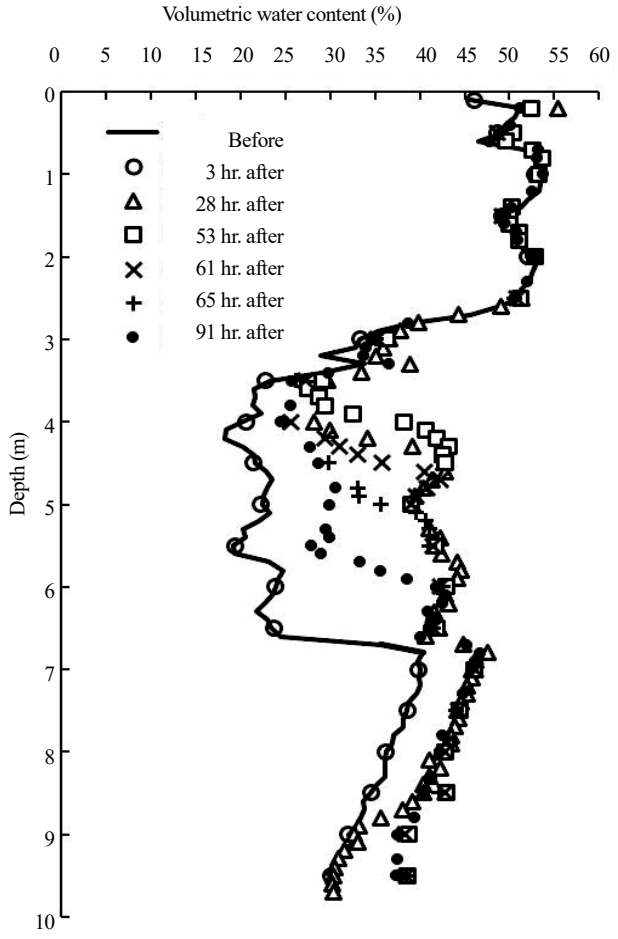

Fig.21 Volumetric water content (%) observed in borehole B1 before, during (3, 28 and 53 hr. passed), and after (61, 65 and 92 hr. passed) the recharge experiment.

3.3 Field experiment

3.3.1 The water filled range in the recharge area

Figure 22 illustrates the range that was filled with water after recharge experiment started. The gray region with a solid border is the range that was filled in the early stages of the recharge test, while the shaded region with a dotted border is the range that was filled by the end of the test. In this early stage, after the start of recharging, water did not spread in all recharge area and spread mostly near line A in RA2 and near the west corner in RA1, because the recharge area surfaces were not flat. The volume of water supplied in 1 hr. could raise the water height to more than 10 cm, if no infiltration occurs in the recharge areas. However, water did not cover the major parts of the recharge areas. This means that a large amount of water infiltrated the loam layer quickly. In a later stage, however, most parts of the recharge areas were covered with recharge water. After the end of recharging, the supplied water fully infiltrated into the loam layer within 1hr. This indicates that fast infiltration zones exist in the loam layer.

3.3.2 Resistivity distribution before the start of recharging

Figure 23 shows the resistivity distribution before recharging. The residuals of inversion at each survey line

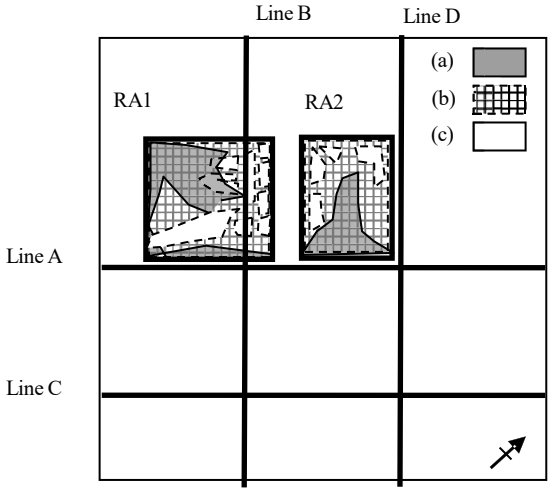

Fig.22 The range that was filled with water. (a) The gray colored region with a solid line border is the range that was filled with water at the early stage of the recharge test. (b) The shaded region with a dotted border is the range that was filled with water at the end of the recharge test. (c) The white colored region is the range that was not filled with water during the recharge test.

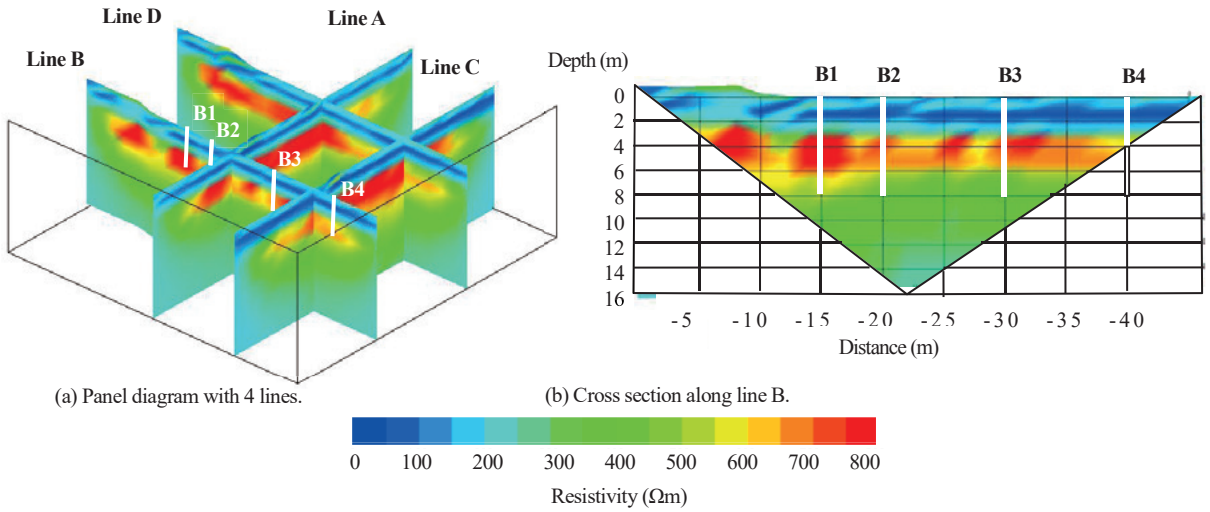

Fig.23 Inverted resistivity distribution before the recharge test. (a) Panel diagram with 4 lines. (b) Cross section along survey line B.

came close to convergence within six iterations. The residual values of 5.6, 6.6, 6.5 and 5.2 were recorded at survey lines A, B, C and D, respectively as plotted in **Fig.24**. The distributions at each survey line demonstrated a layered structure, and with a resistivity of 50–200 Ωm at depths less than 3 m, 500–800 Ωm at depths between 3 and 7 m, and 200–500 Ωm at depths greater than 7 m. The resistivity distribution along survey line B in **Fig.23** (b) corresponded to the geological structure, which were assumed the loam layer, the secondary Shirasu layer, and the Shirasu layer.

3.3.3 Resistivity change distribution after recharge

Figure 25 compares the resistivity change ratio after the recharge experiment began. Although the results for all four survey lines are shown together, the measurement times of the lines were not the same but had a delay of less than 3 hr. The inversion residuals converged to values less than 6% within six iterations.

Figure 26 shows the maximum resistivity change ratios and residuals levels of the inversions in the inverted resistivity sections along the survey lines at each time. Although the maximum resistivity change ratio along survey line C at 3 to 4 hr. after the start of recharging was less than the level of the residual, the other maximum resistivity change ratios were sufficiently large to indicate the resistivity change.

Along survey line B after the recharge started, the resistivity decreased at a depth of 4 m under the recharge area in **Fig.25 (a)**. This decrease zone spread horizontally in **Figs.25 (b)** and **(c)** and shrank after the recharge terminated in **Figs.25 (c)** and **(d)**. At the other survey lines, the resistivity change was similar to that at survey line B, although the changes at the intersections did not always correspond to each other.

3.4 Discussions

The resistivity distribution derived from survey line B before the recharge began corresponded to the geological structure observed at the boreholes being layered. The resistivity distributions from survey lines A, C and D also showed a layered structure in **Fig.23 (a)**. This suggests that the geology of the site was layered structure and almost uniform horizontally.

The panel diagram of the resistivity changes from the four survey lines after the recharge experiment started in **Fig.25** correspond to the changes in volumetric water content at different depths observed in borehole B1 as shown in **Fig.21**. These results suggested that the change in resistivity resulted

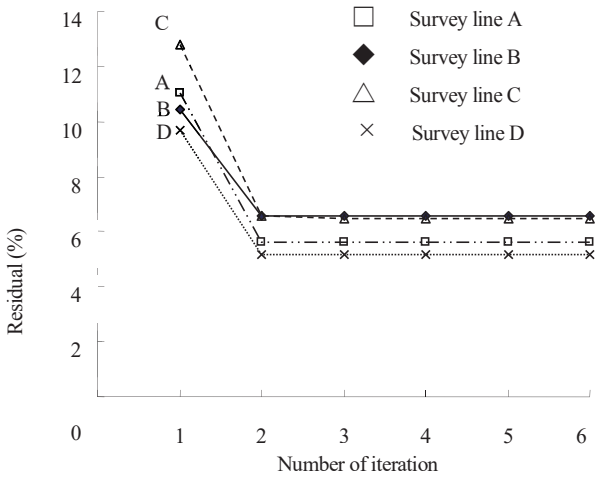

Fig.24 Residual levels at each iterations of the resistivity inversion before the recharge test started. A – D: Residual levels of the inversions of survey lines A – D.

from the recharge water changing the saturation level of the soil and reflected the water flow though the soil. The cross section along survey line B did not show resistivity changes at depths less than 4 m in **Fig.25**. This is because the change in volumetric water content was relatively small in the loam layer, as shown in **Fig.21**. The resistivity changes in the secondary Shirasu appeared earlier than the time estimated from the saturated hydraulic conductivity of the loam layer measured near the site, which was 5.5×10^{-7}–3.1×10^{-5} m/s (Inoue et al., 2004). This suggests that water infiltrated the loam layer more quickly than expected. Factors that encourage the infiltration include macro pores produced by plant root traces, or cracking by other causes.

The decreased resistivity zone that appeared beneath the recharge area after the recharge began and spread horizontally corresponded to the zone of high resistivity as shown in **Fig.23**. The recharging of soil water increased the volumetric water content mainly in the secondary Shirasu layer. This is because the hydraulic conductivity of the Shirasu layer was lower than that of the secondary Shirasu layer. As described by Kubota et al. (2007), this reduced vertical infiltration into the Shirasu layer, by slowing the recharge velocity, so that soil water spread horizontally. Inoue et al. (2004) reported the hydraulic conductivity of the Shirasu layer and the secondary Shirasu layer to be 1.3×10^{-5} m/s and 1.7×10^{-5}–1.3×10^{-4} m/s, respectively, in agreement with these results.

Figure 27 shows the resistivity change along survey lines

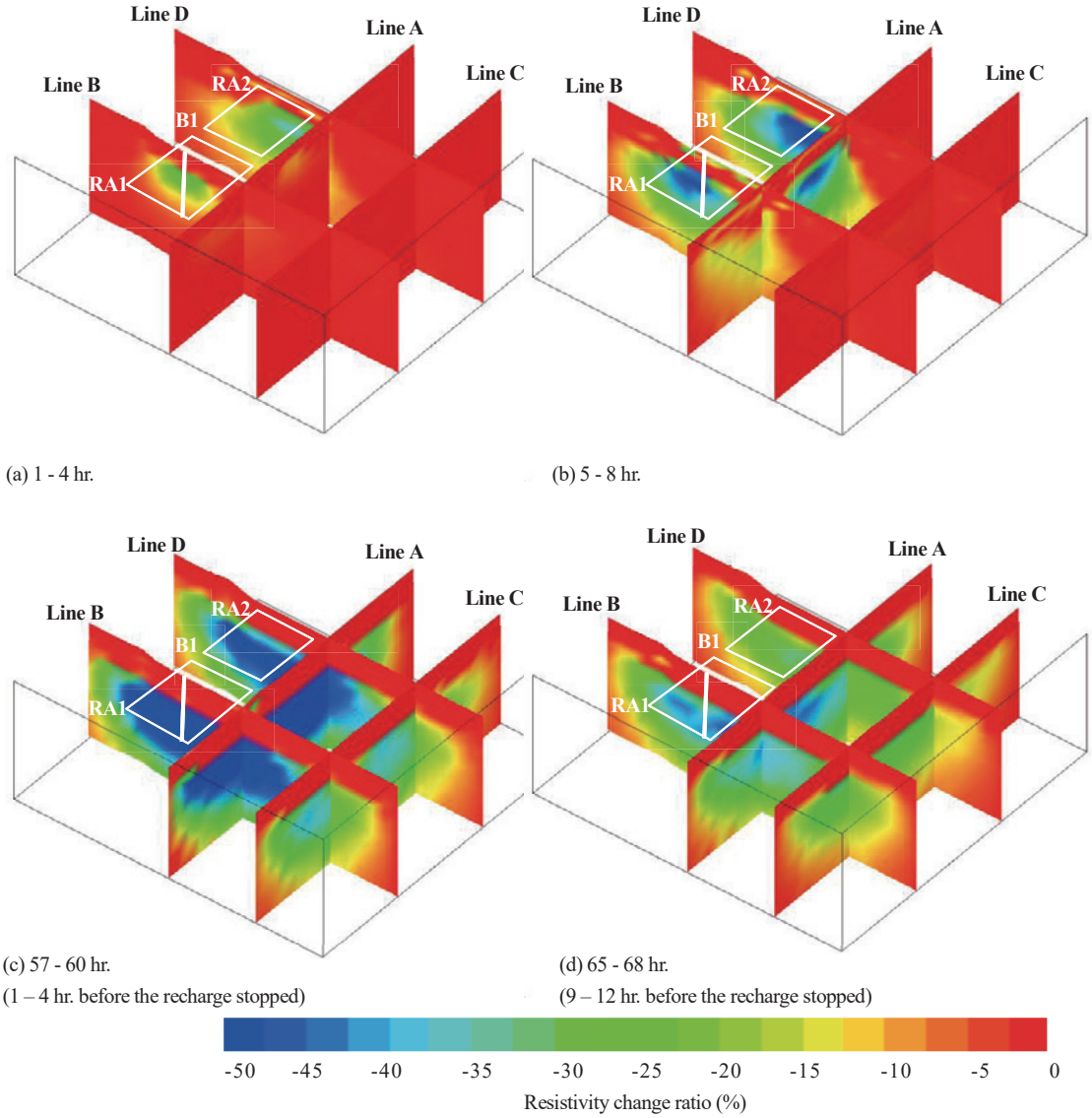

Fig.25 Distribution of the resistivity change ratio. (a) From 1 to 4 hr. after the recharge test started. (b) From 5 to 8 hr. after the recharge test started. (c) From 57 to 60 hr. after the recharge test started (From 1 to 4 hr. before the recharge test stopped). (d) From 65 to 68 hr. after the recharge test started (From 9 to 12 hr. after the recharge test stopped).

A, B and D from **Fig.25 (b)**. In **Fig.27 (a)**, resistivity decreased at a depth of 5 m beneath recharge area RA2 along survey line A, although no decrease was found beneath area RA1. This difference is because water did not cover the entire recharge area in the early stages as shown in **Fig.22**. The surface range that was filled with water in recharge area RA2 spread near survey line A, whereas the surface range that was filled with water in recharge area RA1 spread near the west corner. The different changes in resistivity reflect the difference in these water-filled ranges. Moreover, at a depth of 5 m, the center of resistivity changed at the cross section along survey line D in **Fig.27 (c)** is more near to survey line A than that along survey line B in **Fig.27 (b)**. This indicates the nonuniformity of the surface range that was filled with water. These results confirm that 2D resistivity survey can be used to model a semi 3D nonuniform surface range sequentially filled with water. However, the resistivity changes failed to correspond at the intersection of survey lines A and D, despite the almost same measurement time at each survey line. This demonstrates the difficulty of estimating a spatially continuous 3D distribution.

3.5 Conclusions

In this chapter, we described the 3D estimation of soil water flow based on resistivity changes derived from a 2D difference inversion using four traversal survey lines in a recharge experiment on the Shirasu Plateau. The conclusions are as follows.

1. Before the recharge experiment started, the resistivity distribution along boreholes reflected the geological structure. When the resistivity distributions from the other survey lines were added, the geology of the site was estimated to have a layered structure.
2. The change in resistivity matched the change in saturation level recorded in the recharge experiment. The 2D difference inversion could be used to estimate a semi 3D sequential soil water flow.
3. Preferential flows were assumed in the loam layer, because no change in volumetric water content was detected by the neutron moisture meter or from resistivity changes in the difference inversion.
4. After recharging began, a zone of decreased resistivity spread in the secondary Shirasu layer. This suggested that the soil water infiltrated vertically and then spread horizontally along this layer.
5. In the early stage of recharging, nonuniform infiltration may have occurred, because the surface range that was filled with water did not spread across the entire recharging area. The resistivity changes at the cross sections of the survey lines reflect this nonuniform filling. This confirms that 2D difference inversions from 2D resistivity survey lines can be used to detect nonuniformities in the range that was filled with water.

Our results suggest that 2D difference inversions from 2D resistivity survey data of four traversal survey lines can be

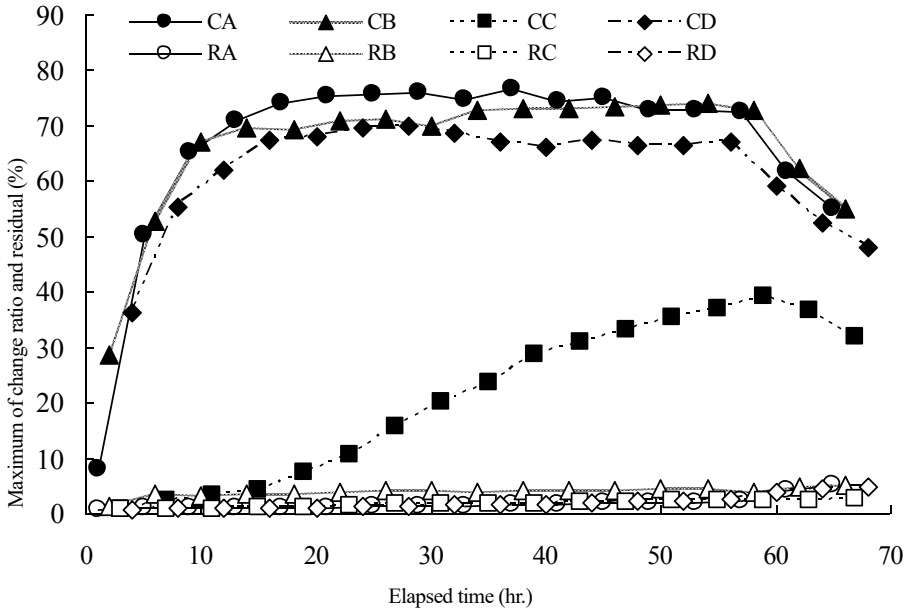

Fig.26 The maximum levels for the resistivity change ratios and residuals levels of the inversions in the inversed resistivity sections along the survey line for each time. CA – CD: Maximums levels of the resistivity change rations along lines A – D. RA – RD: Residual levels of the inversions of lines A – D.

used to estimate vertical and horizontal water flow and to three-dimensionally model nonuniform sequential recharging. This method can be used to monitor the infiltration of large amounts of water during heavy rainfall or filling water in a paddy field. However, the resistivity changes at the intersections of each survey line do not always correspond to each other, because the inversions at each survey line assume a 2D resistivity structure. Therefore, problems remain in the estimation of spatial recharging. Although this chapter showed that 3D infiltration could be estimated using 2D inversion from 2D resistivity survey data, 3D difference inversion is still needed to more precisely estimate the sequential 3D resistivity change.

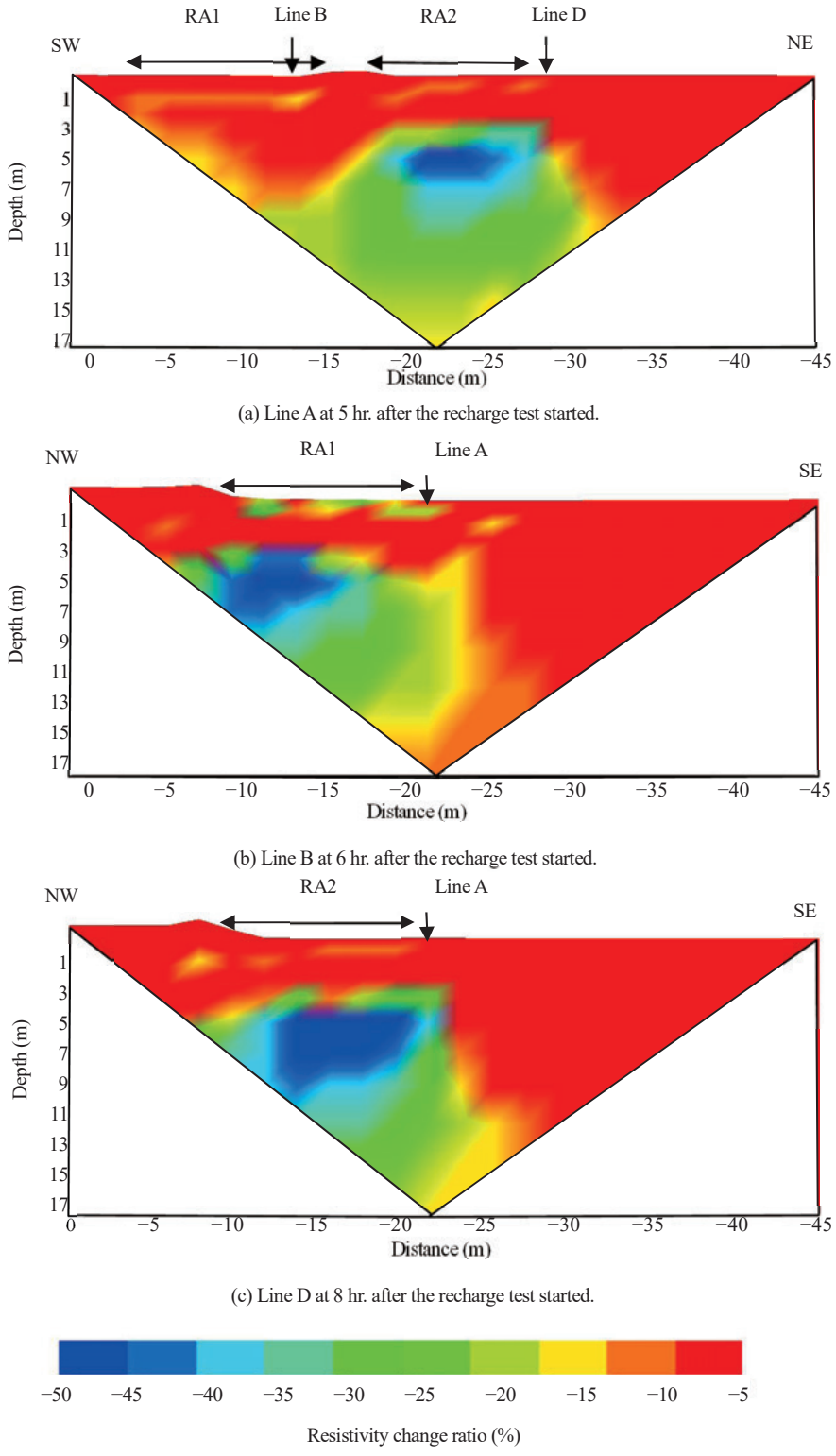

Fig.27 Distribution of the resistivity change ratio at (a) 5 hr., (b) 6 hr. and (c) 8 hr. after the recharge test started.

4. Line arrangement of 2D resistivity surveys for 3D inversion

In the preceding two chapters, we described the methods to use 2D inversion of 2D resistivity data. Although 3D inversion requires more time than 2D inversion, 3D inversion provide more precise information than 2D inversion. In this chapter and next chapter, we propose methods to use 3D inversion of 2D resistivity data.

When a 3D inversion of the 2D resistivity survey data is conducted, the arrangement of the survey line for 2D resistivity survey is also important. This effective arrangement has to be investigated.

This chapter describes numerical experiments to investigate the applicability of electrode configurations and line layouts commonly used for 2D resistivity surveys from 3D inversion. We propose effective electrode configurations and line arrangements of 2D resistivity surveys for 3D inversion. We also conduct field experiments in a loam area including a backfilled pit. Finally, we apply these electrode configurations and line arrangements to the investigation of geological structure near the Nojima Fault in Awaji Island.

4.1 Introduction

When electrodes are arranged on lines on the surface, 3D inversion of resistivity data obtained from 3D resistivity survey is the most accurate way to reconstruct a 3D resistivity distribution. In the 3D resistivity survey, the current and potential electrodes are positioned along not only one line, but also different lines. Since a 3D model involves many unknown parameters to be determined and requires a large amount of data for reliable inversion, the resulting high cost often makes this approach impractical. In general, 2D inversion is carried out to interpret resistivity data obtained from 2D measurements, where the current and potential electrodes are positioned on one line. However, when the resistivity structure is 3D, 2D inversion may produce artifacts. To address these issues, 3D terrain corrections for 2D measurements have been conducted (Holcombe and Jiracek, 1984; Imamura and Fukuoka, 2004; Nakazato et al., 2006), and 3D inversion of resistivity data gathered from 2D measurements has been conducted (Jackson et al., 2001; Sugimoto et al., 2004; Gharibi and Bentley, 2005; Inoue et al., 2016). Sugimoto et al. (2004) and Nakazato et al. (2004) showed that 3D inversion is more accurate than 2D inversion, even if the same data are used. Sasaki et al. (2005) determined a 3D resistivity structure of the ground via 3D inversion of 2D resistivity data measured along three parallel lines.

It is important to select effective electrode configurations and line arrangements. Gharibi and Bentley (2005) suggested that parallel survey lines should be separated by two electrode spacings, if near surface resolution is important, and should be separated by four electrode spacings, if it is not important or if orthogonal lines are used. Moreover, they demonstrated that the dipole-dipole array produces a more accurate subsurface image than the Wenner array and that parallel lines can be more efficient than orthogonal lines, if the number of electrodes and lines are same with the other line. Sugimoto et al. (2004) examined sensitivity based on a pole-pole array and showed that a line interval less than ten electrode spacings is enough to efficiently obtain an overall resistivity distribution. Also, they demonstrated that adding a few current sources could significantly improve the result.

The criteria for selecting an electrode configuration and line arrangement in 2D resistivity surveys depends on the properties of the target and the aim of the survey. The parallel-line arrangement is expected to be efficient to obtain an overall resistivity distribution, while the orthogonal-line arrangement is expected to give a more reliable resistivity distribution near the line intersections. It is useful for improving an inversion result to add other lines after a 2D resistivity survey has been completed. Therefore, the characteristics of the electrode configuration and line arrangement in 2D resistivity surveys should be examined for an efficient survey and reliable data analysis.

This chapter describes numerical and field experiments with orthogonal and parallel lines and three different arrays. We show characteristics of the electrode configuration and line arrangement and a contour map of root-mean-squares (RMS) errors between resistivities given in the model and reconstructed from the inversion. Then we propose effective electrode configurations and line arrangements for 2D resistivity surveys that will undergo 3D inversion. We also conduct field experiments in a loam area including a backfilled pit. Finally, we apply these electrode configurations and line arrangements to the investigation of geological structure near the Nojima Fault in Awaji Island.

4.2 Numerical experiment

4.2.1 Materials and methods

Figure 28 illustrates the resistivity model used in the numerical experiment. A single 10 Ωm conductive body is located with its top at a depth of 2 m in a homogeneous 100 Ωm half-space. The body is a cube with a 4 m side. Sixteen alternative locations of the body are considered in the experiment and are shown as black squares in **Fig.28**. We examine two types of line arrangements, orthogonal and

parallel, which have two or four lines as shown in **Fig.29**. The parallel-line arrangement is expected to be useful for obtaining an overall resistivity distribution, because the entire survey area is effectively covered by the lines in **Figs.29 (a)** and **29 (c)**. In contrast, the orthogonal-line arrangement is efficient for successfully producing an accurate resistivity distribution near the intersecting point of lines in **Figs.29 (b)** and **29 (d)**. We also consider three kinds of electrode configurations: dipole-dipole, pole-pole, and both dipole-dipole and pole-pole array. **Table 5** is the specifications of electrode configurations. The number of electrodes per line is 41 and the electrode spacing is 1 m. The number of data is 620 and 295 for the dipole-dipole and pole-pole arrays, respectively. Dipole spacings (a-spacings) are 1 m, 2 m and 4 m, and the maximum separation is set to 8.

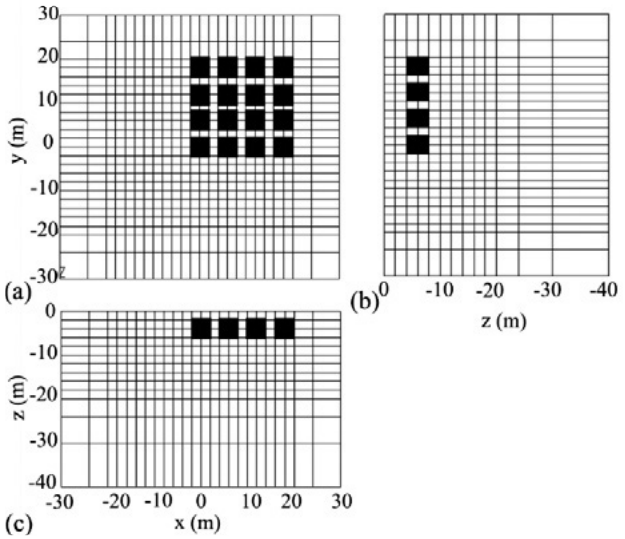

Fig.28 (a) x-y, **(b)** y-z and **(c)** x-z planes showing a resistivity model. The 16 locations of a conductive 10 Ωm body (black) in a homogeneous 100 Ωm half-space, as shown.

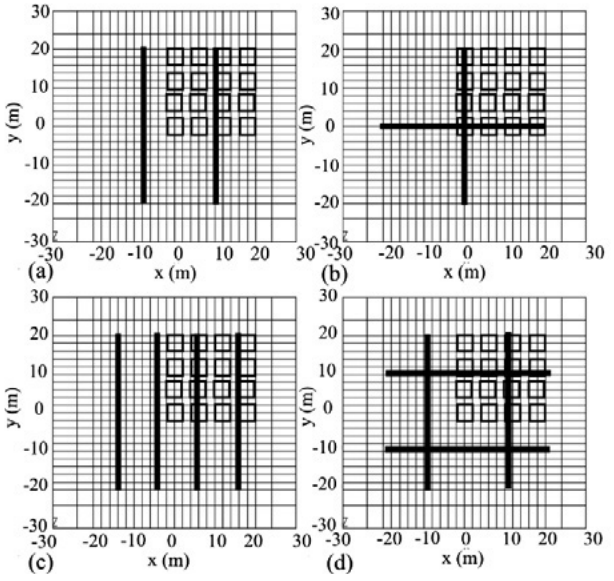

Fig.29 Survey lines on the surface: (a) two parallel, (b) two orthogonal, (c) four parallel and (d) four orthogonal lines.

Table 5 Specifications of survey lines.

Electrode configuration	dipole-dipole	pole-pole
Number of electrodes	41	
Electrode spacing	1 m	
Line length	40 m	
Number of data	620	295

Resistivity data were generated for each line arrangement in a 2D resistivity survey using FEM, E-Tomo 3D (Sugimoto et al., 1998). This FEM with tetrahedral elements was used for the 3D forward modeling for the 3D model shown in **Figs.28** and **29**. The model space was divided more roughly according to the distance from an electrode using the Delaunay triangulation. **Table 6** is the specifications of the forward modeling. Because this chapter aims to examine the characteristics of electrode configurations and line arrangements, no noise was added to the synthetic data.

For this chapter, we conducted 3D inversion of 2D resistivity data. **Table 6** also shows the specifications for the 3D inversion. Unknown parameters (resistivities) were assigned to the grid shown in **Figs.28** and **29**. The size of the inversion grid is 2 m × 2 m × 2 m inside an area of 40 m × 40 m × 10 m and gradually increased outside the area. E-Tomo 3D (Sugimoto et al., 1998) is used for the forward modeling and inversion. The inversion scheme is based on a nonlinear least-squares method with an initial-value constraint expressed in Section 2. In this chapter, $\boldsymbol{C}$ is the unit matrix and α is chosen such that

$$\mathrm{ABIC} = N\log(2\pi\sigma^2) - \log|\alpha^2\boldsymbol{C}^{\mathrm{T}}\boldsymbol{C}| + \log|\boldsymbol{A}^{\mathrm{T}}\boldsymbol{A} + \alpha\boldsymbol{C}^{\mathrm{T}}\boldsymbol{C}| + N + 2 \quad (15)$$

is minimized (Sugimoto, 1988), where ABIC is Akaike's Bayesian Information Criterion (Akaike, 1978), N is the number of observed data and

$$\sigma^2 = \frac{1}{N}\left\{\left\|\boldsymbol{d} - F(\boldsymbol{p}_0+\Delta\boldsymbol{p})\right\|^2 + \alpha^2\|\boldsymbol{C}\Delta\boldsymbol{p}\|^2\right\} \quad (16)$$

The initial model was assumed to be an average value of apparent resistivities, and partial derivatives with respect to model parameters were calculated at each iteration.

4.2.2 Numerical results

Figures 30 and **31** compares resistivity planes at a depth of 4 m derived from 3D inversion of 2D resistivity survey data. When using two parallel lines as shown in **Figs.30 (a) – 30 (c)**, an image of the conductive body can be recognized

Table 6 Specification of 3D forward and inverse modeling.

Arrangement of survey lines	orthogonal		parallel	
Number of survey lines	2	4	2	4
Number of FEM nodes	30,174	50,268	32,735	56,307
Number of FEM elements	178,828	299,813	193,666	334,547
Modeling region	450×450×500 m			
Inversion region	116×116×50 m			
Number of inversion blocks	7,935			

as a low-resistivity zone, although an artifact appears on the opposite side of the line. In the case of using two orthogonal lines as shown in **Figs.30 (d) – 30 (f)**, a low-resistivity zone is not obvious, if the conductor is located outside a square area formed by connecting the four end points of the lines. However, if the target body is located near the intersecting point of the lines, a low-resistivity zone appears at the exact location of the target body. The artifact is reduced by increasing the number of lines as shown in **Fig.31**. The low-resistivity zone appears lower in value and narrower in size in the dipole-dipole array than in the pole-pole array. When both dipole-dipole and pole-pole data are used as shown in **Figs.30 (c)**, **30 (f)**, **31 (c)** and **31 (f)**, the low-resistivity zone is best identified. To evaluate the performance of the line arrangement, RMS error between resistivities given in the model and reconstructed from the inversion is calculated as

$$\mathrm{RMS}=\frac{1}{M}\sum_{i=1}^{M}\left(\frac{R_i^{\mathrm{mdl}}-R_i^{\mathrm{inv}}}{R_i^{\mathrm{mdl}}}\right)^2 \qquad (17)$$

where R_i^{mdl} (Ωm) is the resistivity assigned to the model, R_i^{inv} (Ωm) is the resistivity reconstructed from the inversion, and M is the number of unknown parameters.

The RMS error for each model is plotted at the location of the conductive body at a depth of 4 m. After gathering all RMS errors for the 16 models, a contour map is drawn as seen in **Fig.32**. Note that these illustrations show only the first quadrant of the contour map. Using the parallel-line arrangement as shown in **Figs.32 (a)**, **(b)**, **(c)**, **(g)**, **(h)** and **(i)**, the RMS error increases as the distance from a line increases. Using the orthogonal-line arrangement as shown in **Figs.32 (d)**, **(e)**, **(f)**, **(j)**, **(k)** and **(l)**, the RMS error outside an area formed by connecting the end points of lines is high, whereas it is low inside the area and lowest beneath the intersection of lines. In general, the RMS error is lower when four lines are used in **Figs.32 (g) –32 (l)** compared to when two lines are used in **Figs.32 (a) – 32 (f)**. Similarly, the RMS error is lower when both arrays are used in **Figs.32 (c)**, **(f)**, **(i)** and **(l)** compared to when a single array type is selected.

4.3 Field experiment

A resistivity survey was conducted in an experimental field at the Institute for rural engineering, part of the National Agriculture and Food Research Organization. In the test field, a 2-m-deep pit with a size of 2 m × 0.5 m was dug in a loam area and backfilled with soil six months before the survey. Four lines were set in the field using an electrode spacing of 0.5 m and each line had 20 electrodes. Resistivity data were collected through a 3D survey with the pole-pole array and a 2D survey with the dipole-dipole array. For the 3D pole-pole survey, the number of data was 3,160, and the measurement time was about 3 hr. In the case of the 2D dipole-dipole survey, it took about 1 hr. to obtain 808 data. Resistivity data of a 2D survey with the pole-pole array were sampled from the 3D pole-pole data. A McOHM Profiler-4 and Scanner 64 were used for the measurements. In 3D inversion, the grid size was 0.5 m inside the survey region and gradually increased outside the region.

Figure 33 shows a 3D resistivity distribution derived from 3D inversion of full data collected through both 3D pole-pole and 2D dipole-dipole surveys. The backfilled pit is successfully imaged as low resistivities, while the other areas are generally recovered as high resistivities as shown in **Fig.33 (a)**. The low-resistivity zone occurs in the center of the survey area with a slight shift to the x direction from the intersection of lines B and D.

Figure 34 compares inverted resistivity planes at a depth of 1.5 m. When using only three parallel lines of A, B and C, a low-resistivity zone appears at the center of the survey area in **Figs.34 (a) – 34 (c)**. The resistivity contrast is generally higher in the dipole-dipole array than in the pole-pole array. In the pole-pole array, the high-resistivity zone appears wider than in the dipole-dipole array. When using both arrays, the resistivity contrast is higher and the high-resistivity zone is more extensive than using a single array. When the orthogonal-line data (line D) is added in 3D inversion, the central low-resistivity zone appears at a position shifted

(a) dipole-dipole array with parallel line.

(b) pole-pole array with parallel line.

(c) dipole-dipole and pole-pole arrays with parallel line.

(d) dipole-dipole array with orthogonal line.

(e) pole-pole array with orthogonal line.

(f) dipole-dipole and pole-pole arrays with orthogonal line.

Fig.30 A resistivity slice at depth of 4 m reconstructed from 3D inversion of synthetic data obtained along two parallel lines (a, b and c) and two orthogonal lines (d, e and f). The square black box shows the location of the conductive body in the half-space.

(a) dipole-dipole array with parallel line.

(b) pole-pole array with parallel line.

(c) dipole-dipole and pole-pole arrays with parallel line.

(d) dipole-dipole array with orthogonal line.

(e) pole-pole array with orthogonal line.

(f) dipole-dipole and pole-pole arrays with orthogonal line.

Fig.31 A resistivity slice at depth of 4 m reconstructed from 3D inversion of synthetic data obtained along four parallel lines (a, b and c) and four orthogonal lines (d, e and f). The square black box shows the location of the conductive body in the half-space.

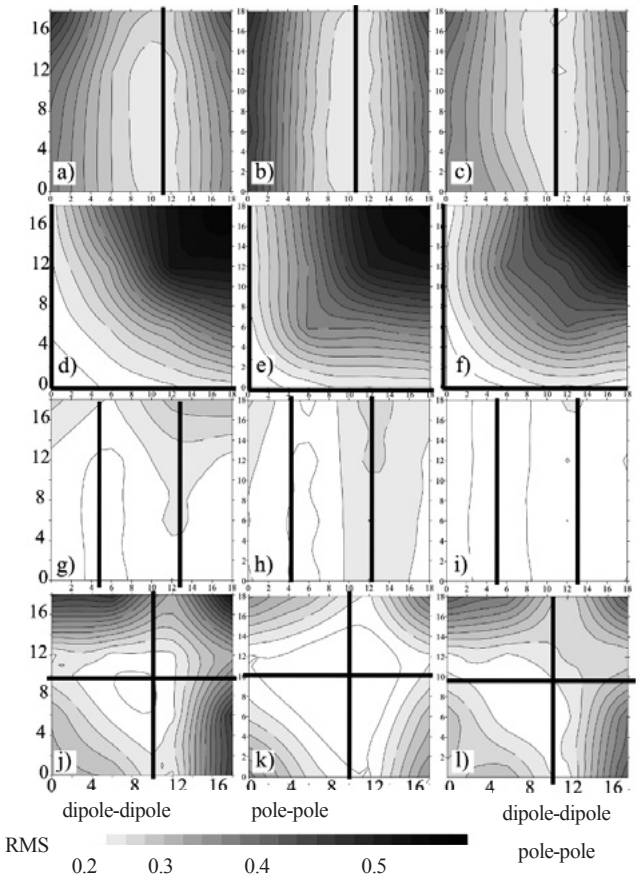

Fig.32 Map of RMS error in resistivity for (a, b and c) two parallel lines, (d, e and f) two orthogonal lines, (g, h and i) four parallel lines and (j, k and l) four orthogonal lines. Only the first quadrant of the contour map is shown. The RMS error is assigned to the position of body.

slightly to the *x* direction that coincides well with the actual location of the backfilled pit in **Figs.34(d) - 34(f)**. The reconstructed resistivities near the intersections of lines C and D, and lines A and D are higher than those in the parallel-line arrangement.

4.4 Field application

4.4.1 Method

To access the applicability of the approach described above to a field, a resistivity survey was conducted in the Nojima Fault area in Awaji Island. **Figure 35** illustrates the study site, the geology of which is a gravel quarry located to the south of Origaya Pond in Awaji City. The general geological strike in this area is N-S, and weathered granite, lignite-containing mudstone of the Iwaya Formation of the Kobe Group, and conglomerate of the Osaka Group are distributed from east to west. The horizontal width of the Iwaya Formation is from 10 to 15 m on the south bank of Origaya Pond. An earthquake fault lies at the boundary of the Iwaya Formation and the Osaka Group, and the Iwaya Formation and weathered granite are in contact at the fault. The fault plane is N2°W, 65°E, there is right-lateral fault displacement of 25 cm, and the upheaval is 5 cm on the east side (Awata and Mizuno, 1998).

The survey area was approximately 100 m square, including the earthquake fault running from north to south. **Figure 36** illustrates the survey area. Six survey lines labelled A to F laid out with an electrode spacing of 2 m and each line had 48 electrodes. The boundary of the Iwaya

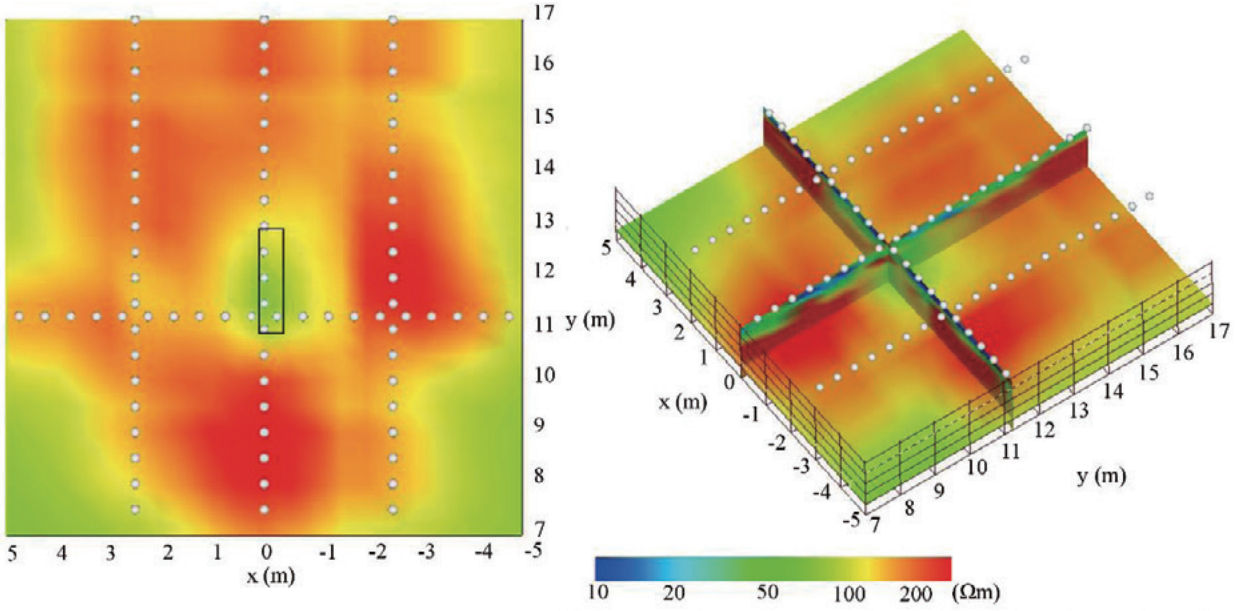

(a) Plane at a depth of 1.5 m.

(b) Cross sections along line B and D and the 1.5-m-deep plane.

Fig.33 Resistivity plane at a depth of 1.5 m and cross sections along lines B and D reconstructed from 3D inversion of synthetic data gathered using 3D and 2D data obtained from the pole-pole and dipole-dipole arrays.

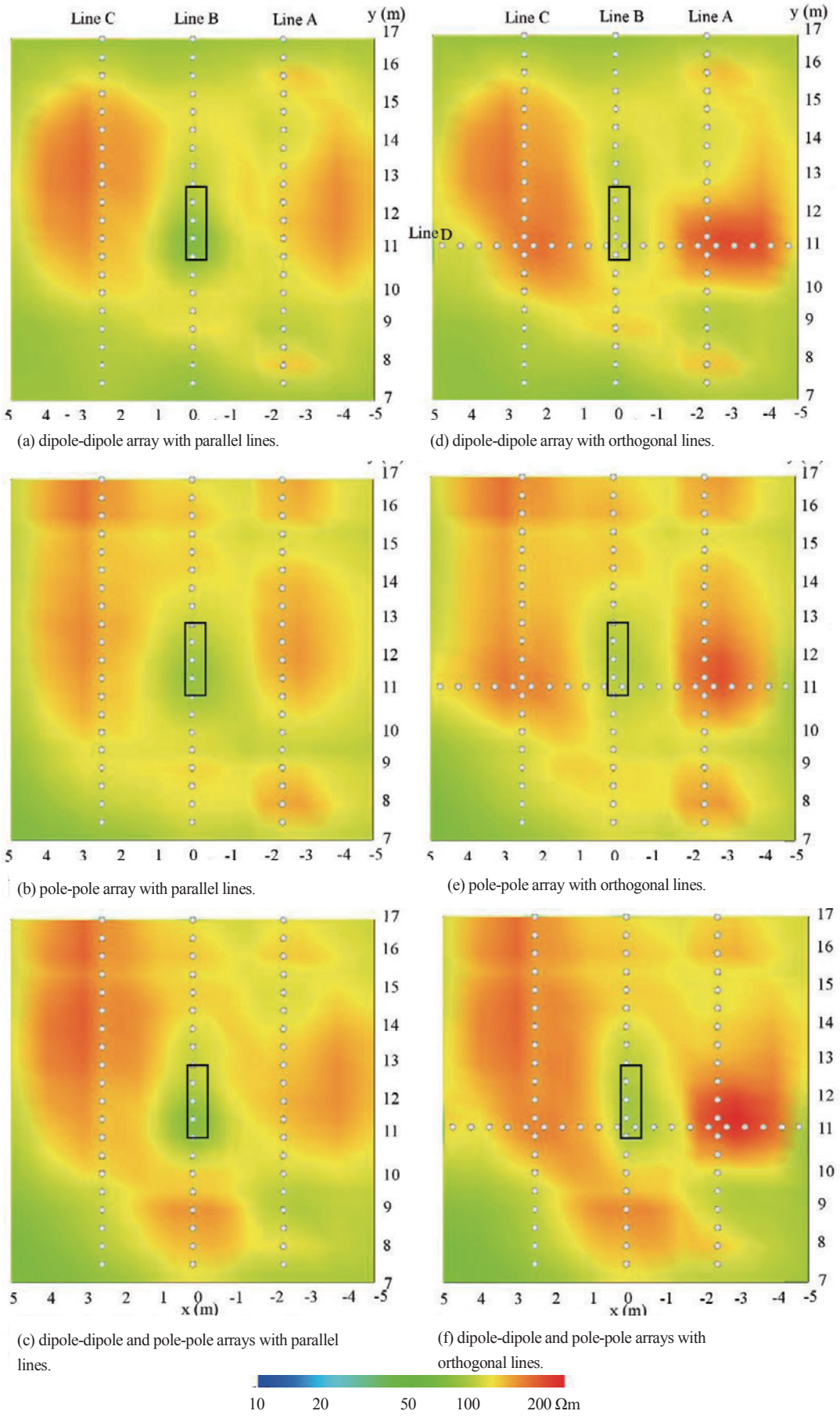

(a) dipole-dipole array with parallel lines.

(b) pole-pole array with parallel lines.

(c) dipole-dipole and pole-pole arrays with parallel lines.

(d) dipole-dipole array with orthogonal lines.

(e) pole-pole array with orthogonal lines.

(f) dipole-dipole and pole-pole arrays with orthogonal lines.

Fig.34 Resistivity plane at a depth of 1. 5 m with (a, b and c) three parallel lines and (d, e and f) four lines including an orthogonal line.

Formation and weathered granite was observed at (1 m, 36 m), shown by a dashed line, in **Fig.36** (Nakazato et al., 2005). A McOHM Profiler-4 and Scanner 64 were used for resistivity measurements. After two survey lines were connected to the instrument, 2D resistivity data were collected automatically, measuring four channels simultaneously for each source. In the pole-pole array, the source and receiver remote electrodes were placed at points C2 (1 m, 60 m) and P2 (9 m, −42 m), respectively.

Since the remote electrodes were not separated enough as the pole-pole array, we calculated an apparent resistivity of the pole-pole array as a general 4-electrode array. For the dipole-dipole array, the number of data for each line was 788, and the measurement time was about 1 hr. In the case of the pole-pole array, it took about 1.5 hr. to obtain 1,128 data. The FEM mesh consists of 473,609 elements and 78,769 nodes

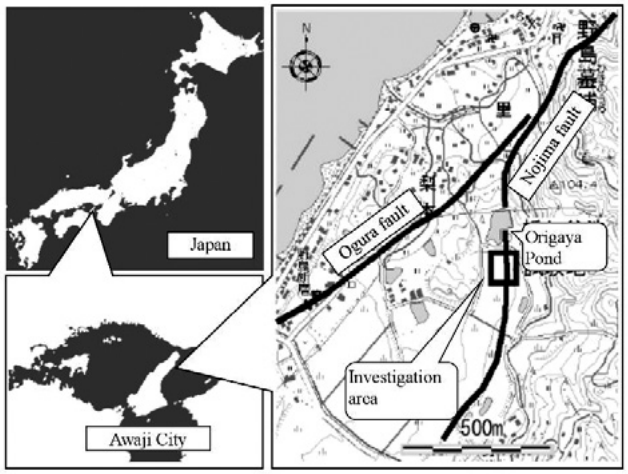

Fig.35 Maps showing the survey area in Awaji City, Japan.

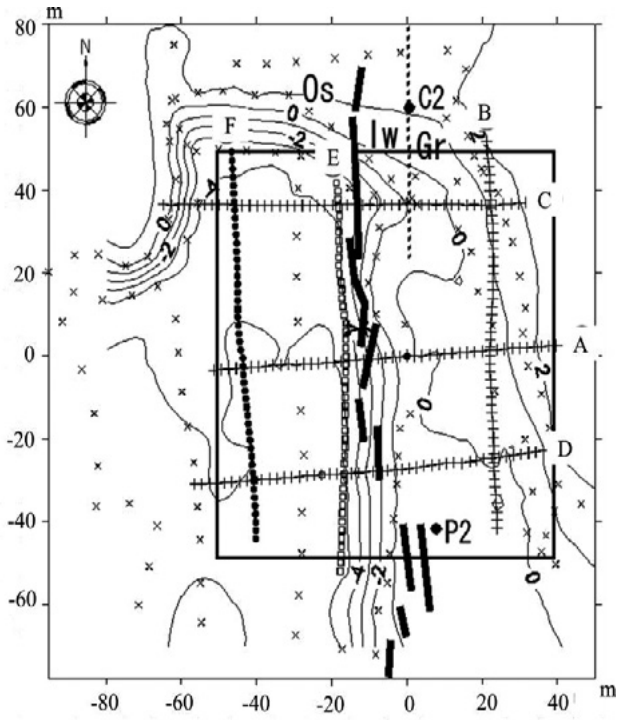

Fig.36 Six lines laid on the survey area. Symbols C2 at (1 m, 60 m) and P2 at (9 m, −42 m) represent the source and receiver remote electrodes for the pole-pole array. Symbols Os, Iw, and Gr represent the Osaka Group, the Iwaya Formation, and weathered granite, respectively. Thick line segments indicate faults (Awata and Mizuno, 1998). The dotted line shows the boundary of the Iwaya Formation and weathered granite.

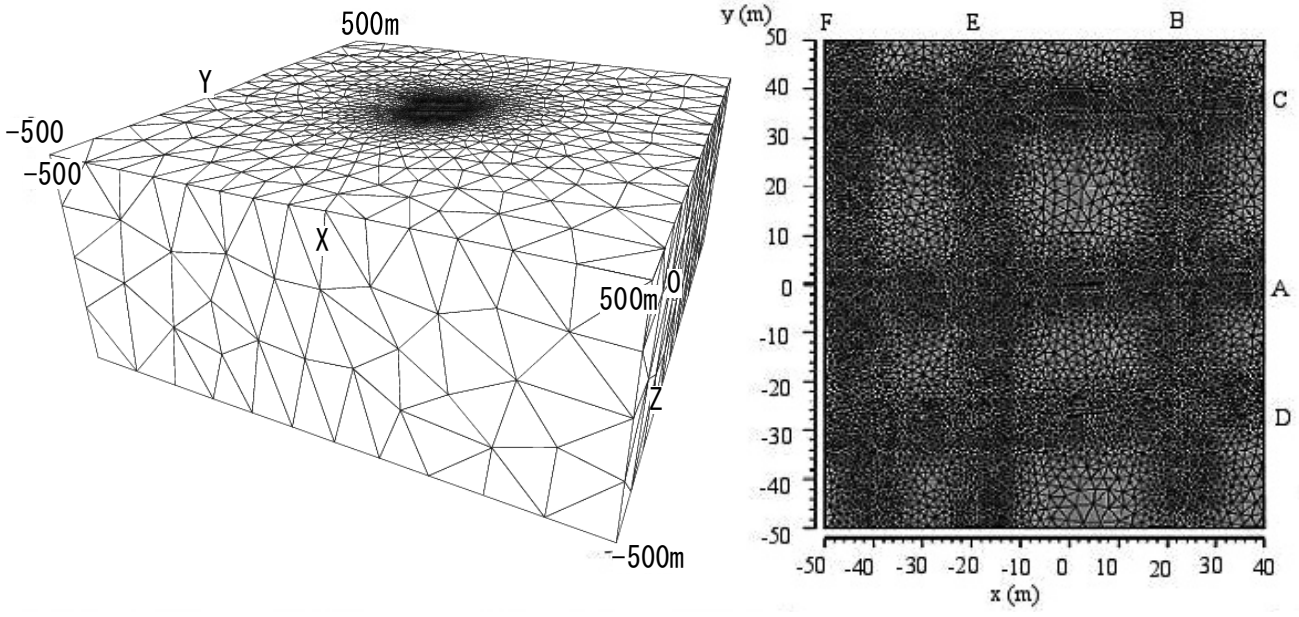

(a) Three-dimensional view. (b) Surface view.

Fig.37 (a) Three-dimensional view and **(b)** surface view of the FEM mesh used to generate synthetic data.

as shown in **Fig.37**. The inversion region ranges were x = −80 to 60 m, y = −70 to 70 m, and z = 0 (surface) to 50 m, the cell size was 4 m inside the survey area, so the inversion volume included 7,840 (28 × 28 × 10) unknown parameters.

4.4.2 Field results

Figure 38 shows resistivity distributions at depths of 10 and 20 m determined by 3D inversion of dipole-dipole data measured along the six lines. A low-resistivity (40 Ωm or less) belt with a width of about 15 m is distributed from north to south in the central part of the survey area. This low-resistivity belt corresponds well to the Iwaya Formation, because the boundary of granite and the Iwaya Formation was observed at (1 m, 36 m). The high-resistivity zone on the east side coincides with the area of granite, while the high-resistivity zone on the west side represents the Osaka group. Suzuki et al. 1996 carried out another 3D resistivity survey with electrodes arranged in a lattice with an interval of 5 m (154 electrodes and 11,781 data points) in investigating the Nojima Fault in Ogura in Awaji City, 700 m west of the present study site, and the orientation of the fault was determined three-dimensionally. The results of our study meet well with Suzuki et al. (1996).

As an example of using less data, **Fig.39 (a)** illustrates a resistivity distribution at a depth of 10 m determined from 3D inversion of dipole-dipole data observed along two lines A and E that intersect at the center of the study area. In the resistivity distribution derived from the two lines, the continuity of the low-resistivity belt at the center and the overall resistivity contrast are slightly less when compared to those derived from the six lines as shown in **Fig.38 (a)**. **Figure 39 (b)** illustrates the results of 3D analyses based on both pole-pole and dipole-dipole data. From this illustration, we can find the low-resistivity belt, and this indicates that adding different array data is useful to improve the resistivity image.

4.5 Discussions

In the numerical experiment, the dipole-dipole array produces a clear image of the low-resistivity body in **Figs.30 (a)**, **30 (d)**, **31 (a)** and **31 (d)**, while the pole-pole array yields a broader image of the body in **Figs.30 (b)**, **30 (e)**, **31 (b)** and **31 (e)**. When the data from both arrays are used, the most reliable image of the low-resistivity zone is obtained as shown in **Figs.30 (c)**, **30 (f)**, **31 (c)** and **31 (f)**. After survey lines have been installed by planting electrodes, using of several arrays is efficient, because fast measuring equipment has been developed and the effort of measurements is relatively smaller than that of setting survey lines.

The numerical experiment shows that a low-resistivity zone can be recovered nearly at the target location when using the parallel-line arrangement as shown in **Figs.30 (a)** – **30 (c)** and **31 (a)** – **31 (c)**, although a low-resistivity artifact may occur on the opposite side of the line to the target. The resistivity reconstructed is constrained with only one line

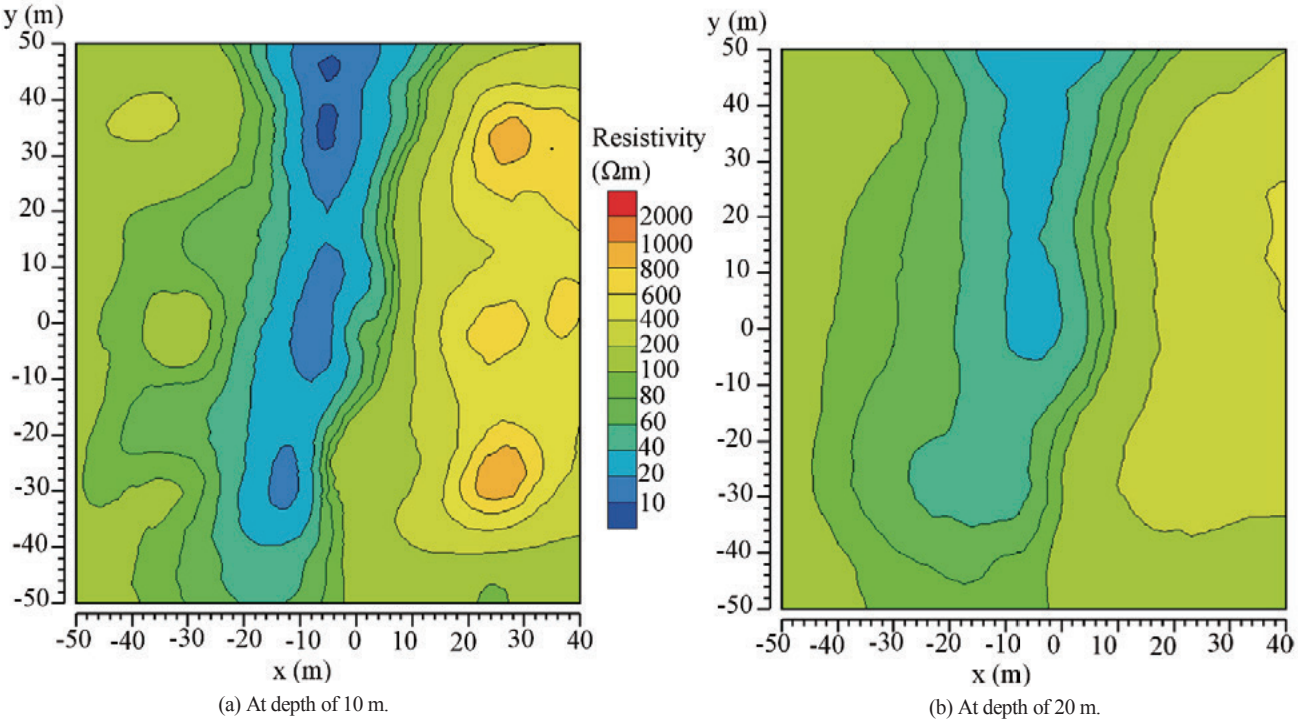

(a) At depth of 10 m.　　(b) At depth of 20 m.

Fig.38 Resistivity distributions at depths of **(a)** 10 m and **(b)** 20 m reconstructed from 3D inversion of field data gathered using six dipole-dipole arrays.

when the line interval is wide. Moreover, a 3D sensitivity distribution exhibits axial symmetry with respect to the survey line (Sasaki, 1994). Therefore, a conductive body off the line in one side produces a low-resistivity artifact at a position equal to the offset distance in the other side.

If the conductive body is located outside an area formed by connecting the line ends, its image is not clear when using the orthogonal-line arrangement. On the other hand, a low-resistivity zone can be recognized near the intersecting point of lines, although an artifact may also occur on the opposite side of the line. This means that sensitivity is very low in the outside area, while it is high near the intersecting point, and the resistivity is constrained by the two lines. Uncertainty in recovering the low-resistivity zone may be reduced by increasing the number of lines, because the distance of the conductive body from a line then becomes relatively less and sensitivity increases.

The parallel-line arrangement is more useful to identify the location of a target body than the orthogonal-line arrangement, if the target is located at some distance from the intersection of lines. The orthogonal-line arrangement has its maximum sensitivity at the intersection. Thus, it may be effective to conduct a resistivity survey in two stages. An initial survey with parallel lines reveals the presence of a survey target that is subsequently explored using an intersecting line. It is useful for improving an inversion result by adding other lines to obtain additional data after the initial resistivity survey has been completed. Both data gathered before and after adding the new lines would be combined for 3D inversion. The additional lines could be set only for an area including the survey target so saving time and money.

In the field experiment, the approximate location of the backfilled pit can be identified as a low-resistivity zone by using parallel lines. However, the backfill pit is located actually at a position slightly shifted to the *x* direction from the intersection of lines B and D as shown in **Fig.33 (a)**. The reconstructed resistivity contrast is higher when the dipole-dipole array is used compared to when the pole-pole array is selected. The pole-pole array is useful as it detects the high-resistivity zone more broadly than the dipole-dipole array. Using both pole-pole and dipole-dipole arrays, the resistivity contrast is higher than that using a single array, and high-resistivity zones appear more extensively. When orthogonal lines are added, the low-resistivity zone occurs at the location shifted to the direction of line D from the intersection of lines B and D, and coincides with the exact location of the backfill pit. Furthermore, the high-resistivity zones recovered near the other intersections of lines A and D, and C and D are also clearer in the orthogonal-line arrangement than in the parallel-line arrangement. These features correspond to the results of the numerical experiment.

The 3D inversion of 2D survey data for the field application in the Nojima Fault area provides a resistivity distribution similar to the geological structure in the survey site. Even when the resistivity distribution is derived from only two orthogonal lines, a low-resistivity belt can be

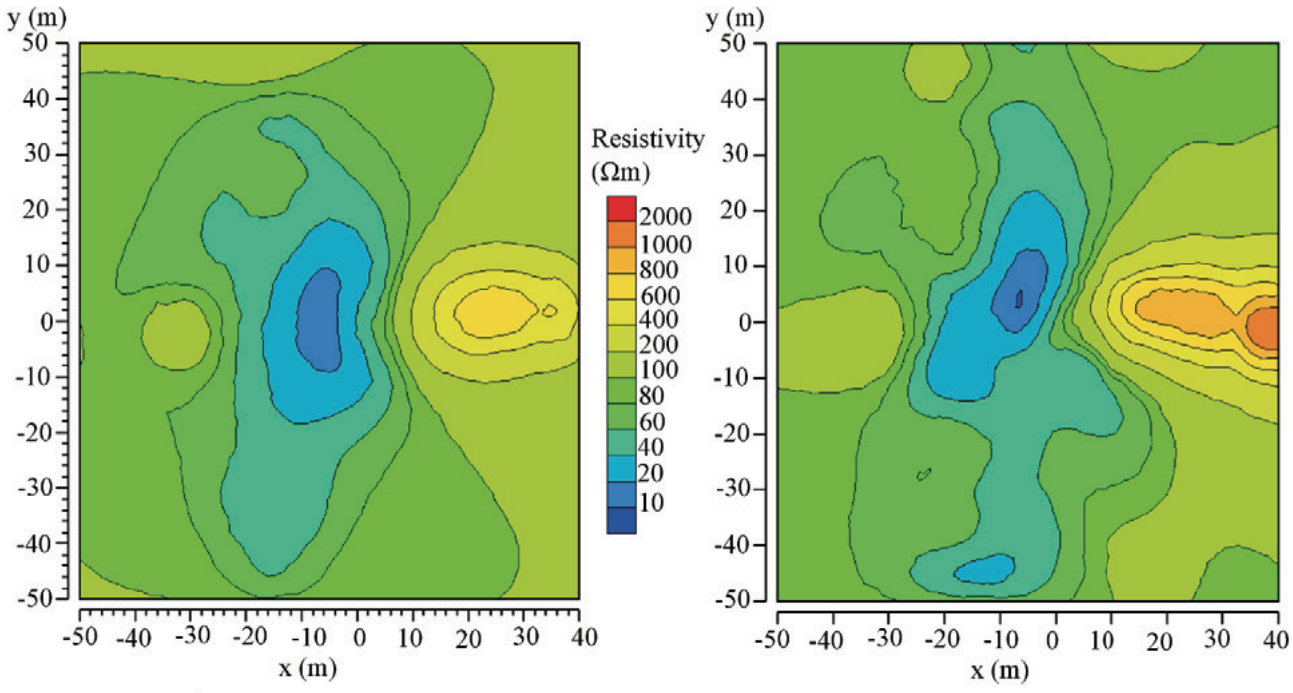

(a) dipole-dipole array.

(b) dipole-dipole and pole-pole arrays.

Fig.39 Resistivity distributions at depths of 10 m reconstructed from 3D inversion of field data gathered using (a) two dipole-dipole arrays and (b) two pole-pole and dipole-dipole arrays.

recognized. Since the area in which the resistivity distribution is successfully recovered has low RMS errors as shown in **Figs.32 (d)** and **32 (f)**, the inversion result can be interpreted easily by reference to the contour map of RMS errors shown in **Fig.32**. Three-dimensional inversion of 2D resistivity data may also be useful in investigating an area where the survey lines have not arranged with specific reference to the subsurface geology. The reconstructed resistivity structure can be improved by adding survey lines and measuring supplementary data in an area in which there are insufficient data (Sugimoto et al., 2004) and by conducting orthogonal-line measurements (Sasaki et al., 2005). Collecting data using different electrode arrays that have different sensitivities is also an effective approach that can reduce a total amount of fieldwork required.

4.6 Conclusions

We investigated different electrode configurations and line arrangements for 3D inversion of 2D resistivity survey data. We conducted numerical experiments for three kinds of electrode configurations and two types of line arrangements for 16 models of a conductive body in a homogeneous half-space.

The dipole-dipole array produced a clearer image of the low-resistivity body, while the pole-pole array yielded a broader image of the body. Using the parallel-line arrangement, a low-resistivity zone appeared near the conductive body and the RMS error between resistivities given in the model and reconstructed from the inversion was low. Using the orthogonal-line arrangement, the low-resistivity zone appeared to more accurately locate the target body beneath the line intersections. In the orthogonal-line arrangement, the RMS error was minimized inside the area formed by connecting the ends of lines. In this regard, it may be desirable to take place a resistivity survey in two stages. A first round of the resistivity survey with parallel lines may highlight areas of particular interest where further detailed work with an intersecting line to be carried out. The field experiment showed that, by using a resistivity survey with parallel lines, a low-resistivity zone appeared near the backfilled pit. The orthogonal lines were useful to improve an image of the backfill pit. These features corresponded to the results of the numerical experiment. Finally, resistivity surveys were performed near the Nojima Fault in Awaji Island to examine the effectiveness of the approach proposed in this chapter. The 3D inversion of 2D survey data provided a resistivity distribution similar to the geology in the field. Although the resistivity distribution was derived using only two orthogonal lines, the direction of the low-resistivity belt can be recognized. Collecting data from different electrode arrays that had different sensitivities was shown to be an effective approach.

The criteria for selecting an electrode configuration and line arrangement in 2D resistivity surveys for 3D inversion depends on the properties of the target and the aim of the survey. It may be desirable to take place a resistivity survey in two stages as described above by considering the characteristics of the electrode configuration and line arrangement in 2D resistivity surveys. However, this chapter showed results for the survey lines that are parallel or orthogonal to the anomaly. Additional considerations are needed when the survey lines are diagonal to the direction of the anomaly.

5. Three-dimensional monitoring of groundwater using 3D inversion

In the preceding chapter, we described effective arrangements of 2D resistivity survey for 3D inversion. When the water content varies with time, the distribution derived from 3D inversion of the 2D resistivity survey data includes data at different measurement times. The interpretation of the results based on the characteristics of inversion results is needed.

This chapter describes the applicability of 2D resistivity survey data for 3D inversion to monitoring of soil-water flow in the vadose zone. Distributions of the resistivity change ratio are verified by the volumetric water content observed in a borehole in the test site. Furthermore, other 3D resistivity change ratio distributions are recovered from a 1-hr. time-shifted dataset to investigate the time dependency of measurements.

5.1 Introduction

Soil water flow on a field scale is in 3D because of the heterogeneous hydraulic conductivity of soil. Therefore, for a detailed understanding of soil water flow, a 3D distribution of resistivity is required. A cross-hole resistivity survey with electrodes placed along boreholes (Daily et al., 1992; Binley et al., 2002; Slater et al., 2002; Daily et al., 2004; Singha and Gorelick, 2005; Oldenborger et al., 2007; Coscia et al., 2011), or a resistivity survey with electrodes around a soil column in the laboratory (Binley et al., 1996; Chambers et al., 2004; Koestel et al., 2008; Garre et al., 2011) provides detailed information, because the electrodes are placed close to the unknown resistivity structure. However, such a resistivity survey is of limited application in an actual field environment, because the electrodes must be placed underground, so

boreholes must be drilled. Thus, 3D resistivity survey with surface electrodes has often been applied to monitoring infiltration of soil water (Sasaki, 1994; Park, 1998; Bentley and Gharibi, 2004; Jackson et al., 2001; Sugimoto et al., 2004; Gharibi and Bentley, 2005).

The images of water flow in layers of high hydraulic conductivity, derived from 3D resistivity inversion, may be distorted if the water content varies during the actual measurement process. To deal with this uncertainty, Day-Lewis et al. (2003) adopted a method to account for the time taken to acquire ground penetrating radar (GPR) difference-attenuation data, and Kim et al. (2009) and Karaoulis et al. (2011) regularized the time lapse data to account for the data acquisition time. A quick survey is also effective, because the accuracy of the 3D image is highly dependent on measurement time. Since 2D resistivity survey collects resistivity data along a line, it can save measurement time compared with 3D resistivity survey. Soil water flow may be estimated from several 2D inversions of resistivity data as shown in Chapter 3 (Inoue et al., 2008). However, 2D resistivity survey may provide a less accurate image than 3D resistivity survey for 3D targets (Batlle-Aguilar et al., 2009; Bentley and Gharibi, 2004). Thus, 3D inversion of 2D resistivity survey data is frequently conducted to investigate a site with 3D geology (Jackson et al., 2001; Sugimoto et al., 2004; Gharibi and Bentley, 2005). When the water content varies with time, the distribution derived from 3D inversion of the 2D resistivity survey data includes data at different measurement times. The interpretation of the results based on the characteristics of inversion results is needed.

This chapter investigates the applicability of 2D resistivity survey data for 3D inversion to monitoring of soil-water flow in the vadose zone. To this end, a groundwater recharge experiment is conducted in a pyroclastic plateau in Kagoshima, Japan, and the resistivity data is continuously measured along four intersecting lines, each from 2D resistivity survey during the recharge experiment. In this chapter, distributions of the RCR are derived from 2D and 3D inversions of the 2D resistivity survey data. These RCR distributions are verified by the volumetric water content observed in a borehole in the test site. Furthermore, other 3D RCR distributions are recovered from a 1-hr. time-shifted dataset to investigate the time dependency of measurements.

5.2 Resistivity survey

Chapter 3 described time-efficient multiple 2D resistivity surveys during an artificial groundwater recharge experiment in a pyroclastic plateau in Kagoshima. Dipole-dipole resistivity surveys were continuously performed during the recharge experiment along the four lines shown in **Fig.17**. This chapter estimates the time-lapse 3D resistivity change distributions during the recharge experiment shown in Chapter 3. In resistivity surveys, electrical currents are introduced into the soil through a pair of electrodes and induced potential differences are measured with other pairs of electrodes. If all electrodes are confined to a single line, a 2D profile image can be obtained. A 3D image of the subsurface can be obtained from 3D resistivity surveys, where the current and potential electrodes may be positioned not only along one line but also along different lines. Although the 3D resistivity survey is helpful for gathering 3D information, the increase in data acquired results in an increase in measurement time. On the other hand, data collection along several lines distributed over the survey area from 2D resistivity survey, where the current and potential electrodes are positioned on one line in each case, can save measurement time. In this chapter, 2D resistivity survey data measured along four intersecting survey lines are used, because a relatively fast water flow is expected in the pyroclastic plateau.

Table 7 Modelling and inversion specifications.

	3D	2D
FEM modeling region	450 × 450 × 500 m	517 × 234 m
Number of FEM nodes	39,716	1,587
Number of FEM elements	235,173	2,998
Inversion region	116 × 116 × 50 m	107 × 49 m
Number of unknown parameter	7,935	495

Resistivity distributions are derived from the 2D and 3D inversions of the 2D survey data. E-Tomo 2D (Sugimoto et al., 1995) and E-Tomo 3D (Sugimoto and Inoue, 1998) are used for the inversions. **Figure 40** presents a schematic view of the mesh for FEM modelling, and the inversion grid. The forward and inverse modelling specifications are listed in **Table 7**. The FEM mesh is generated in such a way that the density of the nodes is higher near the electrodes and gradually decreases away from the electrodes (Sugimoto and Hishiya, 1993) as shown in **Figs.40 (a)** and **(c)**. The cell of the inversion grid in the horizontal direction is 3 m inside the survey site and 6 to 24 m outside. The cell size is also increased gradually in the vertical direction as shown in **Figs.40 (b)** and **(d)**. Time-lapse RCR distributions during the recharge experiment are estimated using the method described above, in which the distribution before the change is used as the initial state and the normalised apparent

resistivity is inverted rather than the measured apparent resistivity itself. Each 3D RCR distribution is derived by inverting each dataset composed of the four lines A to D.

5.3 Results

To calculate the RCR distribution during the recharge experiment, the initial distributions of resistivity were derived from both 2D and 3D inversion of 2D resistivity survey data obtained before the experiment as shown in **Fig.41**. The inversion processes were quite stable, and residual errors between the observed and predicted data were reduced to 7.5% in 3D and 6.6% in 2D inversions and changed insignificantly after ten and six iterations, respectively. The 2D and 3D inversions provides similar resistivity images in **Fig.41**. The reconstructed images show an almost 1D layered structure. A low-resistivity layer from the surface to 4 m depth, which corresponds to the loam layer, whereas a high-resistivity layer at 4 – 7 m depths corresponds to the secondary Shirasu layer shown in **Fig.18**.

Figure 42 illustrates time-lapse RCR distributions obtained from the 3D inversion of the 2D survey data collected in the recharge experiment. The inversion almost converged within ten iterations and the residual error for each stage was reduced to less than 6.2%. Since it take 1hr. to collect the resistivity data for each survey line, each RCR distribution is regarded as a 4 hr. averaged image. A clear decrease in resistivity was observed at depth of 4 m in the recharge area 0 – 4 hr. after the recharge experiment started, while little resistivity change occurred in the surface layer shallower than 4 m in **Fig.42 (a)**. The region with decreased resistivity extended horizontally in the secondary Shirasu layer at relatively early times during the recharge experiment

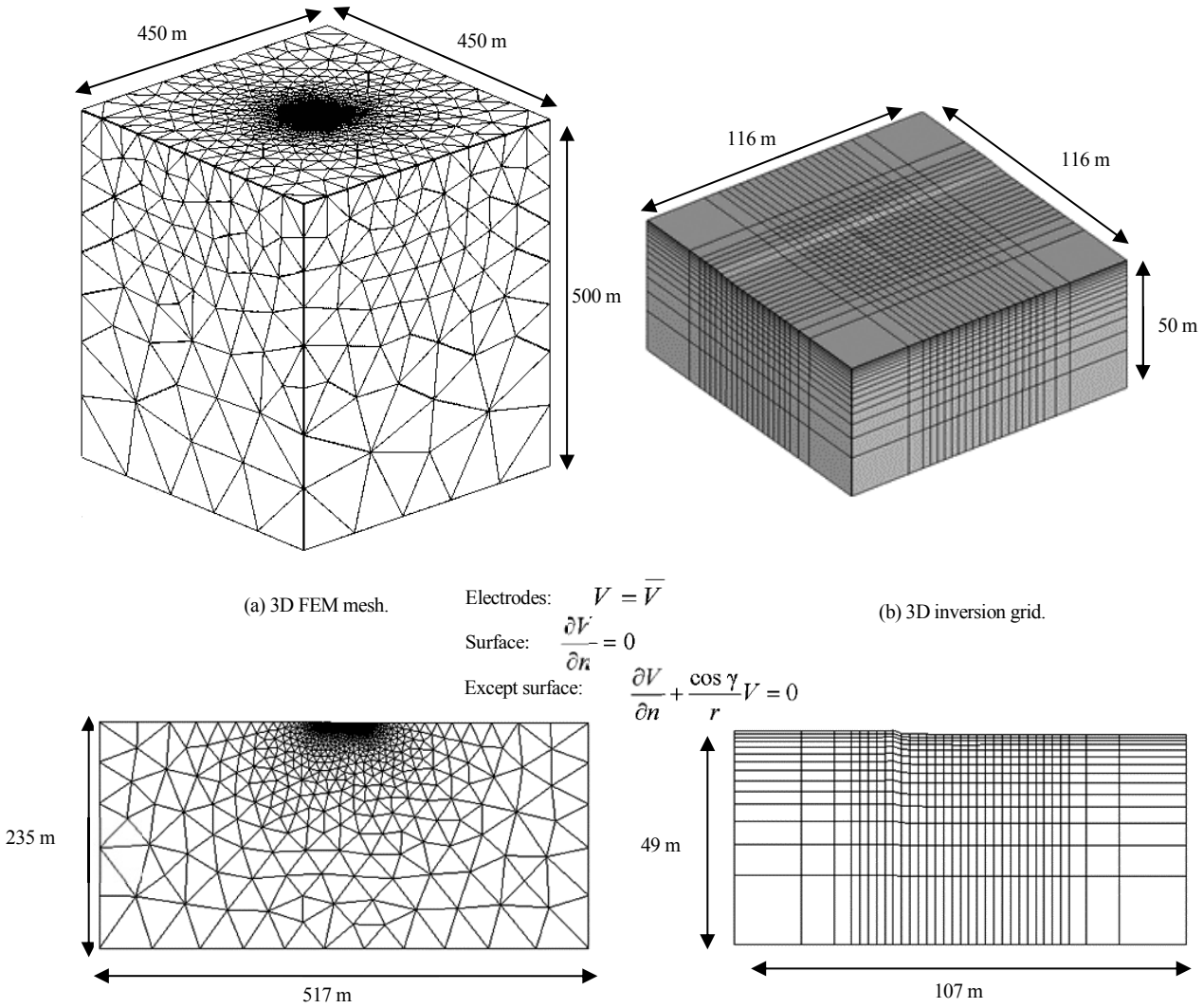

(a) 3D FEM mesh.

(b) 3D inversion grid.

(c) 2D FEM mesh along line B.

(d) 2D inversion grid along line B.

Fig.40 Schematic views of the 3D FEM mesh **(a)** and the inversion grid **(b)**, and 2D FEM mesh **(c)** and inversion grid **(d)** along line B.

in **Fig.42 (b)**, then penetrated the underlying the Shirasu layer in **Fig.42 (c)**, and finally, shrank after the water supply ended in **Fig.42 (d)**.

Figure 43 compares the RCR distributions along survey line B derived from the 2D and 3D inversions of the 2D survey data gathered 52 – 56 hr. after the recharge started (0 – 4 hr. befor e the recharge terminated). The RCR profile reconstructed from the 3D inversion in **Fig.43 (a)** presents a decreased resistivity zone of less than −50% at depths of 5 – 9 m near borehole B1. The maximum change in resistivity occurs at 7 m, and the resistivity gradually increases with depth in a deeper zone. By contrast, the RCR profile obtained from 2D inversion in **Fig.43 (b)** presents a decreased resistivity zone of less than −50% at depth of 5 – 11 m, and the maximum resistivity change appears at depth of 5 m. **Figure 43 (c)** shows that θ mainly increases in a narrow zone at depth of from 3 m to 7 m, and its maximum appears at depth of 5.5 m. The decreased resistivity zone recovered from the 3D inversion matches well with the zone showing a significant change in θ observed in borehole B1, compared

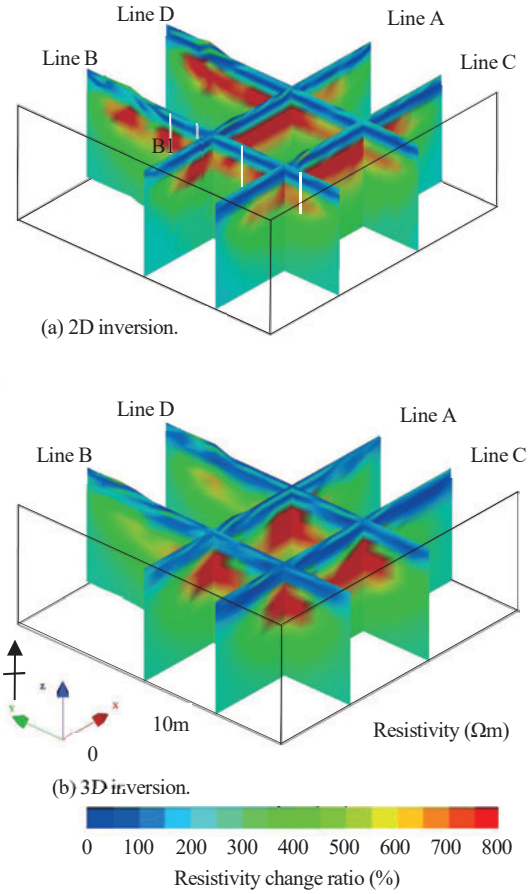

Fig.41 Resistivity distributions derived from **(a)** 2D and **(b)** 3D inversions of electrical resistivity data measured before the recharge experiment.

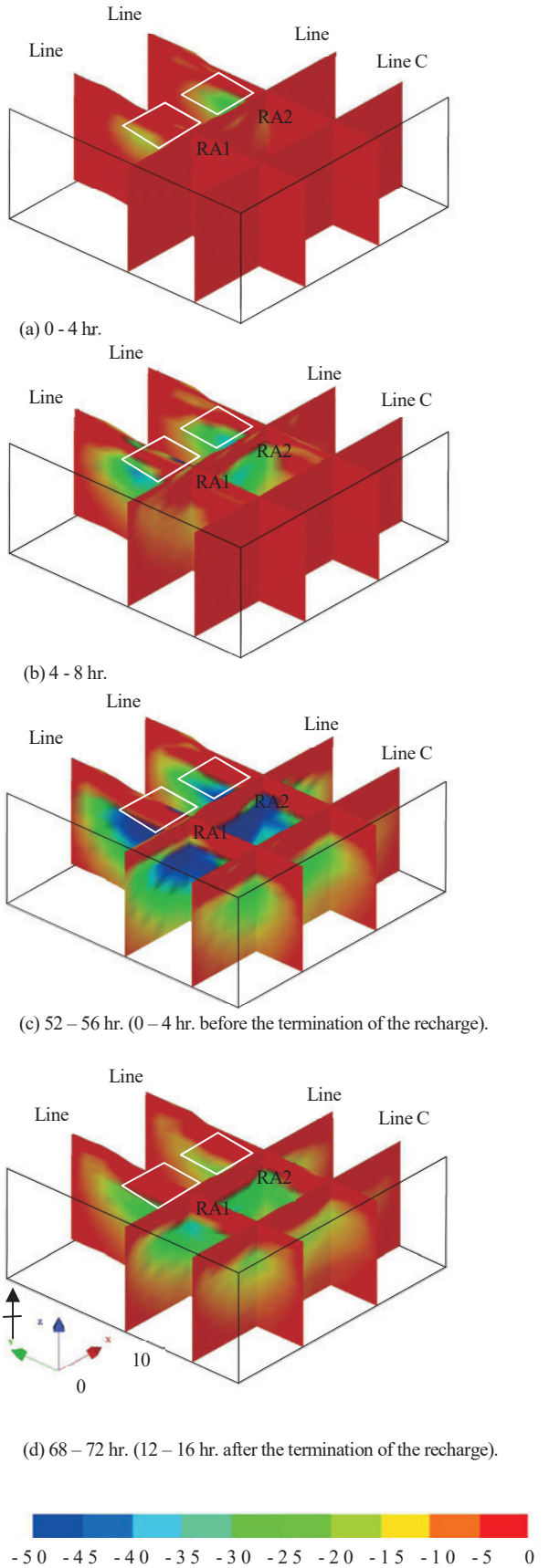

Fig.42 Resistivity change ratio distributions. **(a)** 0 – 4 hr., **(b)** 4 – 8 hr., **(c)** 52 – 56 hr. and **(d)** 68 – 72 hr. after the recharge experiment started.

with the zone indicated by the 2D inversion result, whereas the depth of the maximum change in θ appears to coincide better results with the 2D than that with the 3D.

Figure 44 compares the RCR profiles derived from the 2D and 3D inversions near borehole B1 and the change rate in volumetric water content observed in borehole B1. The RCR near borehole B1 increases at depths of greater than 4 m after recharge starts and decreases after recharge terminates in **Figs.44 (a)** and **44 (b)**. The RCR starts to increase rapidly in the profile of 0 – 4 hr. from 3D and 1 – 2 hr. from 2D, although the change rate in volumetric water content varies only a little even after 5 hr. in **Fig.44 (c)**. The slight change in the volumetric water content suggests that fast infiltration did not occur near borehole B1. This is partly in agreement with the observation that recharge water spreads to the opposite side of line B at an early stage as shown in **Fig.22** . On the other hand, the RCR increase in the early stages may reflect the change in volumetric water content not beneath line B but beneath the west area of recharge area RA1, because the recharge water spread only to the west side of recharge area RA1 and preferential infiltration would be expected there at an early stage. The RCR at depths of 7 – 10 m in 2D in **Fig.44 (b)** is around −50%, and almost constant over time. This observation coincides with the change in volumetric water content in **Fig.44 (c)** rather than with the observations provided by the 3D inversion in **Fig.44 (a)**.

Figure 45 illustrates RCR contour lines along line B after the re charge experiment started. The zone of decreased resistivity expands with time and spreads horizontally during recharge, and reaches farthest away from borehole B1 at a depth of 7 m. **Figure 46** shows the distances of the RCR contour lines from borehole B1 at a depth of 7 m along line B. From the variation in the volumes of the decreased resistivity zone with time, we can estimate the velocity of groundwater flow. The rate of expanding of the decreased resistivity volumes 20 – 54 hr. after the recharge started are estimated to be at 2.93×10^{-6} m/s (10%), 2.87×10^{-6} m/s (20%), 2.63×10^{-6} m/s (30%), 1.51×10^{-6} m/s (40%) and 1.10×10^{-6} m/s (50%). Unsaturated hydraulic conductivity is generally lower than saturated hydraulic conductivity, and these values are one order of magnitude lower than the saturated hydraulic conductivity of $1.3 – 1.7 \times 10^{-5}$ m/s in the

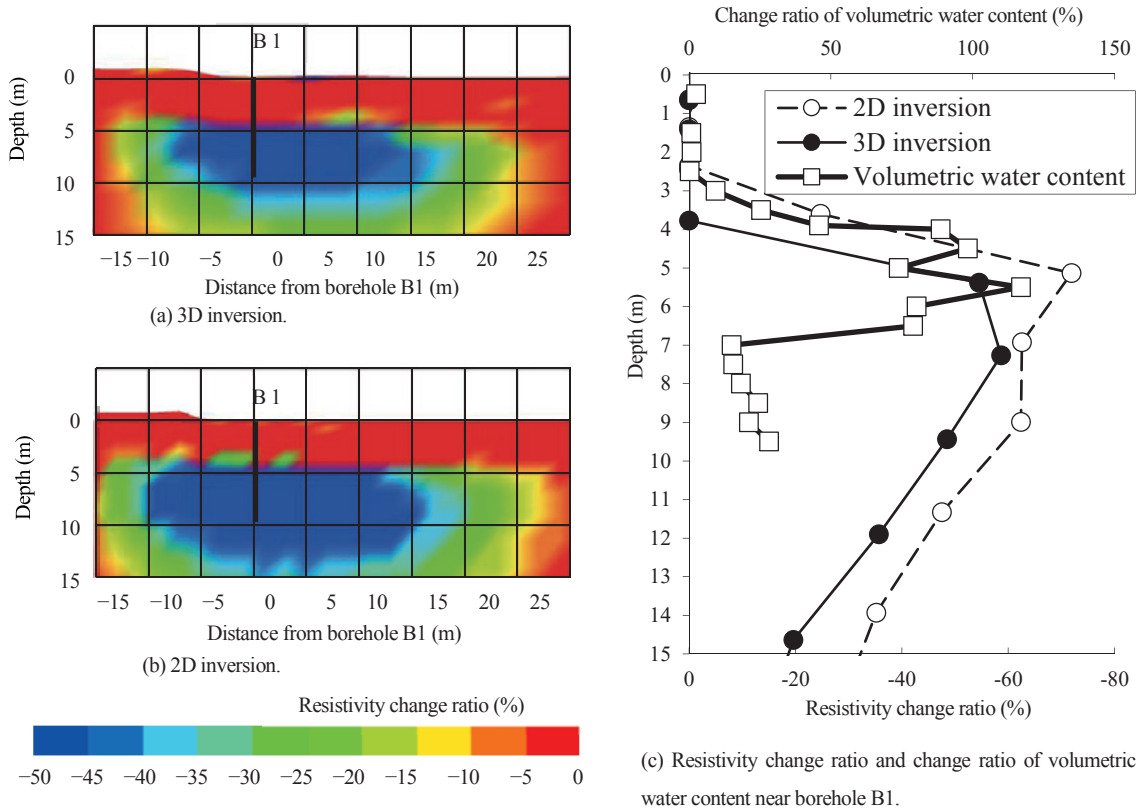

(c) Resistivity change ratio and change ratio of volumetric water content near borehole B1.

Fig.43 Resistivity change ratio sections along line B derived from **(a)** 3D and **(b)** 2D inversions of normalized resistivity data and **(c)** the change ratio of volumetric water content at bore hole B1 and resistivity change ratio near borehole B1 derived from 2D and 3D inversions of normalized resistivity data gathered 52 – 56 hr. after the recharge started (0 – 4 hr. before the recharge terminated). The change ratio of volumetric water content was observed 53 hr. after recharge started and was compared with the volumetric water content before the recharge experiment.

secondary Shirasu layer.

Figure 47 shows variations with time of volumes surrounded by an equi-RCR surface. The volume expands during the recharge experiment and shrinks after recharge termination. The volume expansion matches well with the increase in the total amount of recharged water, and thus reflects an increase in the saturation level in soil. The volume shrinkage responds to the termination of recharge, and thus

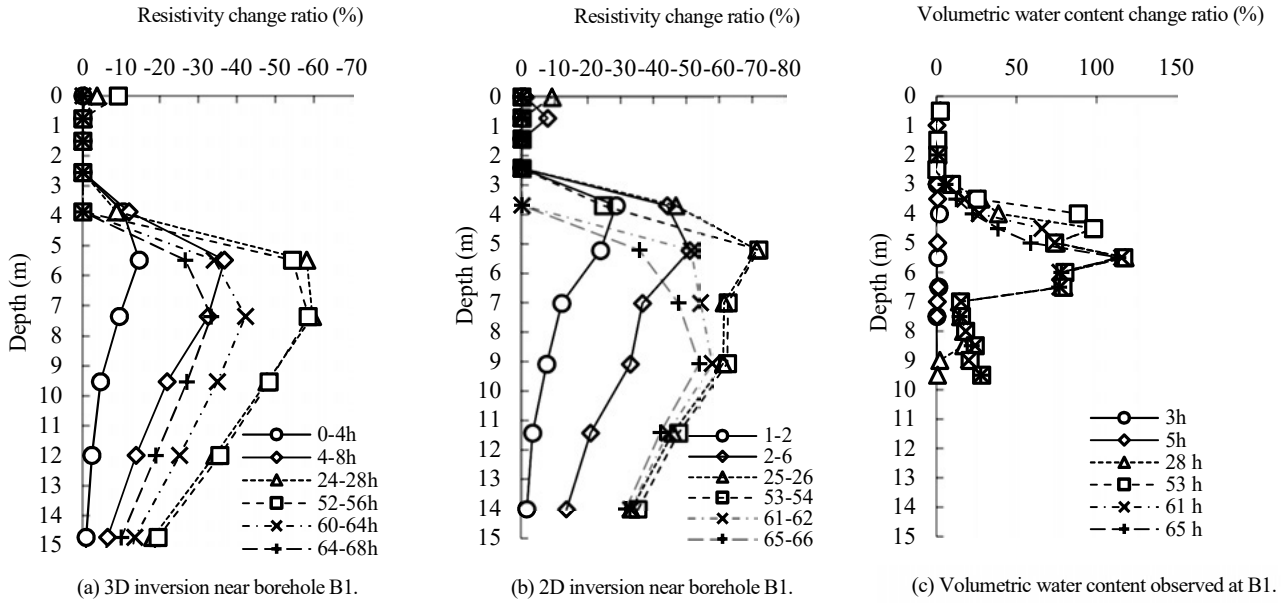

(a) 3D inversion near borehole B1. (b) 2D inversion near borehole B1. (c) Volumetric water content observed at B1.

Fig.44 Profiles of the RCR and the volumetric water content change ratio. **(a)** 3D RCR near borehole B1, **(b)** 2D RCR near borehole B1, and **(c)** volumetric water content at borehole B1.

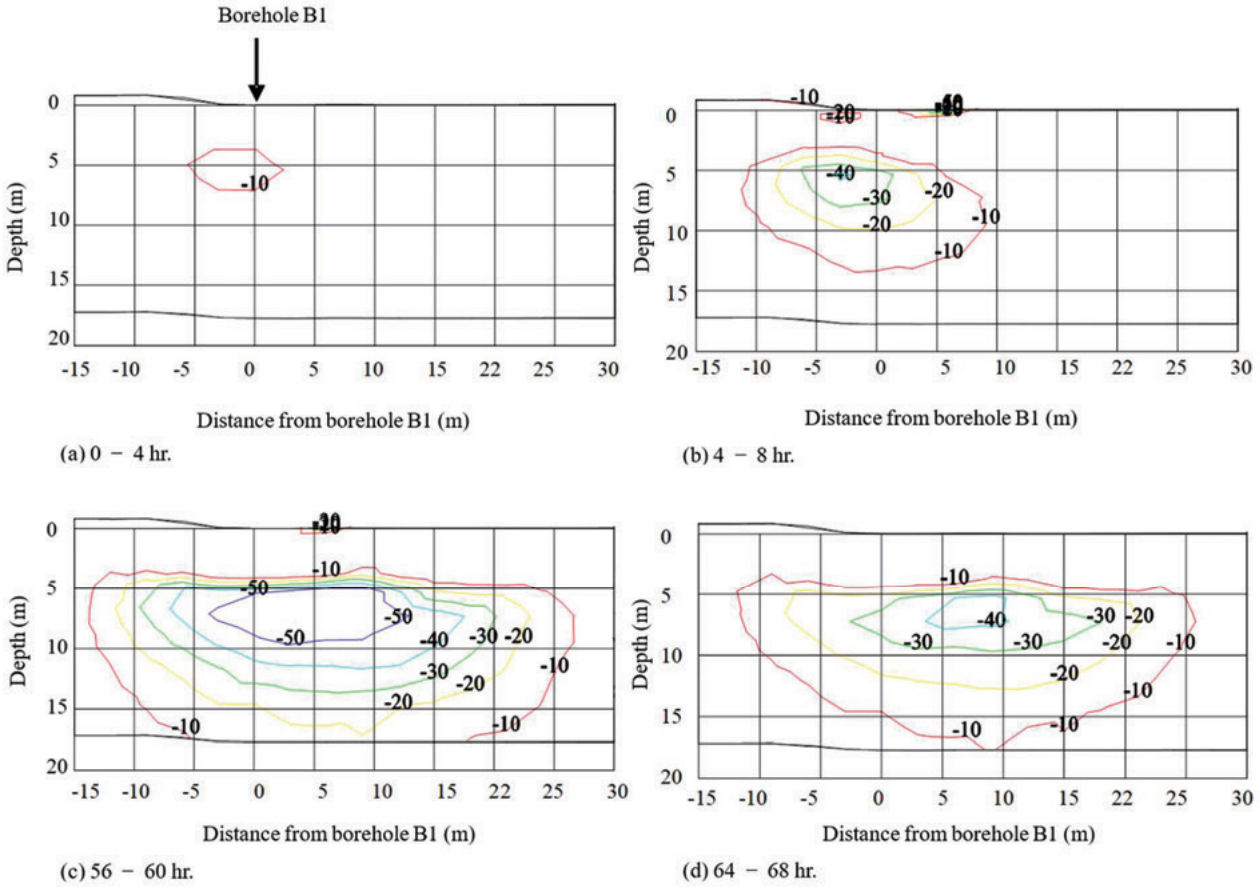

Fig.45 RCR contour lines along line B derived from 3D inversion of resistivity data collected **(a)** 1 – 4 hr., **(b)** 5 – 8 hr., **(c)** 57 – 60 hr. and **(d)** 65 – 68 hr. after the recharge experiment started.

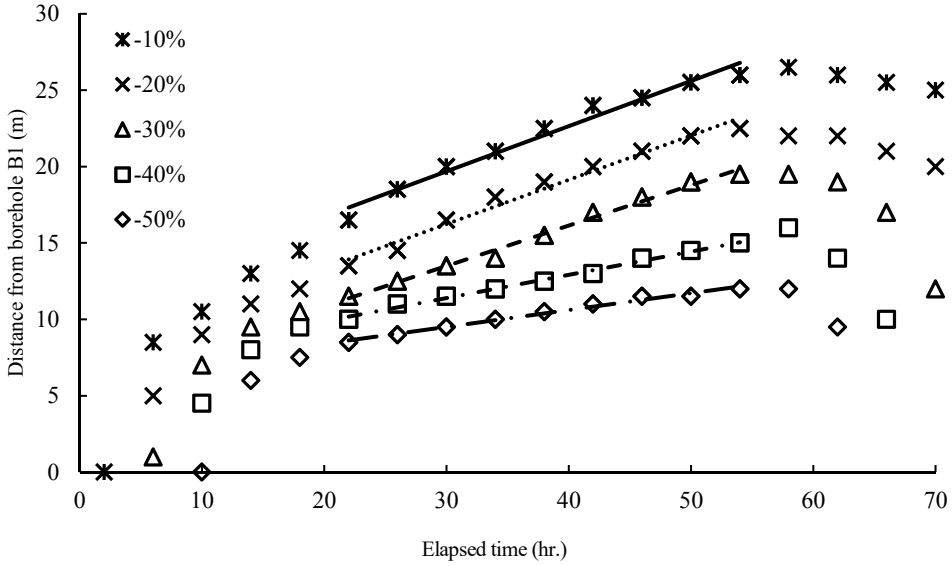

Fig.46 Distances of the RCR contour lines in **Fig.45** from borehole B1 at 7 m depth (positive to the right).

reflects a gradual migration of water away from the site.

The time-lapse volumes derived from the RCR distributions are illustrated in **Fig.48**. In the early stage of the experiment, −30% RCR appeared beneath the recharge areas RA1 and RA2 in **Fig.48 (a)** and extended from near the west corner of recharge area RA1 to near line A in recharge area RA2. This volume increased during the recharge experiment, and −40% RCR appeared 20 hr. after the recharge experiment started in **Figs.48 (b)** and **(c)**. Then, the volume in **Fig.48 (d)** diminished with time after the recharge experiment was completed.

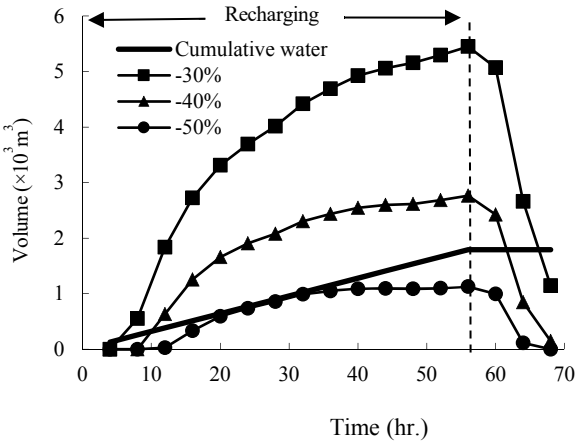

Fig.47 Cumulative water supplied (thick line) and variations in volumes of RCR of −30% (rectangles), −40% (triangles), and −50% (circles) in the recharge experiment.

5.4 Discussions

In this chapter, resistivity and RCR distributions were obtained in an artificial groundwater recharge experiment to monitor groundwater flow in a pyroclastic plateau. The geological setting in the experiment site was deduced from the resistivity distribution inverted from resistivity survey data that were obtained before the recharge experiment. The resistivity distribution showed an almost 1D layered structure shown in **Fig.41** and corresponded well with the log of the four boreholes along line B shown in **Fig.18**. Such a layered structure may be recovered successfully even with the 2D inversion method.

In the recharge experiment, soil resistivity changed with time because of the changes in the saturation level in the vadose zone. The zone where resistivity decreased significantly was derived from the 3D inversion shown in **Fig.43 (a)**, and appeared much narrower than that from the 2D inversion shown in **Fig.43 (b)**. This observation coincides well with the change in θ observed in borehole B1 shown in **Fig.43 (c)**. Newman et al. (2003) showed that 3D inversion tends to focus on anomalies. Batlle-Aguilar et al. (2009) reported that a 3D inversion method is more suitable to describe infiltration under an infiltrometer disc. However, the depth of the maximum resistivity change was 5 m according to the 2D results and matches well with that of the maximum change in θ observed in borehole B1, where θ was maximum at a depth of 5.5 m shown in **Fig.44 (c)**.

Since groundwater flow may cause environmental problems such as leakage from paddy fields or slope failure, an estimate of water flow velocity is very important for the

assessment of the problem. However, the estimate of the water flow velocity is difficult, because the water flow velocity also depends on pressure heads and water content, which are difficult to measure in the field. In this chapter, the velocities of expansion of the decreased-resistivity volumes were estimated in the secondary Shirasu layer as shown in **Fig.46**.

The change in the RCR volume over time can be used to generate a 3D image of the recharged water spreading in the vadose zone as shown in **Fig.48**. This feature is useful for visualizing the recharge process in the vadose zone. To detect a preferential flow in the ground, one or more of direct sampling methods (Ritsema and Dekker, 2000), tensiometry, TDR (Huisman et al., 2002), or GPR (al Hagrey and Müller, 2000; Huisman et al., 2001; Garambois et al., 2002) are often utilized. Since 3D inversion of resistivity data can give 3D geological information non-invasively, it can be used to conduct a feasibility study before a quantitative investigation.

Since one cycle of 2D resistivity survey data was collected in order from lines A to D and required 1 hr. for each line, the resultant RCR distribution for lines A to D contains some variation in resistivity over the total 4 hr. interval. When multiple-line survey data are used for inversion, the data acquisition time should be considered. Many approaches have been suggested previously to take account for data acquisition time (Day-Lewis et al., 2003; Kim et al., 2009, 2011; Karaoulis et al., 2011).

In this chapter, we examined four 3D RCR distributions derived from 2D survey data measured after 3 – 7 hr., 4 – 8 hr., 5 – 9 hr. and 6 – 10 hr. We can see that the volume of −30% RCR close to line D is larger in **Fig.49 (b)** than in **Fig.49 (a)**, whereas those close to the other lines are almost the same between the two figures. This is because the image close to line D in **Fig.49 (b)** is mainly reconstructed from data acquired 4 hr. later than the data in **Fig.49 (a)**, whereas the images close to the other lines are recovered from the same data. Similarly, the volume close to line B is larger in **Fig.49 (d)** than in **Fig.49(c)**. Thus, the time-lapse RCR images display the water spreading in the vadose zone. Furthermore, the RCR distribution in **Fig.49 (d)** has the same heterogeneous tendency as that in **Fig.49 (b)**, although the west side was measured after the east side. These results indicate that the heterogeneous RCR distribution mainly reflects a non-uniform water flow in the soil shown in **Fig.22** rather than the difference in measurement times.

Little resistivity change was observed in the first layer shallower than 4 m. This suggests that little change occurred in the saturation level at that depth range, although a high volume of water was supplied through the recharge areas. By contrast, the zone of decreased resistivity spread horizontally

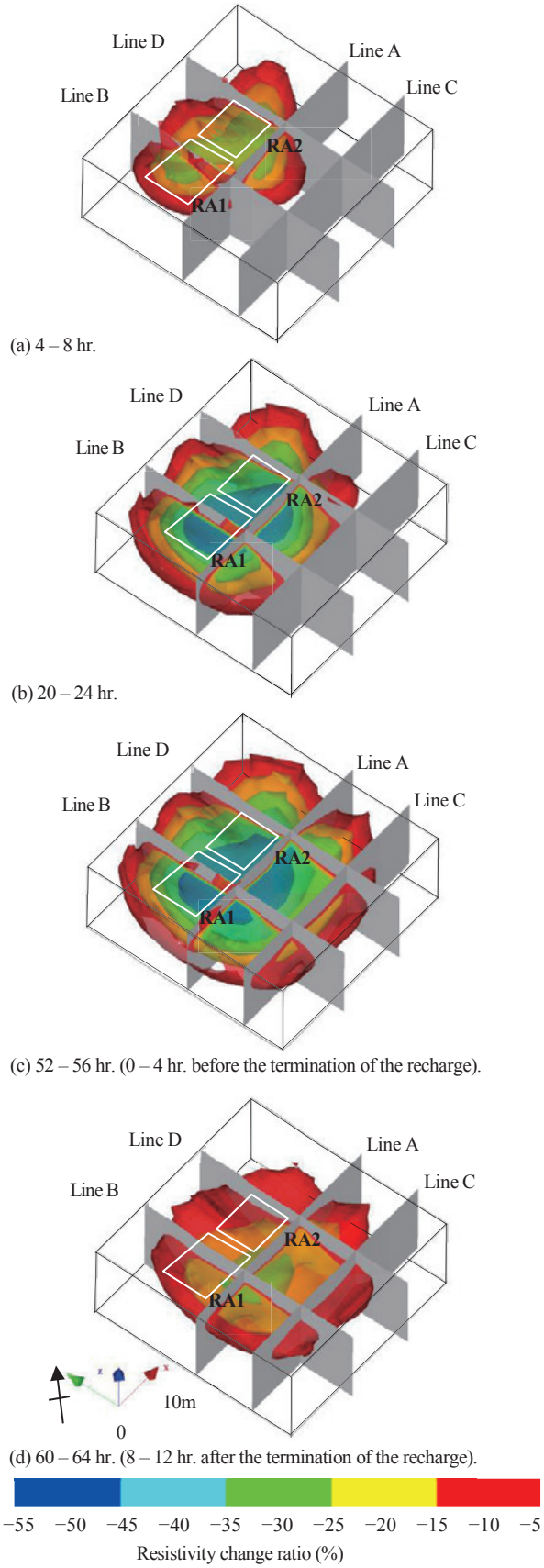

Fig.48 Change in the volume of resistivity change ratio derived from 3D inversion of resistivity data measured **(a)** 4 – 8 hr., **(b)** 20 – 24 hr., **(c)** 52 – 56 hr. and **(d)** 60 – 64 hr. after the recharge experiment started.

during the recharge experiment in a layer beneath the first layer, which had been observed to be a high-resistivity zone before the experiment in **Fig.41**. Consequently, we can conclude that a clear image of infiltration in the secondary Shirasu layer (3 – 7 m depth) is obtained from the RCR distribution. It should take at least 24 hr. for soil water to migrate 3 m in the loam layer with its low hydraulic conductivity, whereas the resistivity of the secondary Shirasu layer starts to change less than 4 hr. after recharging starts as shown in **Fig.42 (a)**. This implies that a faster flow than that expected from the measured hydraulic conductivity has occurred in the loam layer. It may be preferential infiltration, as observed in the recharge areas during the recharge experiment. This preferential flow may cause little change in the saturation level of the loam layer.

5.5 Conclusions

In this chapter, the distribution of resistivity changes was derived from 3D inversion of resistivity data collected in an

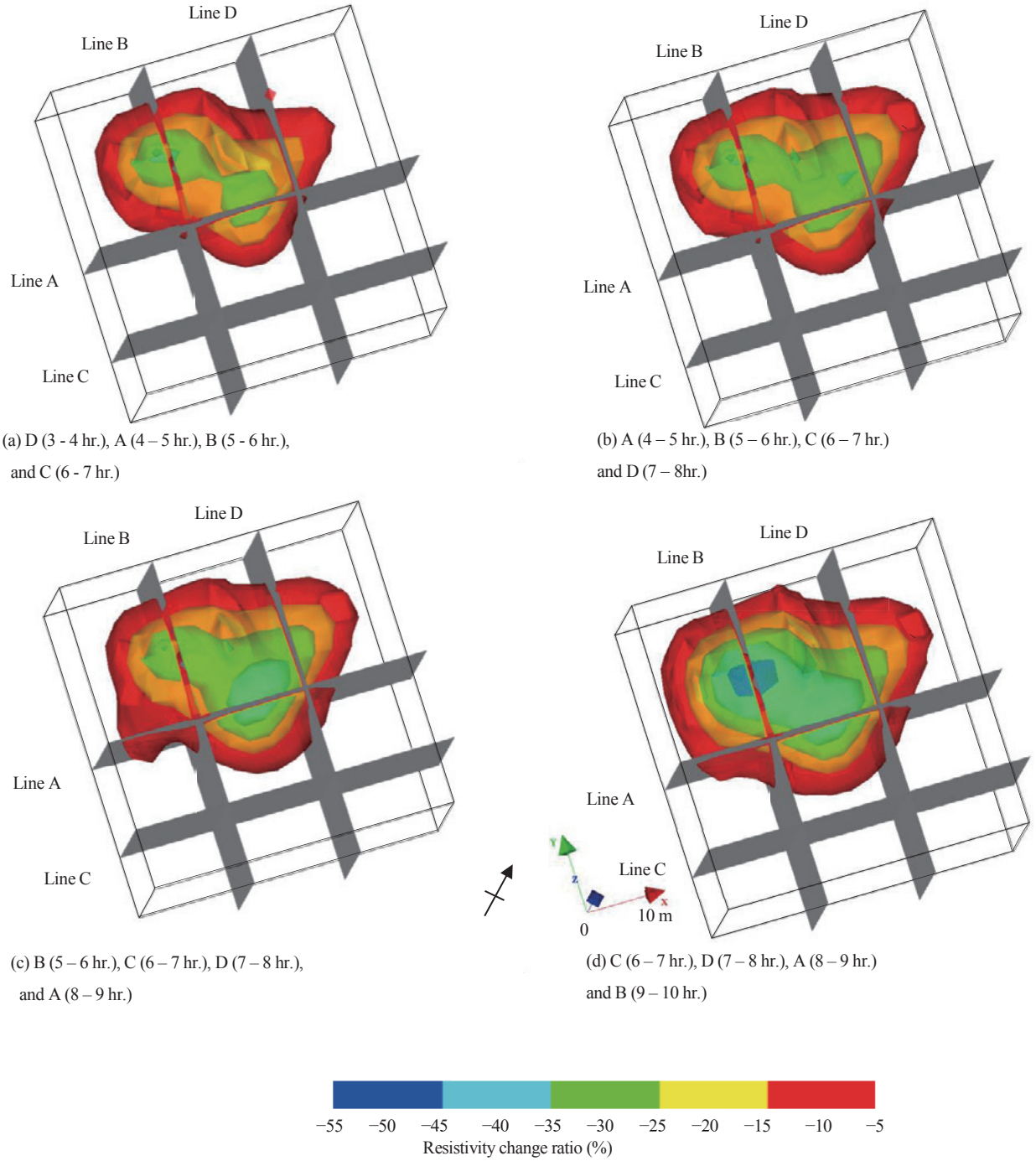

(a) D (3 - 4 hr.), A (4 – 5 hr.), B (5 - 6 hr.), and C (6 - 7 hr.)

(b) A (4 – 5 hr.), B (5 – 6 hr.), C (6 – 7 hr.) and D (7 – 8hr.)

(c) B (5 – 6 hr.), C (6 – 7 hr.), D (7 – 8 hr.), and A (8 – 9 hr.)

(d) C (6 – 7 hr.), D (7 – 8 hr.), A (8 – 9 hr.) and B (9 – 10 hr.)

Fig.49 Change in the volume of resistivity change ratio derived from 3D inversion of resistivity data collected **(a)** 3 – 7 hr., **(b)** 4 – 8 hr., **(c)** 5 – 9 hr., and **(d)** 6 – 10 hr. after the recharge experiment started.

artificial recharge experiment. To save measurement time, 2D resistivity surveys were conducted, which required about 1 hr. per line. The 3D inversion results clearly showed a heterogeneous resistivity distribution in the vadose zone and changes in the saturation level, especially in the secondary Shirasu layer, during the recharge experiment. The 3D inversion of the 2D survey data was more suitable than the 2D inversion to describe the 3D phenomena associated with groundwater recharge. These results indicate that this method can be applied to monitoring of relatively fast infiltration in the vadose zone. However, the infiltration flow in the loam layer was hardly detected, because little change occurred in the resistivity. This indicates that little change occurred in the saturation level. This method may be useful when the target layer has low saturation before the recharge experiment. Further investigations using other indicators such as changes in water resistivity are required to understand the groundwater flow in the loam layer.

6. Estimation of high hydraulic conductivity locations through 3D simulation of water flow in soil and resistivity survey

In the preceding chapters, we described the method to estimate damaged zones using resistivity distributions from 2D and 3D inversions of 2D resistivity survey data. Since the infiltration is governed by infiltration phenomena, considering the water flow simulation may improve the results, because the constraint is added to the resistivity structure.

This chapter describes a method that uses 3D simulation data of soil water flow and 2D resistivity survey data during a groundwater recharge experiment to estimate high hydraulic conductivity locations. First, we show the difficulty in estimating the infiltration path from the inversion of the 2D resistivity survey data. Next, proposed method is described in detail. Finally, numerical and field experiments are conducted to evaluate this method.

6.1 Introduction

The high hydraulic conductivity zone of soil often leads to problems such as leakage of water from a reservoir or a paddy field and slope failures after heavy rain. It is difficult to estimate such high hydraulic conductivity locations. Although a change in resistivity using 3D inversion of 2D resistivity survey data before and after infiltration provides a 3D image of the water flow, the high hydraulic conductivity zone cannot be obtained because of the inherent limitation of the observation data, i.e., number of measurements, time represented and measuring sensitivity. However, a method that uses data from resistivity surveys and seepage analyses would be effective because a resistivity change is caused by the water flow in soil and the water flow is governed by the seepage phenomenon. Estimation methods of water flow model are developed, which compares the water content converted from inversion of resistivity survey data with water content simulated from hydraulic models (Farzamian et al., 2015a; 2015b; Li et al., 2015). Although this method provides not only the image of the water flow but also the properties of the hydraulic conductivity, the resistivity obtained from inversion remains uncertain because of spatially varying resolution. Thus, comparing of water content values converted from resistivity with those from water flow simulations includes a 3D inversion uncertainty. However, according to the coupled approach, the observed apparent resistivity data are directly used for determining the hydrological properties (Looms et al., 2008; Huisman et al., 2010; Takeshita et al., 1995). In this method, water content simulated from water flow analysis is converted to a resistivity model, and then apparent resistivity data are created by the simulated survey. The simulated apparent resistivity data are compared with the field observations to estimate the hydraulic properties. This method can reduce the spatial uncertainty of the 3D invasion, because the resistivity model is constrained by the seepage analysis data. One dimensional hydraulic properties were inverted from 1D water flow simulations (Looms et al., 2008), and 2D hydraulic properties were inverted from Bayesian and multi-criteria inversion (Huisman et al., 2010) or from neural networks (Takeshita et al., 1995). However, few studies investigated 3D hydraulic properties using 3D water flow simulation and 3D resistivity survey data, because reconstruction of the 3D conditions is complex, and there are many unknown parameters. Since the resistivity obtained from inversion can provide an approximate image of infiltration, making certain assumptions in terms of infiltration can reduce the unknown parameters.

This chapter proposes a simple method to estimate high hydraulic conductivity locations in the shallow soil layer, which causes many hydraulic problems in the field. This method assumes that fast infiltration occurred in the first layer and compares observed field resistivity data with 3D simulated apparent resistivity data based on the volumetric water content, which are obtained from possible 3D water flow models. First, we introduce a survey data, which were obtained through a resistivity monitoring of groundwater recharge experiment, and show the difficulty in estimating the infiltration path from the inversion of the 2D resistivity survey data. Next, proposed method is described in detail.

Finally, numerical and field experiments are conducted to evaluate this method.

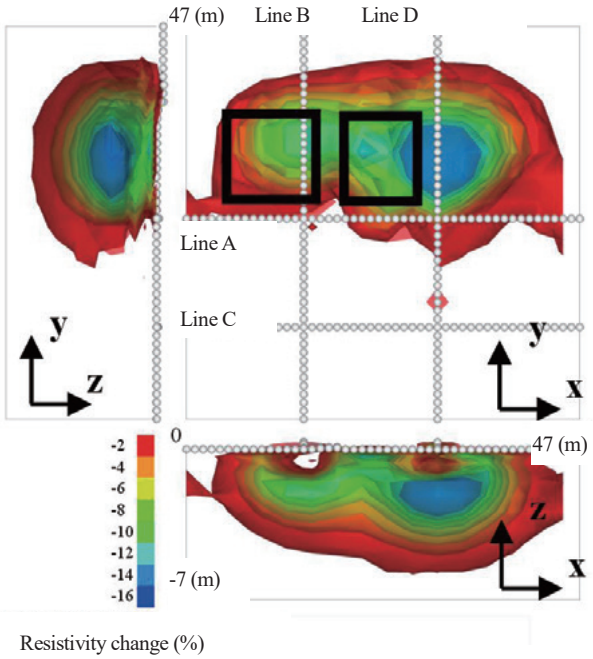

Fig.50 Isosurfaces of resistivity change derived from 3D inversion of 2D resistivity data measured 0 – 4 hr. after the recharge experiment started displaying surfaces of constant data value in three dimensions. The transparency level of the isosurfaces is set to 50% to display inner isosurfaces that are obscured by ouater isosurfaces. Figures with *x*-*y*, *z*-*x* and *y*-*z* axis are views from *z*, *y* and *x* directions, respectively. Open circles show electrodes.

6.2 Methods

Chapter 3 described time-efficient multiple 2D resistivity surveys during an artificial recharge of groundwater in a pyroclastic plateau in Kagoshima Prefecture. Dipole–dipole resistivity surveys were continuously performed during the recharge along the four lines shown in **Fig.17**. Chapter 5 estimated the time-lapse 3D resistivity change distributions during the recharge experiment. **Figure 50** shows the distribution of resistivity change derived from 3D inversion with 2D resistivity survey data 0 – 4 hr. after the recharge started. The 3D inversion showed a resistivity change in the secondary Shirasu layer during the early stage. The results revealed that a flow in the loam layer was faster than that expected from the saturated hydraulic conductivity measured near the site. This tendency of the resistivity change zone as shown in **Fig.50** matched with that of the filling water zone as shown in **Fig.22**. However, the resistivity changes showed a donut-like shape around the resistivity survey lines, and the maximum changes were not under the filling water zones. The location of the maximum change in resistivity was below the survey lines B and D. From these results, the location of the preferential infiltration was unclear. To identify the infiltration location more precisely and reduce the above problems, where the resistivity change indicates a donut-like shape and does not correspond to the location of infiltration area, this chapter introduces a new methodology proposed in the next section to combine the resistivity data and 3D seepage analysis.

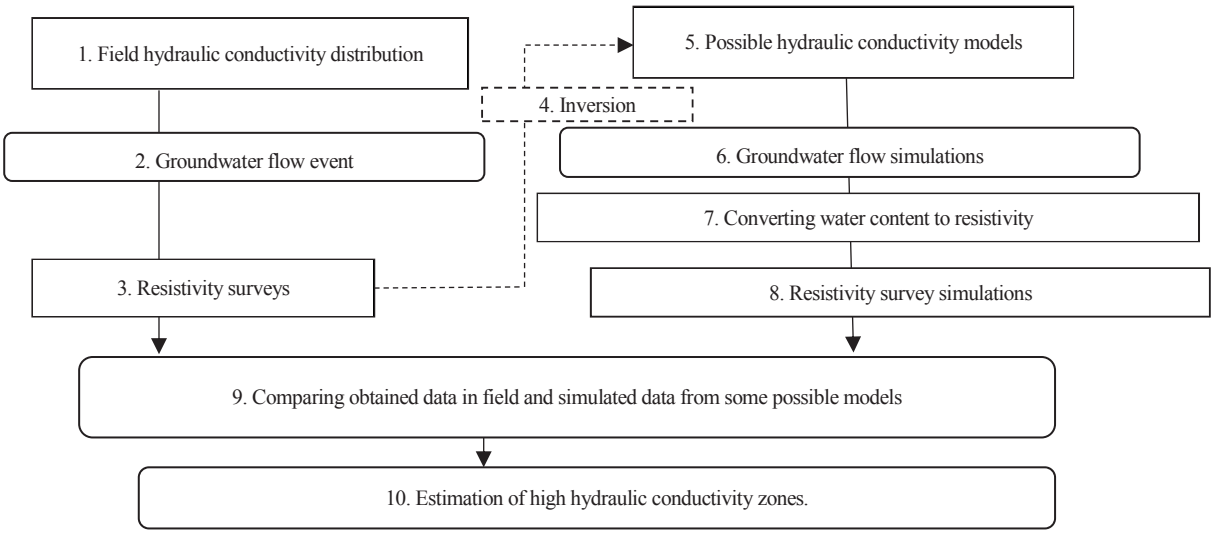

Fig.51 Flow to estimate high hydraulic conductivity zones.

6.2.1 Flow to estimate the location of infiltration

Figure 51 shows the flow to estimate high hydraulic conductivity zones from groundwater-recharge experimental data. There is an unknown hydraulic conductivity distribution in a field. During a groundwater flow event, resistivity surveys are conducted. A resistivity changes are derived from 3D inversion of 2D resistivity survey data and some possible hydraulic conductivity models are assumed. Distributions of volumetric water content are simulated by saturated-unsaturated seepage analysis and are converted to resistivity models. Resistivity survey simulations are conducted with the resistivity models and an optimum model is estimated comparing obtained data in field and simulated data from the possible models.

6.2.2 Analysis of saturated-unsaturated seepage

Using FEM, volumetric water content can be calculated with a hydraulic conductivity model. The partial differential equation governing the behavior of the pressure head is described (Nishigaki, 2001) by

$$\frac{\partial}{\partial x_i}\left\{K_{\mathrm{r}}\left(K_{ij}^{S}\frac{\partial \psi}{\partial x_j}+K_{i3}^{S}\right)\right\}-q=\left(\beta S_{\mathrm{s}}+\frac{\partial \theta}{\partial \psi}\right)\frac{\partial \psi}{\partial t} \tag{18}$$

β = (0 : unsaturated region, 1 : saturated region)

where the subscripts i and j are space direction indicates 1, 2 and 3, the Einstein summation convention is used, K^s is the saturated hydraulic conductivity (m/s), K_{r} is the relative hydraulic conductivity (m/s), ψ is the pressure head (m), t is time (s), q is the source (m^3/s), S_{s} is the storage-coefficient and θ is volumetric water content. In this study, AC-UNSAF3D (Nishigaki, 2001) is used to calculate the water head pressure and volumetric water content.

6.2.3 Converting volumetric water content to resistivity

Archie (1942) developed an empirical formula for the effective resistivity of a formation rock, which considers porosity, ϕ, water saturation of pores, S_{r}, and water resistivity, ρ_{w}, as shown in Equation (1). If ϕ, ρ_{w}, the constants, temperature and geological settings remain constant, resistivity change is occurred by water saturation change. In the recharge experiment, the change in the water saturation is the main factor of resistivity change since resistivities almost never change because of other factors. In the survey site, soil temperature is expected to not change at a depth of 1 m deeper. Since saturation and volumetric water content express a direct proportion using equation:

$$S_{\mathrm{r}}=\frac{\theta}{\phi} \tag{19}$$

resistivity change may be converted from volumetric water content change calculated using the seepage analysis. In this study, the resistivity decrease is converted from the volumetric water content increase using equation:

$$\rho_{s_t}=\rho_{s_0}-\frac{\theta_t-\theta_0}{\theta_0}\times\frac{\dfrac{\rho_{s_{\max}}-\rho_{s_{\min}}}{\rho_{s_{\min}}}}{\dfrac{\theta_{\max}-\theta_{\min}}{\theta_{\min}}} \tag{20}$$

where ρ_{s_t} is bulk resistivity at time t during the recharge experiment, ρ_{s_0} is the initial bulk resistivity before recharge experiment, θ_t is volumetric water content at time t, θ_0 is the initial volumetric water content, $\theta_{\max}$ and $\theta_{\min}$ are the maximum and minimum volumetric water content measured near the field (Nakano et al., 1981), respectively, and $\rho_{s_{\max}}$ and $\rho_{s_{\min}}$ are the resistivities derived from 3D inversion before the recharge started shown in **Fig.41 (b)** and when the recharge stopped shown in **Fig.48 (c)**, respectively. Although resistivity and water saturation are not proportional, the maximum change in resistivity is assumed to correspond to the maximum change in volumetric water content for simplicity of converting. The decreased resistivity is added to the initial resistivity, which is derived from the resistivity survey data before the recharge shown in **Fig.41 (b)**.

6.2.4 Resistivity survey simulation and inversion

The electric potentials can be calculated for the resistivity model using FEM. The partial differential equation governing the behavior of the electric potential is described by Poisson's equation (2). In the inversion of resistivity, the model parameters are updated to fit the calculated data to the observation. In general, a resistivity change is estimated from two resistivity distributions using apparent resistivity data obtained before and after the resistivity change. However, this approach may not identify a resistivity change accurately due to the different noise levels at each measurement and the different convergence levels at each inversion. To reduce these influences, LaBrecque and Yang (2001) presented difference inversion and Daily et al. (2004) described ratio inversion. In this study, to estimate a resistivity change, normalized apparent resistivity data (Sugimoto, 1995; Inoue et al., 2016) are used for the inversion. E-Tomo 3D (Sugimoto, 1995) is used to simulate the observed apparent resistivity data and to conduct the 3D inversion of resistivity.

6.2.5 Comparison between observed and simulated resistivity data

The observed apparent resistivity data are compared with the simulated apparent resistivity data from resistivity models that are converted from the volumetric water content simulated for possible hydraulic models. Let j be number of the possible models, the total error E_k between observed

data and simulated one for possible hydraulic model k (k= 1,⋯, j) is calculated by

$$E_k=\sum_{i=1}^{N}\left(\frac{d_i^{\mathrm{obs}}-d_i^{\mathrm{sim}}}{d_i^{\mathrm{obs}}}\right)^2 \quad (k=1,\cdots,j) \qquad (21)$$

where d_i^{obs} is the observed apparent resistivity data, d_i^{sim} is simulated apparent resistivity data and N is the number of observations in the apparent resistivity data.

6.3 Results

In the resistivity survey during the recharge experiment, the high hydraulic conductivity zones were expected to be located in a recharge area, but their location was difficult to be estimated solely from the 3D inversion of the 2D resistivity survey data. In this study, a numerical experiment and a field application are conducted for the survey site.

6.3.1 Experiment of groundwater flow and resistivity survey simulation

In the numerical experiment, a field model that has a high hydraulic conductivity zone in a recharge area at first layer is considered assuming the survey site. **Figure 52** shows a numerical model of seepage analysis. According to the survey site as described in chapter 5, three layers have different hydraulic conductivity, and Layer 1, 2 and 3 correspond to the loam layer, the secondary Shirasu layer, the Shirasu layer, respectively. Two recharge areas (RA1 and RA2) were configured, and RA1 was divided into nine columns (3 × 3) and RA2 was divided into six columns (3 × 2). Since high hydraulic conductive zones were expected in the survey site, one high hydraulic conductivity zone in layer 1 was located in each recharge area and the hydraulic conductivity in this zone was set to ten times higher than the hydraulic conductivity of layer 1. All nodes were set to −10 m of the total hydraulic head at the initial conditions, because the groundwater level was estimated to be deeper than 10 m at the survey site. The boundary condition included an impermeable boundary, and the surface nodes in the recharge area were set to the pressure head of 0.3 m during the recharge, because the recharge areas were surrounded by plastic plates buried 0.3 m in depth and the water level was less than 0.1 m. The water characteristic curve, which is the relationship between the unsaturated hydraulic conductivity and the water pressure head with the volumetric water content used in the seepage analysis, are shown in **Fig. 53**, and the relationship were based on the unsaturated flow examination conducted near the survey area (Nakano et al., 1981). The smallest mesh size is 3 m in the horizontal direction and 1 m in the vertical direction. The mesh size is same with the grid size of resistivity inversion with the purpose of easily converting water content to resistivity, although this mesh size might be not enough for a water flow simulation.

Table 8 The conditions of an 2D resistivity survey.

Number of electrodes	48
Electrode spacing	1 m
Line length	47 m
Number of data	698
Electrode configuration	dipole-dipole array
Measuring time	1 hr.

In **Fig.52**, white dotted lines show four resistivity survey lines. Resistivity models were converted from the volumetric water content models simulated by seepage analysis before and after the recharge started, and simulations of 2D resistivity surveys were conducted for the resistivity models. **Table 8** shows the conditions of an 2D resistivity survey. Resistivity change was derived from the 3D inversion of the four 2D survey line data.

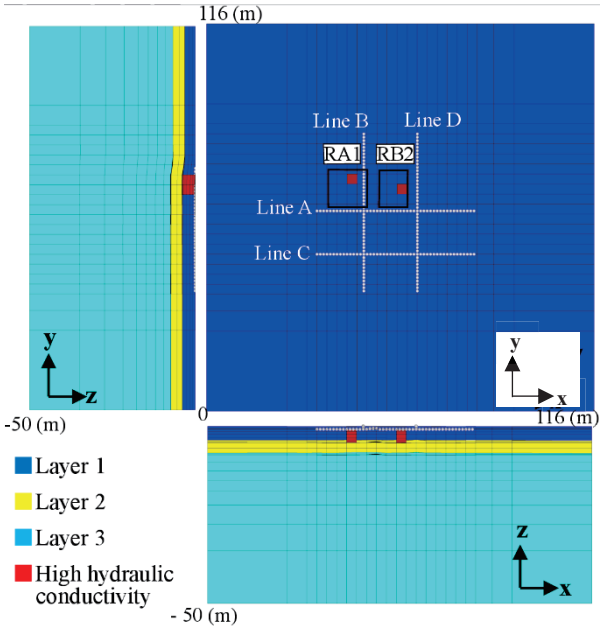

Fig.52 Projection view of FEM mesh for seepage analysis and resistivity survey lines. White dotted lines show four resistivity 2D resistivity survey lines. The smallest mesh size is 3 m in the horizontal direction and 1 m in the vertical direction. This mesh size is same with grid size of inversion of resistivity and it is easy to convert water content to resistivity. All nodes are initially set at −10 m of the hydraulic total head. Surface nodes in the recharge areas have the pressure head at 0.3 m during the recharge experiment. The surface of the site is inclined slightly from north-west to south-east.

Figure 54 shows distribution of water pressure heads simulated with the numerical field model 1 to 4 hr. after the recharge experiment started in **Fig.52**. The water pressure head increased primarily in the high hydraulic conductivity zones, and the increased zone spread vertically and horizontally. The volumetric water content can be converted from the water pressure head by water characteristic curve in **Fig.53**.

Figure 55 shows distribution of resistivity changes 4 hr. after the recharge started in the numerical field model. **Figure 55 (a)** shows the change in resistivity converted from the volumetric water content 4 hr. after the recharge started in **Fig.54 (d)**, against the values before the recharge started. The resistivity changes at layer 2 are higher than those at layer 1, because water characteristic curves of each layer are different, and the increases in volumetric water content at layer 2 are higher than layer 1, although the water pressures are almost same at layers 1 and 2 as shown in **Fig.54 (d)**. **Figure 55 (b)** shows the change in resistivity inverted from the resistivity survey data simulated for the water content 0 – 4 hr. after the recharge started in **Figs.54 (a)** – **(d)**, against the values before the recharge started. **Figure 56** shows resistivity changes 4 hr. after the recharge started in a model of no high hydraulic conductivity zone in layer 1. **Figures 55 (a)** and **56 (a)** present true changes in resistivity and **Fig.55 (b)** and **56 (b)** present changes in resistivity from 3D inversions. In **Fig.55 (b)**, the resistivity decreased near the high hydraulic conductivity zones and resistivity change of −10% was observed at a depth of 3 m deeper, although, in **Fig.56 (b)**, resistivity change is less than −3%, and there is no change below the survey line B. **Figure55 (b)** also shows a donut-like shape of resistivity change around the resistivity survey line, and the maximum resistivity change in **Fig.55 (b)** is not in the location where water content has maximum change in **Fig.55 (a)**. The location of the maximum change in resistivity is below the survey line.

Figure 57 compares high hydraulic conductivity models. **Figure 57 (a)** is the field model shown in **Fig.52**, and **Figs.57**

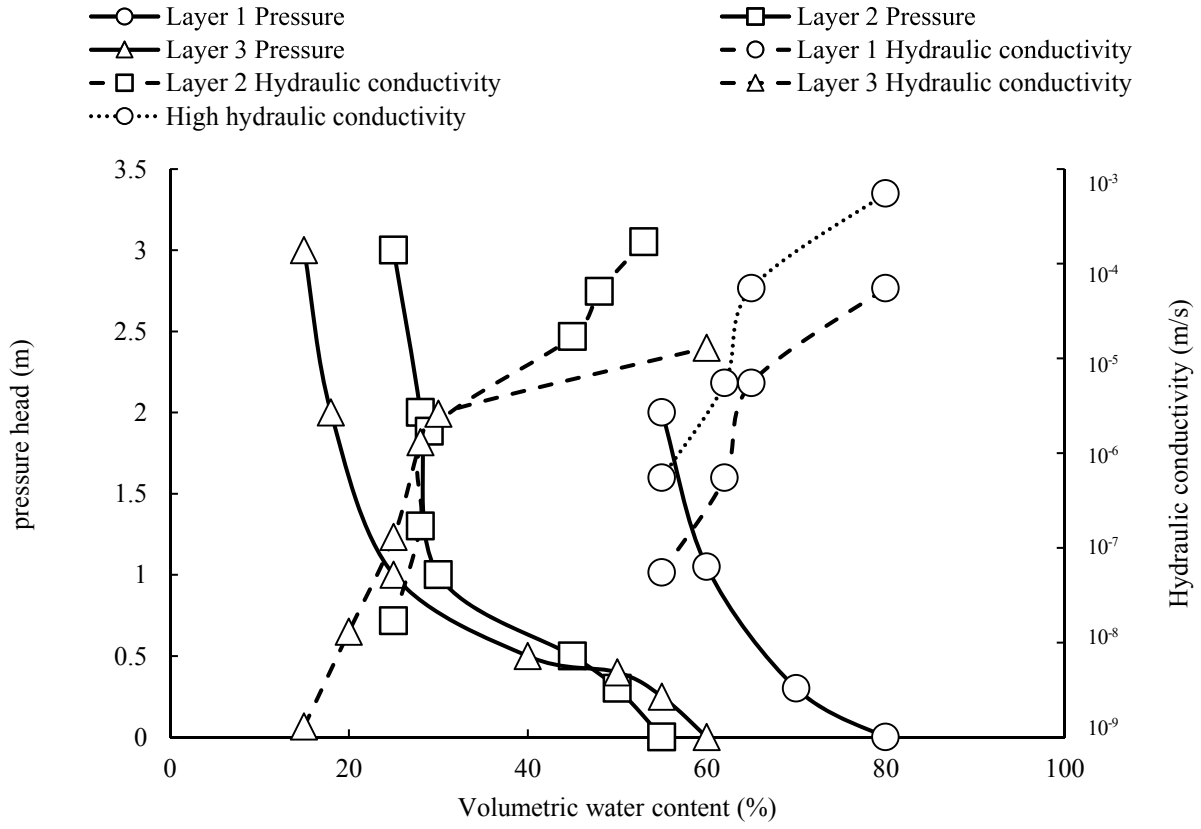

Fig.53 Relationship between the unsaturated hydraulic conductivity and the water pressure head against the volumetric water content used in the seepage analysis. The relation is based on the unsaturated flow examination conducted near the survey area (Nakano et al., 1981) and high hydraulic conductivity in layer 1 is assumed to be ten times higher than the hydraulic conductivity of the layer 1.

(b) and **(c)** are other field models. **Figure 57 (d)** is the location number in recharge areas, and the location *k* is the high hydraulic conductivity location at possible model *k* (*k*= 1, ⋯,15). Possible model 1 has a hydraulic conductivity zone at location 1, possible models 2 – 15 have a hydraulic conductivity zone at location 2 – 15, respectively. Field models 1, 2 and 3 shown in **Figs.57(a)**, **(b)** and **(c)** have two hydraulic conductivity zones at locations 6 and 14, 2 and 10, and 13 and 4, respectively. **Figure 58** shows total errors between the observed apparent resistivity data from the field models and the simulated apparent resistivity data from 15 possible models. The contour level at location 1 in **Fig.58 (a)** indicates the total errors between the observed data in the field model 1 and the simulated data in possible model 1. The contour levels at locations 2 – 15 indicate the errors between the field model 1 and possible models 2 – 15,

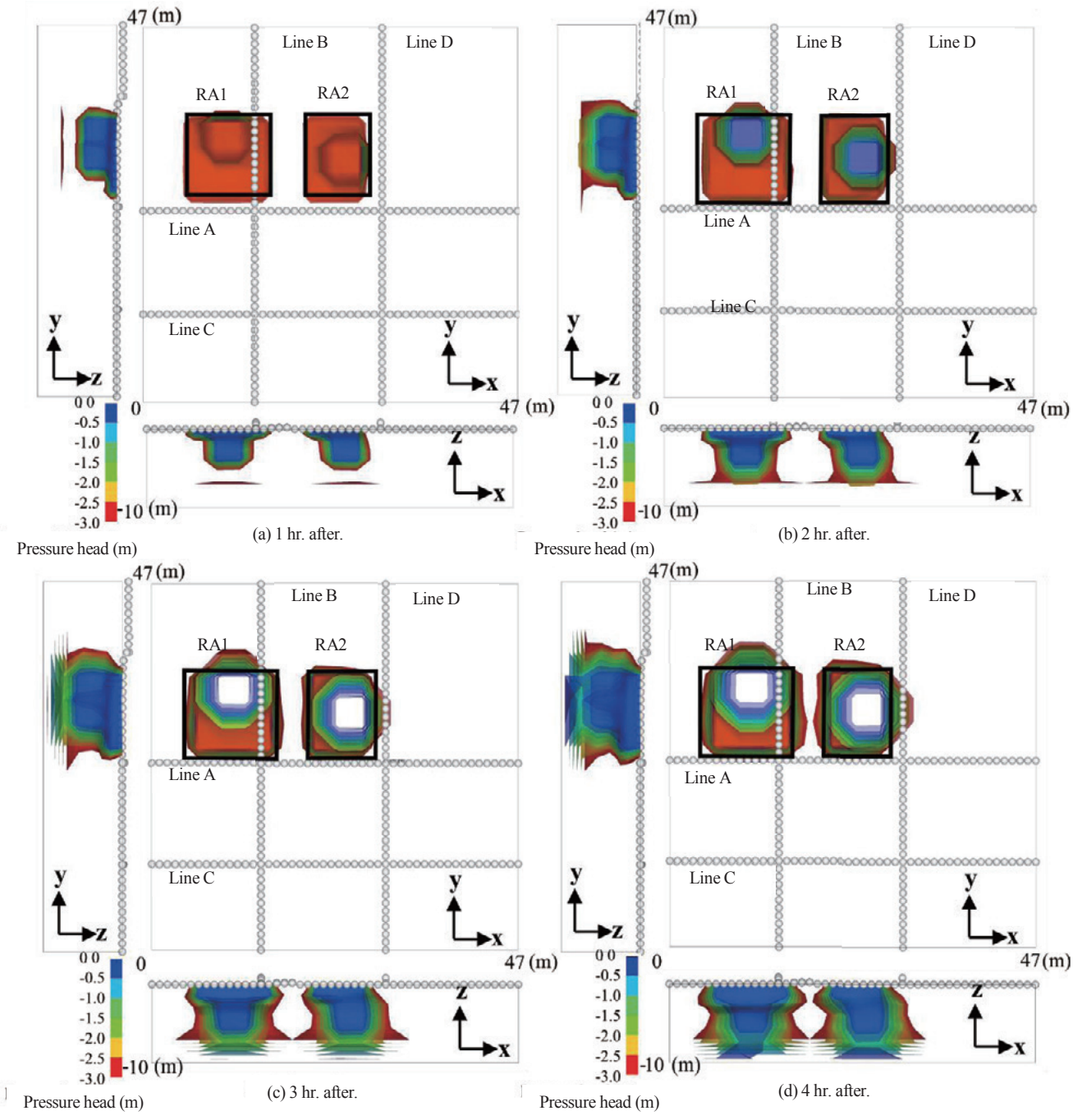

Fig.54 Isosurfaces of pressure head at **(a)** 1 hr., **(b)** 2 hr., **(c)** 3 hr. and **(d)** 4 hr. after the recharge started. displaying surfaces of constant data value in three dimensions. The transparency level of the isosurfaces is set to 50% to display inner isosurfaces that are obscured by outer isosurfaces. Figures with *x*-*y*, *z*-*x* and *y*-*z* axis are views from z, y and x directions, respectively. Open circles show electrodes.

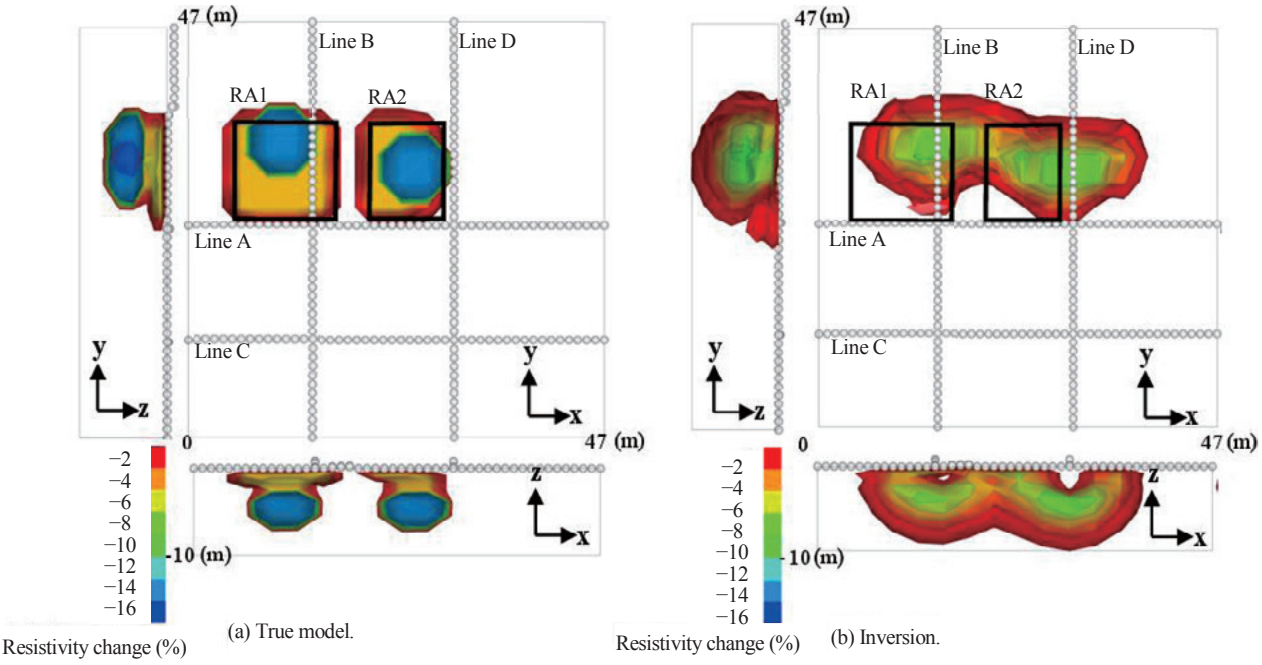

Fig.55 Isosurfaces of resistivity change in the numerical field model shown in Figure 6.3: (a) converted from pressure head at 4 hr. after the recharge experiment started, (b) inverted from resistivity data simulated for the water content 0–4 hr. after the recharge started displaying surfaces of constant data value in three dimensions. The transparency level of the isosurfaces is set to 50% to display inner isosurfaces that are obscured by outer isosurfaces. Figures with *x*-*y*, *z*-*x* and *y*-*z* axis are views from *z*, *y* and *x* directions, respectively. Open circles show electrodes.

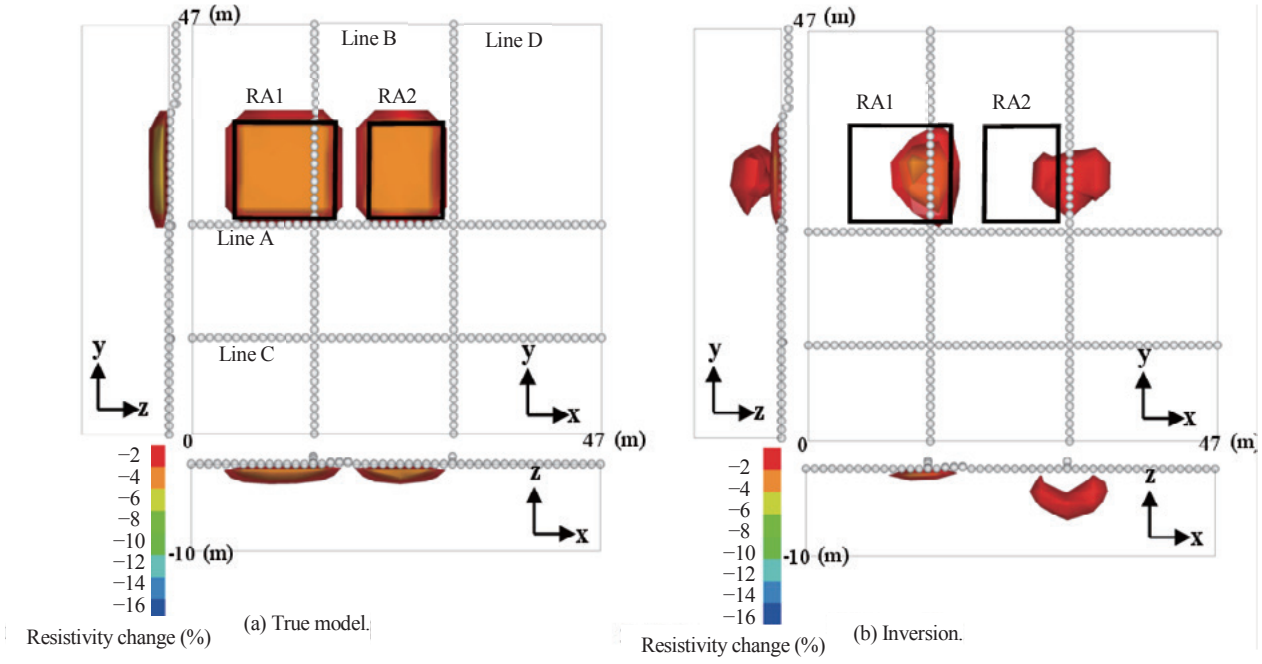

Fig.56 Isosurfaces of resistivity change in the model of no high hydraulic conductivity, (a) converted from pressure head at 4 hr. after the recharge experiment started, (b) inverted from resistivity data simulated for the water content 0–4 hr. after the recharge started displaying surfaces of constant data value in three dimensions. The transparency level of the isosurfaces is set to 50% to display inner isosurfaces that are obscured by outer isosurfaces. Figures with *x*-*y*, *z*-*x* and *y*-*z* axis are views from *z*, *y* and *x* directions, respectively. Open circles show electrodes.

respectively. The minimum error zones in RA1 and RA2 are the locations 2 and 10, respectively. **Figures 58 (b)** and **(c)** plot total errors for the other field models. The minimum error zones in RA1 and RA2 correspond to the zones of high hydraulic conductivity. These results indicate that this method has sufficient sensitivity to seek the location of high hydraulic conductivity zone.

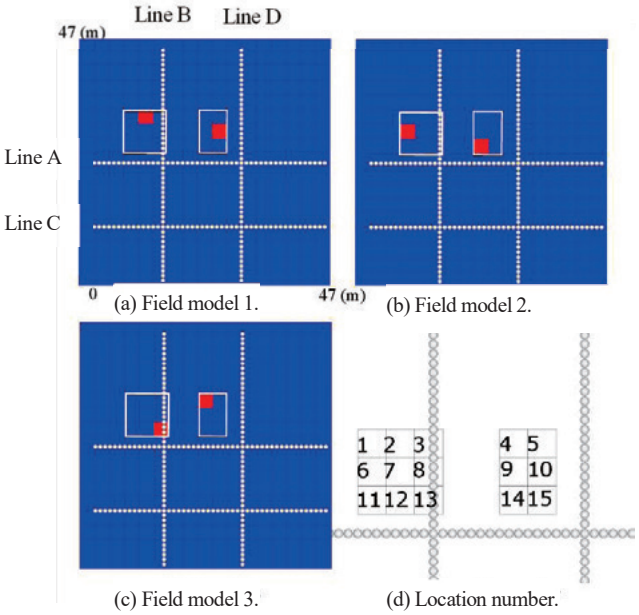

Fig.57 High hydraulic conductivity models. (a), (b) and (c) are numerical field models and (d) is the location number in recharge areas and the location of the high hydraulic conductivity zone at each possible model. Possible model 1 has a hydraulic conductivity zone at location 1, possible models 2 – 15 have a hydraulic conductivity zone at location 2 – 15, respectively. Field models 1, 2 and 3 have two hydraulic conductivity zones at locations 6 and 14, 2 and 10, and 13 and 4, respectively.

6.3.2 Application to the field data of groundwater flow and resistivity survey

The above method was applied to the field data of groundwater recharge experiment described in Chapters 3 and 5. **Figure 59** shows the total errors between the observed data in the field and the simulated data in the 15 possible models shown in **Fig.57 (d)**. In RA1, the total errors of the possible models 1, 2, 6 and 7 are lower than other models and the error in the possible model 2 is minimized. In RA2, the total error of the possible model 10 is minimized. The locations of minimum models coincide with the surface range filled with water 1 hr. after the recharge experiment started in RA1 and RA2 as shown in **Fig.22**, whereas the locations of large total errors coincide with the no filling water zone.

6.4 Discussions

In the numerical experiment, the resistivity decreased near the high hydraulic conductivity zones, and a resistivity change of −10% was observed at a depth of 3 m deeper in **Fig.55 (b)**, although, in the model of no high hydraulic conductivity zone, the resistivity change was less than −3%, and there is no change below the survey line B in **Fig.56 (b)**. These results indicate that the resistivity change derived from 3D inversion with four 2D resistivity survey data can reveal the existence and the approximate location of infiltration. However, the resistivity change exhibited a donut-like shape around the resistivity survey line, and the maximum change was not in the location where water content exhibited its maximum change. The location of the maximum change in resistivity was below the survey line. This reveals difficulty in estimating the precise location of infiltration from 3D inversion with 2D resistivity survey data. The reason is that

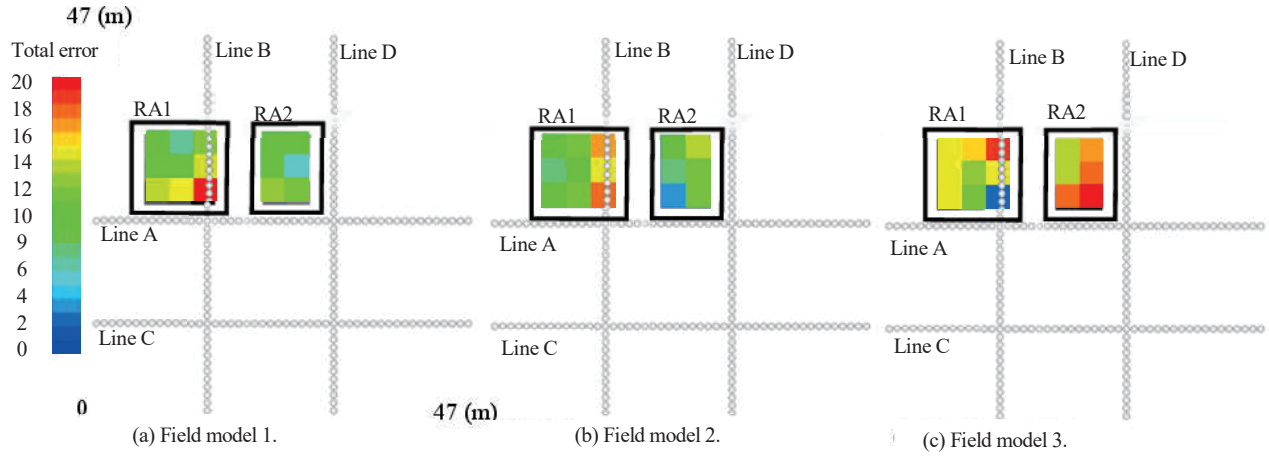

Fig.58 Total errors of observed resistivity data in (a) field model 1 in Figure 6.8 (a), (b) field model 2 in Figure 6.8 (b) and (c) field model 3 in Figure 6.8 (c) against resistivity data of 15 possible models shown in Figure 6.8 (d).

there is low constraint for inversion. More information is needed such as 3D resistivity survey data or water flow data. The reason of the donut-like shape around the resistivity survey line is that a 3D sensitivity distribution exhibits axial symmetry with respect to the survey line (Sasaki, 1994). A conductive body off the line in one side produces a low-resistivity artefact at a position equal to the offset distance in the other side as shown in Chapter 4.

By comparing the observed data from field models with the simulated data from the possible high hydraulic conductivity models, the high hydraulic conductivity location from minimum error models corresponded to the high hydraulic conductivity location from the field models. This result supports that the use of the total errors between the observed data and the simulated data from some possible high hydraulic conductivity model is feasible for identifying the location of the high hydraulic conductivity zone, whereas the resistivity change derived from the 3D inversion using 2D resistivity survey data cannot reveal the location.

In the field experiment, resistivity changes greater than −10% were observed at a depth of 3 m deeper in **Fig.50**, although in the model of no high hydraulic conductivity zone, resistivity changes more than −3% were not observed, and there is no change below the survey line B in **Fig.56 (b)**. The resistivity change under the survey line D in **Fig.56 (b)** may be caused by the resistivity change of −4% in the surface of RA2 shown in **Fig.56 (a)**. If the resistivity change of the surface in RA2 is high, the resistivity change below the survey line D can be high. However, there is no resistivity change under the survey line B in **Fig.56 (b)**, although resistivity changes were observed under the survey line B in **Fig.50**. This result indicates that resistivity changed in the secondary Shirasu layer and there was a high hydraulic conductivity zone in the loam layer. The zone of resistivity change matched with that of the filling water shown in **Fig.22** and the 3D inversion with 2D resistivity survey data revealed a trend of preferential flows. However, as described before, it is difficult to identify the location of high hydraulic conductivity zone using the resistivity change derived from 3D inversion with 2D resistivity survey data.

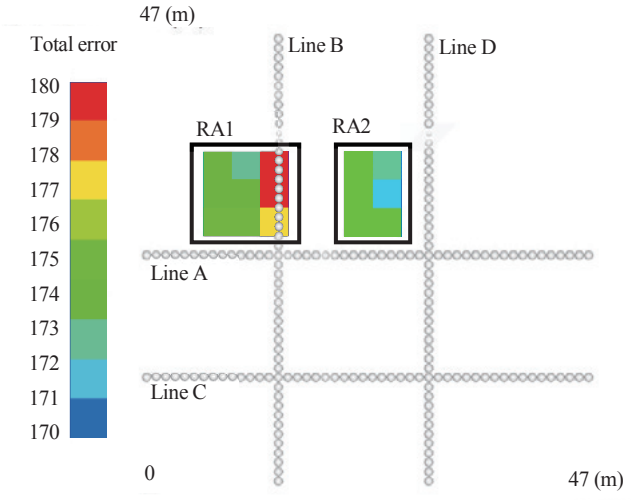

Fig.59 Total errors of the observed data in the field against 15 possible models.

The total errors were estimated between the observed data in the field and the simulated data in the 15 possible models. The locations of the high hydraulic conductivity zones with the minimum error model coincided with the surface zones filled with water 1 hr. after the recharge experiment started in RA1 and RA2, whereas the large total errors models coincided with the no filling water zone. This indicates that the total errors between the observed and the simulated data for some possible high hydraulic conductivity models can indicate the infiltration location.

In this study, hydraulic conductivity was assigned homogeneously in a layer, although it varied due to the heterogeneous geological conditions. It also requires a relationship between the hydraulic conductivity and the water pressure head with the volumetric water content. Direct inversion of hydraulic properties (Looms et al., 2008; Huisman et al., 2010; Takeshita et al., 1995) is a more objective way, however reconstructing the 3D conditions is complex, and there are many unknown parameters such as the shapes of water characteristic curve or its spatial varieties. Since infiltrations were expected from the 3D inversion of 2D resistivity data in this study, many conditions were assumed. Only one high hydraulic conductivity zone in a recharge area was expected at the first layer. If there are many high hydraulic conductivity zones in a first layer or the high hydraulic conductivity zone is narrow, the estimated location becomes unclear. In addition, the depth and the intensity of high hydraulic conductivity cannot be estimated with this method. It is also difficult to apply this method to a field, where there is no change in the water content, because there is no change in resistivity.

We aimed to estimate the location of infiltration, when infiltration is expected and the location is unclear. When an earthquake occurs, there are cracks under the paddy field and failures of filling water. This method can be applied to such cases for the effective repair of paddy fields.

6.5 Conclusions

To identify high hydraulic conductivity locations from the surface, a method to select hydraulic conductivity models was applied to both numerical and field experiments by comparing observed 2D resistivity survey data in field and simulated resistivity survey data for the volumetric water

content simulated from possible hydraulic conductivity models. In the numerical experiment, the 3D inversion of 2D resistivity surveys indicated the preferential flow and an approximate tendency of preferential flow zone. However, the infiltration locations were unclear. By assuming that high hydraulic conductivity zones exist in the first layer, the location of high hydraulic conductivity zone from minimum error model comparing with the 15 possible models of a high hydraulic conductivity zone corresponded to the high hydraulic conductivity location of the field model.

In the field experiment, resistivity surveys were conducted during groundwater recharge experiment in a pyroclastic plateau. The resistivity surveys provided image of the preferential flow. The high hydraulic conductivity location of the model that gave minimum errors corresponded to the zone of filling water, whereas that of the model that produced large errors corresponded to the zone of no filling water. These results suggest that estimation of high hydraulic conductivity location using simulation of groundwater flow and resistivity surveys is possible.

Although it is difficult to estimate the precise location of infiltration via 3D inversion using 2D resistivity survey data, the proposed method could estimate high hydraulic conductivity locations. However, there were many assumptions. For example, it was assumed that fast infiltration occurred in the loam layer and the zone of high hydraulic conductivity is ten times larger than the loam layer zone. Inversion of hydraulic conductivity should be carried out in a more objective manner and further investigation is needed.

7. Summary

7.1 Research summary

In this research, we investigated the applicability of methods that estimate the 3D resistivity structure using 2D resistivity survey data to numerical and field experiments. The results in the preceding chapters will be summarized once again.

In Chapter 2, we proposed a method using 2D resistivity surveys to efficiently detect the range of cracks. In the numerical experiment, the horizontal range estimated by the survey line parallel to the crack was found to be almost equal to the actual crack length. The vertical range estimated by the survey line orthogonal to the crack had low correlation with the depth when the depth was larger than the length. However, high correlation was observed when the depth was smaller than half of the length. In the field experiments, the horizontal range estimated by the survey line parallel to the crack detected the crack length. The vertical range of cracks, estimated by the survey line orthogonal to the cracks, detected the crack depth when the depth was smaller than the length. The results indicate the possibility in detecting the range of cracks by estimating the crack length based on parallel survey lines and the crack depth based on orthogonal survey lines and the results of the crack length.

Chapter 3 presented a semi 3D resistivity monitoring method using 2D resistivity surveys of four traverse survey lines at a groundwater recharge experiment site. The resistivity distributions before the recharge test reflected the geological column at the boreholes and it was assumed that the geology of this site had a layer structure. During the recharge, resistivity changes reflected changes in volumetric water content at the boreholes. This shows that 2D difference inversions can be used to image soil water flows. Decreased resistivity zones spread along the secondary Shirasu layer and it was assumed that the soil water spread horizontally along the secondary Shirasu layer. The volumetric water content using a neutron moisture meter and the resistivity derived from the 2D inversion did not change in the loam layer. This may indicate the occurrence of partial flows in the loam layer. Each survey line gave a non-uniform distribution for the resistivity change ratio that reflected the fact there was no uniform filling of water in the recharge area. These results indicate that multi-line 2D resistivity surveys make it possible to easily monitor semi 3D flows of soil water.

In Chapter 4, we proposed effective electrode configurations and line layouts commonly used for 2D resistivity surveys for 3D inversion. The results of the numerical experiment revealed that the parallel-line arrangement was effective in identifying an approximate location of the conductive body. The orthogonal-line arrangement was optimal for identifying the target body near the intersecting point of lines. As a result, parallel lines were useful to highlight areas of particular interest where further detailed work with an intersecting line to be carried out. In the field experiment, 2D resistivity data were measured on a loam layer with a backfilled pit. The reconstructed resistivity image derived from parallel-line data showed a low-resistivity portion near the backfilled pit. When an orthogonal line was added to the parallel lines, the newly estimated location of the backfilled pit coincided well with the actual location. As a field application, we collected several 2D resistivity data sets in the Nojima Fault area in Awaji Island. The 3D inversion of these data sets provided a resistivity distribution corresponded to the geological structure. In particular, the Nojima Fault was imaged as a western boundary of a low-resistivity belt from only two orthogonal lines.

Chapter 5 presented the applicability of 3D inversion of 2D resistivity survey data to monitoring of soil-water flow in the vadose zone. The 3D inversion results clearly showed a heterogeneous resistivity distribution in the vadose zone and changes in the saturation level, especially in the secondary Shirasu layer, during the recharge experiment. The 3D inversion of the 2D resistivity survey data was more suitable than the 2D inversion to describe the 3D phenomena associated with groundwater recharge. These results indicated that this method can be applied to monitoring of relatively fast infiltration in the vadose zone. However, the infiltration flow in the loam layer was hardly detected, because little change occurred in the resistivity. This suggested that little change occurred in the saturation level. This method may be useful when the target layer has low saturation before the recharge experiment. Further investigations using other indicators such as changes in water resistivity are required to understand the groundwater flow in the loam layer.

In Chapter 6, we proposed a method that uses 3D simulation data of soil water flow and 2D resistivity survey data during a groundwater recharge experiment to estimate high hydraulic conductivity locations. In the numerical experiment, 3D inversion of the resistivity survey provided an image of the preferential flow, although the infiltration locations were unclear. The high hydraulic conductivity location of the possible model that provided the minimum errors corresponded to the high hydraulic conductivity location of the field model. In the field experiment, an 2D resistivity survey was conducted during groundwater recharge experiment in a pyroclastic plateau. The 3D inversion of the 2D resistivity survey provided an image of the preferential flow. By comparing the field resistivity survey data with the simulated resistivity survey data, the high hydraulic conductivity location of the possible model that provides the minimum error corresponded to filling water range, whereas that of the possible model that gives the maximum errors corresponds to no filling water range. These results indicate that estimating high hydraulic conductivity locations using 3D simulations of the groundwater flow and 2D resistivity survey is possible.

7.2 Conclusions

When the resistivity structure is in 3D and does not match the assumption of 2D inversion, the resistivity distribution derived from 2D inversion can result in artifacts. However, 2D inversion using 2D resistivity survey data can estimate the depth of the target body with orthogonal survey lines after estimating the length of the target body with parallel survey lines. Moreover, 2D difference inversions from multiple 2D resistivity survey data could estimate the vertical and horizontal water flow and help in 3D modeling of nonuniform sequential recharging. When 3D inversion of 2D resistivity survey data is conducted, parallel lines are useful to highlight areas of particular interest where further detailed work with an intersecting line should be carried out. The 3D inversion of 2D resistivity survey data is more suitable than 2D inversion to describe the 3D phenomena associated with groundwater recharge. This method can be applied to monitor relatively fast infiltration in the vadose zone. Moreover, 3D simulations of the groundwater flow and 2D resistivity survey can estimate high hydraulic conductivity locations. Although these methods use 2D resistivity survey data, 3D information of the subsurface can be estimated considering proper line arrangement, estimation order, or a combination of simulations.

7.3 Future works

The infiltration flow in the loam layer is barely detected, because the change in resistivity is small. It is difficult to estimate the condition under the water table or in a layer where the change in volumetric water content is small. Resistivity monitoring using a conductive liquid should be investigated. Although 3D simulations of the groundwater flow and 2D resistivity survey could estimate high hydraulic conductivity locations, there were many assumptions. For example, it was assumed that fast infiltration occurred in the loam layer and the zone of high hydraulic conductivity is ten times larger than the loam layer zone. Inversion of hydraulic conductivity should be carried out in a more objective manner and further investigation is needed.

ACKNOWLEDGMENTS: The work presented in this manuscript is based on the author's doctoral dissertation. The author wishes to express his sincere gratitude to Dr. Akira MURAKAMI, Kyoto University Professor and Chairperson of the Examination Committee, for his guidance, valuable suggestions, and constructive criticism during the completion of this thesis. The author wishes to extend his sincere appreciation to the members of the Examination Committee, Professor Shigeto KAWASHIMA and Professor Masayuki FUJIHARA, for their discussions and constructive suggestions when reviewing and improving the thesis. In addition, the author wishes to express his sincere appreciation to Professor Satoshi HOSHINO, Dr. Koichi UNAMI, Dr. Junichiro TAKEUCHI, and Dr. Kazunori FUJISAWA, for their discussions and constructive suggestions.

The author is very grateful to Dr. Hiroomi NAKAZATO of the Institute for Rural Engineering for guidance, encouragement, and

instruction during his research. The author gives special thanks to Dr. Mutsuo TAKEUCHI, Chief Executive Officer of Geo Vest, Inc., Professor Hee Joon KIM of the Pukyong National University, Dr. Yoshihiro SUGIMOTO of DIA Consultants Co., Ltd, Mr. Tomijiro KUBOTA, Chief of the Hydrology and Water Resources Unit, Dr. Koji FURUE of the Kagoshima Prefectural Institute for Agricultural Development, and Dr. Teruhito MIYAMOTO, Chief of the Soil Physics and Irrigation Unit, for their writing guidance, technical support, and field cooperation.

The author express his thanks to Dr. Shigeyasu AOYAMA, Professor Emeritus at Kyoto University, Professor Akira KOBAYASHI of Kansai University, Dr. Shoichi KIYAMA of Kyoto University, Dr. Kazuya INOUE of Kobe University, Dr. Yosuke KUDO of Osaka Prefecture University, and Professor Shinichi NISHIMURA of Okayama University for their continuing guidance and encouragement.

The author thanks Dr. Susumu MASUKAWA, Director of the Division of Facilities and Geotechnical Engineering, Dr. Shigeru TANI, Fellow of the National Agriculture and Food Research Organization, Professor Junji TAKAHASHI of Akita Prefecture University, Professor Yoshiyuki MOHRI of Ibaraki University, Dr. Tamotsu FURUYA, Professor Osamu KAWAMOTO of Nihon University, Dr. Norio NAKANISHI of the Agricultural and Rural Development Information Center, and Dr. Takeshi KOIZUMI of the Japanese Society of Irrigation, Drainage and Rural Engineering for their technical support and valuable advice.

The author thanks all members of the Disaster Prevention Unit, Dr. Hiroshi YOSHISAKO, Dr. Tetsushi SHIGEOKA, Mr. Michiaki KONNO, Dr. Daisuke SHODA, and Ms. Reiko KUNIMATSU, for their kind advice and hospitality. The author extends a thank you to all members of the Institute for Rural Engineering, with special thanks to Dr. Tatsuo NAKA, Dr. Isamu ASANO, Dr. Mitsuhiro MORI, Dr. Toshikazu HORI, Dr. Hisato SUZUKI, Mr. Seiji YASUNAKA, Dr. Satoshi ISHIDA, Dr. Takeo TSUCHIHARA, Dr. Shuhei YOSHIMOTO, Dr. Masaru YAMAOKA, and Dr. Fumiko ORITATE, for their sincere cooperation and assistance.

REFERENCES

Akaike, H. (1978): A Bayesian analysis of the minimum AIC procedure. *Annals of the Institute of Statistical Mathematics*, **30**, 9–14. doi:10.1007/BF02480194

Al Hagrey, S. A., and Müller, C. (2000): GPR study of pore water content and salinity in sand. *Geophysical Prospecting*, **48**, 63–85. doi:10.1046/j.1365-2478.2000.00180.x

Amidu, S. A., and Dunbar, J. A. (2007): Geoelectric studies of seasonal wetting and drying of a Texas Vertisol. *Vadose Zone Journal*, **6**, 511–523. doi:10.2136/vzj2007.0005

Archie, G. E. (1942): The electrical resistivity log as an aid in determining some reservoir characteristics. *Transactions of the AIME*, **146**, 54–62.doi:10.2118/942054-G

Awata, Y., and Mizuno, K. (1998): The strip map of the surface fault ruptures associated with 1995. Hyogo-Ken Nanbu earthquake, central Japan, scale 1:10,000, *Geological survey of Japan*, **12**, 74. [in Japanese]

Batlle-Aguilar, J., Schneider, S., Pessel, M., Tucholka, P., Coquet, Y., and Vachier, P. (2009): Axisymetrical infiltration in soil imaged by noninvasive electrical resistivimetry. *Soil Science Society of America Journal*, **73**, 510–520. doi:10.2136/sssaj2007.0278

Bentley, L. R., and Gharibi, M. (2004): Two- and three-dimensional electrical resistivity imaging at a heterogeneous remediation site. *Geophysics*, **69**, 674–680. doi:10.1190/1.1759453

Binley, A., Shaw, B., and Henry-Poulter, S. (1996): Flow pathways in porous media: electrical resistance tomography and dye staining image verification. *Measurement Science & Technology*, **7**, 384–390. doi:10.1088/0957-0233/7/3/020

Binley, A., Winship, P., West, L. J., Pokar, M., and Middleton, R. (2002): Seasonal variation of moisture content in unsaturated sandstone inferred from borehole radar and resistivity profiles. *Journal of Hydrology*, **267**, 160–172. doi:10.1016/S0022-1694(02)00147-6

Blome, M., Maurer, H., and Greenhalgh, S. (2011): Geoelectric experimental design — Efficient acquisition and exploitation of complete pole-bipole data sets. *Geophysics*, **76**, F15–F26. doi:10.1190/1.3511350

Chambers, J. E., Loke, M. H., Ogilvy, R. D., and Meldrum, P. I. (2004): Noninvasive monitoring of DNAPL migration through a saturated porous medium using electrical impedance tomography. *Journal of Contaminant Hydrology*, **68**, 1–22. doi:10.1016/S0169-7722(03)00142-6

Coggon, J. H. (1971): Electromagnetic and electrical modeling by the finite element method. *Geophysics*, **36**, 132-155.

Coscia, I., Greenhalgh, S. A., Linde, N., Doetsch, J., Marescot, L., Günther, T., Vogt, T., and Green, A. G. (2011): 3D crosshole ERT for aquifer characterization and monitoring of infiltrating river water. *Geophysics*, **76**, G49–G59. doi:10.1190/1.3553003

Daily, W., Ramirez, A., Binley, A., and LeBrecque, D. (2004): Electrical resistance tomography. *The Leading Edge*, **23**, 438–442. doi:10.1190/1.1729225

Daily, W., Ramirez, A., LaBrecque, D., and Nitao, J. (1992): Electrical resistivity tomography of vadose water movement. *Water Resources Research*, **28**, 1429–1442. doi:10.1029/91WR03087

Day-Lewis, F. D., Lane, J. W., Harris, J. M., and Gorelick, S. M. (2003): Time-lapse imaging of saline-tracer transport in fractured rock using difference-attenuation radar tomography. *Water Resources Research*, **39**, 1290. doi:10.1029/2002WR001722

Dey, A., and Morrison, H. F. (1979): Resistivity modeling for arbitrarily shaped three-dimensional structures. *Geophysics*, **44**, 753–780.

Farzamian, M., Santos, F. A. M., and Khalil, M. A. (2015a): Application of EM38 and ERT methods in estimation of saturated hydraulic conductivity in unsaturated soil. *Journal of Applied Geophysics*, **112**, 175–189. doi:10.1016/j.jappgeo.2014.11.016

Farzamian, M., Santos, F. A. M., and Khalil, M. A. (2015b): Estimation of unsaturated hydraulic parameters in sandstone using electrical resistivity

tomography under a water injection test. *Journal of Applied Geophysics*, **121**, 71–83. doi:10.1016/j.jappgeo.2015.07.014

Faybishenko, B., (2000): Tensiometer for shallow and deep measurements of water pressure in vadose zone and groundwater. *Soil Science*, **165**, 473–482. doi:10.1097/00010694-200006000-00003

Garambois, S., Senechal, P., and Perroud, H. (2002): On the use of combined geophysical methods to assess water content and water conductivity of near-surface formations. *Journal of Hydrology*, **259**, 32–48. doi:10.1016/S0022-1694(01)00588-1

Garre, S., Javaux, M., Vanderborght, J., Pages, L., and Vereecken, H. (2011): Three-dimensional electrical resistivity tomography to monitor root zone water dynamics. *Vadose Zone Journal*, **10**, 412–424. doi:10.2136/vzj2010.0079

Geological Survey of Japan, AIST, ed. (2015): Seamless digital geological map of Japan 1 : 200,000. May 29, 2015 version. Geological Survey of Japan, National Institute of Advanced Industrial Science and Technology. [in Japanese]

Gharibi, M., and Bentley, L. R. (2005): Resolution of 3-D electrical resistivity images from inversions of 2-D orthogonal lines. *Journal of Environmental & Engineering Geophysics*, **10** , 339–349. doi:10.2113/JEEG10.4.339

Holcombe, H. T., and Jiracek, G. R. (1984): Three-dimensional terrain corrections in resistivity surveys. *Geophysics,* **49**, 439–452. doi: 10.1190/1.1441679

Hori, T., Ueno, K., and Matsushima, K. (2012): Damages of small earth dams induced by the 2011 off the pacific coast of Tohoku earthquake. *Technical report of the National Research Institute of Agricultural Engineering*, (213), 175–199. [in Japanese with English abstract]

Huisman, J. A., Rings, J., Vrugt, J. A., Sorg, J., and Vereecken, H. (2010): Hydraulic properties of a model dike from coupled Bayesian and multi-criteria hydrogeophysical inversion. *Journal of Hydrology*, **380**, 62–73. doi:10.1016/j.jhydrol.2009.10.023

Huisman, J. A., Sperl, C., Bouten, W., and Verstraten, J. M. (2001): Soil water content measurements at different scales: accuracy of time domain reflectometry and ground-penetrating radar. *Journal of Hydrology*, **245**, 48–58. doi:10.1016/S0022-1694(01)00336-5

Huisman, J. A., Weerts, A. H., Heimovaara, T. J., and Bouten, W. (2002): Comparison of travel time analysis and inverse modeling for soil water content determination with time domain reflectometry. *Water Resources Research*, **38**, 13.1–13.8. doi:10.1029/2001WR000259

Imamura, S. (2007): The possibility of an instantaneous resistivity profiling by the simultaneous multi-channel current injection using CDMA method (I: the principle and the basic experiment). *Proceedings of the 117th SEGJ Conference*, 219–222. [in Japanese with English abstract]

Imamura, S., and Fukuoka, K. (2004): An approach of 3D terrain correction for 2D resistivity survey data. *Proceedings of the 110th SEGJ Conference*, 67–69. [in Japanese]

Inoue, K., and Nakazato, H. (2014) Simplified method for detection of open crack using 2-D resistivity survey. *Irrigation, Drainage and Rural Engineering Journal*, (290), 43–53. [in Japanese with English abstract]

Inoue, K., Nakazato, H., Kawamoto, O., Yamada, Y., Shoda, D. (2010): Material experiment for monitoring earthquake crack by resistivity survey. *Proceedings of the JSIDRE Conference*, 332–333. [in Japanese]

Inoue, K., Nakazato, H., Kubota, T., Takeuchi, M., and Furue, K. (2008): Semi-3-D resistivity monitoring for groundwater recharge tests using 2-D difference inversions. *Butsuri-Tansa*, **61**, 313–321. [in Japanese with English abstract]. doi:10.3124/segj.61.313

Inoue, K., Nakazato, H., Kubota, T., Takeuchi, M., Sugimoto, Y., Kim, H. J., and Furue, K. (2017a): Three-dimensional inversion of in-line resistivity data for monitoring a groundwater recharge experiment in a pyroclastic plateau. *Exploration Geophysics*, **48**(3), 332-343. doi:10.1071/EG16035.

Inoue, K., Nakazato, H., Nakanishi, N., Ootsuka, F., and Kikuchi, S. (2006): Resistivity monitoring for groundwater flow survey in an landslide area. *Technical report of the National Research Institute of Agricultural Engineering*, (204), 287–294. [in Japanese with English abstract]

Inoue, K., Nakazato, H., Takeuchi, M., Sugimoto, Y., Kim, H. J., Yoshisako, H., Konno, M., and Shoda, D.(2017b): Investigation of the line arrangement of 2D resistivity surveys for 3D inversion. *Exploration Geophysics*, in press. doi:10.1071/EG17019.

Inoue, K., Nakazato, H., Kubota, T., Furue, K., Yoshisako, H., Konno, M, and Shoda, D.(2017c): Estimating high hydraulic conductivity locations through a 3D simulation of water flow in soil and a resistivity survey. *Exploration Geophysics*, in press. doi:10.1071/EG17054.

Inoue, M. (1988): The measuring method of variably apparent resistivities by rain at the ground surface. *Proceedings of the 78th SEGJ Conference*, 187–188. [in Japanese]

Inoue, Y., Matsumoto, J., Mochida, T., and Nagatomo, Y. (2004): A soil monolith of a cumulative Andisol profile in Kasanohara Ignimbrite Plateau in southern Kyushu, Japan. *Bulletin of the Kagoshima Prefectural Institute for Agricultural Development*, **32**, 99–108. [in Japanese with English abstract]

Ishida, S., Tsuchihara, T., and Imaizumi, M. (2005): Development of automatic neutron moisture logging system for measurement of volumetric water content in unsaturated zone. *Transactions of The Japanese Society of Irrigation, Drainage and Rural Engineering*, **73**, 113–121. doi: 10.11408/jsidre1965.2005.313 [in Japanese with English abstract]

Jackson, P. D., Earl, S. J., and Reece, G. J. (2001): 3D resistivity inversion using 2D measurements of the electric field. *Geophysical Prospecting*, **49**, 26–39. doi:10.1046/j.1365-2478.2001.00241.x

Karaoulis, M. C., Kim, J. H., and Tsourlos, P. I. (2011): 4D active time constrained resistivity inversion. *Journal of Applied Geophysics*, **73**, 25–34. doi:10.1016/j.jappgeo.2010.11.002

Kim, K. J., and Cho, I. K. (2011): Time-lapse inversion of 2D resistivity monitoring data with a spatially varying cross-model constraint. *Journal of Applied Geophysics*, **74**, 114–122. doi:10.1016/j.jappgeo.2011.04.010

Kim, J. H., Yi, M. J., Park, S. G., and Kim, J. G. (2009): 4D inversion of DC resistivity monitoring data acquired over a dynamically changing earth model. *Journal of Applied Geophysics*, **68** , 522–532. doi:10.1016/j.jappgeo.2009.03.002

Koestel, J., Kemna, A., Javaux, M., Binley, A., and Vereecken, H. (2008): Quantitative imaging of solute transport in an unsaturated and undisturbed soil monolith with 3-D ERT and TDR. *Water Resources Research*, **44**, W12411. doi:10.1029/2007WR006755

Kubota, T., Inoue, K., Nakazato, H., Ishida, S., Furue, H., and Takeuchi, M., (2007): Visualization of the deep soil moisture movement in artificial recharge experiment. *Proceedings of the 49th JSSP Conference,* 52–53. [in Japanese]

Kubota, T., Masumoto, T., Matsuda, S., and Furue, K. (2005): Hydrogeological features of Kasanohara plateau based on water quality and its circulation. *Technical report of the National Research Institute of Agricultural Engineering*, (203), 81–100. [in Japanese with English abstract]

LaBrecque, D. J., and Yang, X. (2001): Difference inversion of ERT data: a fast inversion method for 3-D in situ monitoring. *Journal of Environmental & Engineering Geophysics*, **6**, 83–89. doi:10.4133/JEEG6.2.83

Li, J., Li, X., Lv, N., Yang, Y., Xi, B., Li, M., Bai, S., and Liu, D. (2015): Quantitative assessment of groundwater pollution intensity on typical contaminated sites in China using grey relational analysis and numerical simulation. *Environmental Earth Sciences*, **74**, 3955–3968. doi:10.1007/s12665-014-3980-4

Looms, M. C., Binley, A., Jensen, K. H., Nielsen, L., and Hansen T. M. (2008): Identifying unsaturated hydraulic parameters using an integrated data fusion approach on cross-borehole geophysical data. *Vadose Zone Journal*, **7**, 238–248. doi:10.2136/vzj2007.0087

Lytle, R. J., and Dines, K. A. (1980): Iterative ray tracing between boreholes for underground image reconstruction. *IEEE Transactions on Geoscience and Remote Sensing*, GE-18, 234–240. doi:10.1109/TGRS.1980.4307496

Machida, H., and Arai, F. (2003): Atlas of tephra in and around Japan. *University of Tokyo Press*, 64–70. [in Japanese]

Masukawa, S., Tagashira, H., Kuroda, S., and Hayashida, Y. (2012): Damages of embankment dams for irrigation due to the 2011 off the pacific coast of Tohoku earthquake. *Technical report of the National Research Institute of Agricultural Engineering*, (213), 217–241. [in Japanese with English abstract]

Mohri, Y., Hori, T., Ariyoshi, M., Hayashida, Y., and Tani, S. (2008): Damage to small earth dam due to the Noto Hanto earthquake in 2007. *Technical report of the National Research Institute of Agricultural Engineering*, (208), 15–23. [in Japanese with English abstract]

Morii, T., and Teradate, S. (2006): Some characteristics of mechanical or structural damages of irrigation ponds which were caused by the mid Niigata prefecture earthquake in 2004. *Bulletin of the Faculty of Agriculture, Niigata University*, **59**, 45–50. [in Japanese with English abstract]

Nakano, M., Amemiya, Y, Muto, I., Shiozawa, S., and Nakamura, T. (1981): Physical and hydrologic properties of a Shirasu Hill ―Soil properties and water movement in a volcanic deposit (Shirasu) area(II)―. *Transactions of The Japanese Society of Irrigation*, (93), 7–12. [in Japanese with English abstract]

Nakazato, H., Inoue, K., Nakanishi, N., Ito, Y., Okazaki, K., and Wang, Z., (2004): 3-D terrain corrections in 2-D resistivity survey. *Proceedings of the 111th SEGJ Conference*, 169–172. [in Japanese]

Nakazato, H., Inoue, K., Nakanishi, N., Takeuchi, M., Sugimoto, Y., and Kim, H. J. (2005): 3-dimensional resistivity survey around the Nojima fault in Awaji Island. *Proceedings of the 113th SEGJ Conference*, 85–88. [in Japanese].

Nakazato, H., Inoue, K., Nakanishi, N., and Wang, Z. (2006): New 3-D terrain correction method for 2-D resistivity survey. *Technical report of the National Institute for Rural Engineering*, (204), 281–286. [in Japanese with English abstract]

Nakazato, H., Inoue, K., Takeuchi, M., and Sugimoto, Y. (2009): Labor-saving, three-dimensional electrical prospecting method. *Geotechnical engineering magazine*, **57(**9), 34–35. [in Japanese]

Nakazato, H., Inoue, K., Yoshisako, H., and Hori, T. (2012): Case study of urgent resistivity survey for cracks in dam embankment caused by the 2011 off the pacific coast of Tohoku earthquake. *Technical report of the National Research Institute of Agricultural Engineering*, (213), 23–28. [in Japanese with English abstract]

Nakazato, H., Kuroda, S., Okuyama, T., Park, M., Kim, H. J., and Todoroki, Y., (2003): Application of continuous measuring system of electrical resistivity to geoenvironmental monitoring. *Technical report of the National Research Institute of Agricultural Engineering*, (201), 173–182. [in Japanese with English abstract]

Naruo, H., and Kobayashi, T. (2002): Two large-scale earthquakes triggered by a 6.5 ka BP eruption from Kikai caldera, southern Kyushu, Japan. *The Quaternary Research (Daiyonki-Kenkyu)*, **41**, 287–299. [in Japanese with English abstract] doi:10.4116/jaqua.41.287

Newman, G. A., Recher, S., Tezkan, B., and Neubauer, F. M. (2003): 3D inversion of a scalar radio magnetotelluric field data set. *Geophysics*, **68**, 791–802. doi:10.1190/1.1581032

Nimmo, J. R., Perkins, K. S., Schmidt, K. M., Miller, D. M., Stock, J. D., and Singha, K. (2009): Hydrologic characterization of desert soils with varying degrees of pedogenesis: 1. Field experiments evaluating plant-relevant soil water behavior. *Vadose Zone Journal*, **8**, 480–495. doi:10.2136/vzj2008.0052

Nishigaki, M. (2001): AC-UNSAF3D user's manual. [in Japanese]

Oldenborger, G. A., Knoll, M. D., Routh, P. S., and LaBrecque, D. J. (2007): Time-lapse ERT monitoring of an injection/withdrawal experiment in a shallow unconfined aquifer. *Geophysics*, **72**, F177–F187. doi:10.1190/1.2734365

Park, S., (1998): Fluid migration in the vadose zone from 3D inversion of resistivity monitoring data. *Geophysics*, **63**, 41–51. doi:10.1190/1.1444326

Ritsema, C. J., and Dekker, L. W. (2000): Preferential flow in water repellent sandy soils: principles and modelling implications. *Journal of Hydrology*, 231–232, 308–319. doi:10.1016/S0022-1694(00)00203-1

Samouelian, A., Cousin, I., Richard, G., Tabbagh, A. and Bruand, A. (2003): Electrical resistivity imaging for detecting soil cracking at the centimetric scale. *Soil Science Society of America Journal*, **67**, 1319–1326.

Sasaki, Y., (1993): Pitfalls in 2-D Resistivity inversion - artifacts due to 3-D structures. *Butsuri-Tansa*, **46,** 367–371. [in Japanese with English abstract]

Sasaki, Y. (1994): 3D resistivity inversion using the finite-element method. *Geophysics*, **59**, 1839–1848. doi:10.1190/1.1443571

Sasaki, Y., Goldstein, N. E., and Wilt, M. (1985): Time-lapse monitoring of resistivity changes. *Proceedings of the 73rd SEGJ Conference*, 73–74. [in Japanese]

Sasaki, Y., Hasegawa, N., and Matsuoka, T. (2005): Toward practical 3D resistivity surveys: effects of 3D topography and structures on interpretation. *Proceedings of the 112th SEGJ Conference*, 207–210. [in Japanese]

Singha, K., and Gorelick, S. M. (2005)): Saline tracer visualized with three-dimensional electrical resistivity tomography: field-scale spatial moment analysis. *Water Resources Research*, **41**, W05023. doi:10.1029/2004WR003460

Slater, L., Binley, A., Versteeg, R., Cassiani, G., Birken, R., and Sandberg, S. (2002): A 3D ERT study of solute transport in a large experimental tank. *Journal of Applied Geophysics*, **49**, 211–229. doi:10.1016/S0926-9851(02)00124-6

Suga, T. (2004): Presumption of the osmosis mechanism into the dyke using high density resistivity monitoring method. *Butsuri-Tansa*, **57**, 545–552. [in Japanese with English abstract]

Sugimoto, Y. (1988): A Bayesian approach to geotomographic inversion. *Proceedings of the 79th SEGJ Conference*, 28–33. [in Japanese]

Sugimoto, Y. (1995): Monitoring of electrolyte tracer in groundwater using resistivity tomography -numerical experiment-. *Proceedings of the 92nd SEGJ Conference*, 57–62. [in Japanese]

Sugimoto, Y. (2002): A new inversion technique for time-lapse ER tomography. *Proceedings of the 107th SEGJ Conference*, 207–210. [in Japanese]

Sugimoto, Y., Asakawa, S., Senna, S., and Nishida, K. (1995): 2D resistivity inversion software E-Tomo and some examples of the field survey. *Proceedings of the 92nd SEGJ Conference*, 428–432. [in Japanese]

Sugimoto, Y., and Hishiya, T. (1993): Automatic FEM mesh generation method for resistivity tomography. *Proceedings of the 88th SEGJ Conference*, 307–312. [in Japanese]

Sugimoto, Y., and Inoue, M. (1998): Study on 3-D resistivity tomography in civil engineering. *Butsuri-Tansa*, **51**, 676–687. [in Japanese]

Sugimoto, Y., Nakazato, H., Takeuchi, M., Kim, H. J., Inoue, K., Yamada, N., and Aono, T. (2004): Practical 3-D electrical resistivity survey method using measurements from a few 2 D survey lines. *Proceedings of the 111th SEGJ Conference*, 165–168. [in Japanese]

Sugimoto, Y., Nishida, K., and Tsuchiya, T. (1987): Effect of random noise on geotomographic reconstruction (2) - Choice of optimum solution by using AIC -. *Proceedings of the 77th SEGJ Conference*, 84–88. [in Japanese]

Suryo, E. A., Gallage, C., Trigunarsyah, B., Mochtar, I. B. and Soemitro, R., (2011): Application of electrical resistivity method to detect deep cracks in unsaturated residual soil slope. *Proceedings of AP-UNSAT 2011: 5th Asia-Pasific Conference on Unsaturated Soils*, 901–906.

Suzuki, K. (1997): Application of geophysical prospecting to geological engineering (II). -Application to monitoring the flow of underground water-. *Butsuri-Tansa*, **50**, 497–505. [in Japanese with English abstract]

Suzuki, K., Ito, E., and Chigira, M. (2002): Loosening process of surface area in weathered granite and infiltration of rainwater to excavated slope - Evaluation using geophysical exploration and observed field data-. *Journal of the Japan Society of Engineering Geology*, **43**, 270–283. [in Japanese with English abstract]

Suzuki, K., Fujii, K., and Takahashi, A. (2015): Monitoring groundwater flows using the electrical method at a rock-fill dam during first filling. *Butsuri-Tansa*, **68**, 189–199. [in Japanese with English abstract]

Suzuki, K., Oda. Y., Tani. K., Mogi, T., and Hayashi, H., and Jyomori, A., (1996): 3D electrical survey and step continuous wave radar survey for Nojima Fault area -Results of measurement of resistivity at trenching site-. *Butsuri-Tansa*, **49**, 511–521. [in Japanese with English abstract]

Suzuki, K., Oyama, T., Kawashima, F., Tsukada, T., and Jyomori, A. (2010): Monitoring of grout material injected under a reservoir using electrical and electromagnetic surveys. *Exploration Geophysics*, **41**, 69–79. doi:10.1071/EG09051

Takakura, S. (1991): Monitoring of change of groundwater level by resistivity method. *Butsuri-Tansa*, **44**, 227–231. [in Japanese]

Takakura, S. (1999): Evaluation of the characteristics of various electrode arrays in 2-D electrical prospecting. *Butsuri-Tansa*, **52**, 409–420. [in Japanese with English abstract]

Takakura, S., Yoshioka, M., Ishizawa, T., and Sakai, N. (2013): Geoelectrical monitoring of the slope of an embankment using a large-scale rainfall simulator. *Proceedings of the 11th SEGJ International Symposium*, 228–231.

Takeshita, Y., Konishi, K., Inoue, M., and Kohno, I. (1995): Studies on neural-network approach to the determination of unsaturated soil hydraulic properties by electric prospecting method. *Proceedings of the 92nd SEGJ Conference*, 240–243. [in Japanese]

Takeuchi, M., and Nagae, R. (1990): Geophysical monitoring system of diffusing electrolyte injected into groundwater. *Journal of the Japan Society of Engineering Geology*, **31**, 12–18. [in Japanese with English abstract]

Ushijima, K. (1997): Monitoring of ground water aquifer by electrical prospecting. *Butsuri-Tansa*, **50**, 632–642. [in Japanese with English abstract]

Wada, T., Inoue, M., Yokota, S., and Iwamatsu, A. (1995): Downward infiltration of rainwater by using continuous electric prospecting within pyroclastic plateau (Shirasu-Daichi) in southern Kyushu, Japan. *Journal of the Japan Society of Engineering Geology*, **36**, 349–358. [in Japanese with English abstract]

Zhe, J., Greenhalgh, S., and Marescot, L. (2007): Multichannel, full waveform and flexible electrode combination resistivity–imaging system. *Geophysics*, **72**, F57–F64. doi:10.1190/1.2435081

Received: 2 November 2017

比抵抗モニタリングを用いた土中の損傷領域推定

井上敬資

施設工学研究領域地域防災ユニット

要　旨

地震あるいは洪水により発生・拡大する、ため池や農地の内部における損傷領域は堤体や地盤の安全性低下や湛水不良の原因となるため、早い段階でその領域を特定して必要に応じた対策を施す必要がある。土中の損傷領域を地表面から直接検出することには困難があり、直接視認できる掘削も可能でない場合が多い。非破壊調査法の一つである電気探査による比抵抗モニタリングは、地盤内の浸透を可視化できるため有効な手段である。土中の損傷領域は3次元構造を有するため3次元探査が望ましいが、測定コストや測定時間に制約があるため、迅速に測定ができる鉛直2次元電気探査データを用いて評価することが必要となる。本論文は、電気探査の2次元探査データを用いた鉛直2次元／3次元解析および浸透解析を援用して損傷領域を推定する手法の提案を目的とする。主要な研究成果は、次の5点に要約される。

探査データの2次元解析に基づく提案法では、地震あるいは洪水で発生した土中の亀裂に石灰水を注入し、亀裂に対して平行および直交測線で2次元探査を行い、注入前後の比抵抗変化から亀裂範囲を簡易に推定する。数値実験および模型実験より、亀裂に平行な測線において比抵抗変化がある水平範囲はモデル亀裂長さに対応すること、および亀裂に直交する測線において亀裂長さより亀裂深さが小さい場合は、注入材料の深度方向への広がりを推定できることを明らかにした。以上の結果から、2次元解析では結果に偽像が含まれることがあるが、亀裂に平行な測線からその水平範囲を推定し、その結果に基づいて直交する測線から鉛直範囲を推定することの有用性を示した。

水田の漏水など地表からでは検出が困難な土中水の 3 次元浸透を簡易に把握することを目的として、地下水涵養試験において井桁状に配置した4測線で連続的に2次元探査を行い、2次元の比抵抗変化率分布を解析した。涵養開始後の比抵抗変化はおおむね飽和度の変化を反映していること、不均一な涵養状況を反映していることが示された。これらの結果から、複数測線の2次元解析により、土中水の鉛直および水平方向への浸透を含めた3次元の涵養状態を経時的かつ簡易に把握できることを明らかにした。

探査データの3次元解析により推定する手法においては、高密度に探査測線を設置することが一般的であるが、3次元解析のための効率的な2次元探査の測線配置法を提案した。数値実験の結果から、平行測線配置は対象物のおおよその位置を特定するのに効果的であり、直交測線配置は交差点の周辺で対象物の検出に最適であることを明らかにした。屋外試験では平行測線に直交測線を追加した場合、推定位置は改善されること、現地適用試験では2つの直交測線のみの3次元解析でも、断層を低比抵抗帯として検出できることを検証した。これらより、平行測線によって特定の位置を検出し、交差測線によってより詳細な探査を実施することの効率性を示した。

3次元の浸透状況を推定するため、地下水涵養試験において、複数の2次元探査結果から3次元の比抵抗変化率分布を解析した。複数測線の 2 次元探査データを用いて 3 次元解析を行う場合、異なる時刻で得られた 2 次元データを同時に用いるため、異なる時刻の浸潤領域が重なりあった比抵抗分布を得る。ここでは、2次元探査データの組み合わせを変えて3次元解析を行った結果、時刻に依らない不均一な比抵抗分布が明らかとなった。これにより、2次元探査データであっても、それらの3次元解析によって、より正確な浸潤領域が把握できることを示した。

探査データの 3 次元解析であっても測線数が少ないと偽像が生じ、比抵抗変化率分布のみからでは高透水部の推定が困難な場合がある。これに対し、地下水涵養試験において浸透流と電気探査の3次元解析を用いて高透水部を推定する手法を提案した。本手法は、複数の浸透モデルから計算された水分量分布に対して、2次元探査を実施し、得られた計算探査データと現地探査データを比較することで、最適な湛水不良モデルを選択する。数値実験において、最小誤差を与えるモデルの高透水部の位置は、漏水位置と一致することを明らかにし、地下水涵養試験の現地実験において、不均一な湛水状況を推定できることを新たに示した。

以上から、提案法は、本来は3次元に分布する土中の損傷領域を、容易に収集できる2次元探査データから効率的に推定することを実現し、迅速な機能診断や災害復旧活動を可能にした。本法は災害対策技術に貢献することが期待される。

なお，本論文は京都大学大学院農学研究科学位審査論文であることを付記する。

キーワード：2次元電気探査、3次元比抵抗構造、測線配置、ため池、亀裂、漏水、浸透解析